Gravitational Waves from Compact Objects

Thesis by

Benjamin James Owen

In Partial Fulfillment of the Requirements

for the Degree of

Doctor of Philosophy

California Institute of Technology

Pasadena, California

1998

(Defended May 12, 1998)

Acknowledgements

"He was determined to find the underlying logic behind the universe. Which was going to be hard, because there wasn't one."

Terry Pratchett, *Mort*

I would like to thank my collaborators, from whom I learned many lessons (not all having to do with physics): Nils Andersson, Curt Cutler, Sharon Morsink, Akira Ohashi, Sathyaprakash, Bernard Schutz, Hideyuki Tagoshi, Alberto Vecchio, and especially Lee Lindblom and Alan Wiseman. Alan and I never ended up writing a paper together, but in one way or another more than half of my thesis work has its origins in our many late-night discussions. The last two chapters grew out of 1997 conferences in Bangalore and Pune, India; and I am grateful to Bala Iyer, Gopakumar, and Sanjeev Dhurandhar for helping me through the subcontinent.

I would also like to thank Kip Thorne's research group and frequent visitors, who taught me many lessons and straightened me out when I took wrong turns: Bruce Allen, Haris Apostolatos, Kent Blackburn, Patrick Brady, Jolien and Teviet Creighton, Éanna Flanagan, Scott Hughes, Dan Kennefick, Yuri Levin, Eric Poisson, and Fintan Ryan. Also Shirley Hampton, who navigated me through various mazes of paper.

I will always have fond memories of the Caltech $\mu\alpha\lambda\acute{\alpha}\kappa\varepsilon\varsigma$: Josh Bliss, Hauke Hansen, Darrell Harrington, Rick Jenet, Malik Magdon-Ismail, Jason Maron, Jim Mason, Melissa Midzor, and Tasos Vayonakis. I was fortunate enough to arrive at Caltech in the midst of a large flux of people interested in living like human beings rather than grad students. Thanks for encouraging my vices, guys.

Various others helped me in one way or another to keep my sanity (and to lose it when it became too burdensome): Lynn Cominsky, Matt Davis, Mark Flower, Libby Hays, Michel Jabbour, Mihyung Lee, Naresh Malhotra, Keri-Lynne McDowell, Terry

Pratchett, Greg Sprehn, and Joe Tenn. Not least Cobalt, the campus cat who took over Bridge Hall while I was writing my thesis.

I am grateful to my family, who supported me through five years of crises: Jerry Owen, Sarah Owen and Jesse Crews, Pat and Stacey Stiefer, Margee Stearns, and Beulah Sullivan.

Most of all, I owe Kip Thorne. None of this would have happened without him. I am fortunate beyond words to have found an advisor who is both a great physicist and a great man. I have benefited greatly from his accumulated wisdom, his support, and his encouragement. Not only has he taught me through many patient corrections how to think about and communicate physics, he has been an outstanding example of integrity and compassion. When I leave Caltech for the real world, I will be guided by the memories of my years with him as I strive to live up to the tutelage he has given me.

Abstract

This thesis addresses problems in the generation and detection of gravitational waves from two types of sources: inspiraling compact binaries and rapidly rotating young neutron stars.

Chapters 2 and 3 estimate the computational costs of a basic matched filtering strategy to search for inspiraling compact binaries. Chapter 2 (written in 1995) sets up the machinery for calculating costs and makes a rough estimate based on the waveforms and noise spectra available at the time. It also systematizes previously published methods of choosing the filters. Chapter 3 (written with B. S. Sathyaprakash in 1998) fine-tunes the machinery and updates the estimates of Chapter 2 using more current waveforms and noise spectra.

Chapter 4 (written with Hideyuki Tagoshi and Akira Ohashi) concerns the post-Newtonian generation of gravitational waveforms from inspiraling compact binaries whose component objects spin about their own axes. It lays out a method of calculating post-Newtonian spin effects and calculates the lowest-order such effect not previously known (the second-post-Newtonian spin-orbit contribution to the waveforms in the absence of precession).

Chapters 5 and 6 concern the Chandrasekhar-Friedman-Schutz (CFS) gravitational radiation instability as it applies to the r-modes of rapidly rotating young neutron stars. Chapter 5 (written with Lee Lindblom and Sharon M. Morsink) computes the viscous damping and gravitational radiation timescales of the r-modes and shows that viscosity does not suppress the CFS instability in hot young neutron stars. Chapter 6 (written with Lee Lindblom, Curt Cutler, Bernard F. Schutz, Alberto Vecchio, and Nils Andersson) computes approximate gravitational waveforms from young neutron stars spinning down due to the r-mode instability and estimates that these gravitational waves can be detected by the "enhanced" LIGO interferometers if a suitable data analysis strategy is developed.

Contents

Chapter 1 Introduction

Chapters 2–6 of this thesis consist of five papers, each of which has been published, submitted for publication, or will be submitted for publication in *Physical Review D* (except for Chapter 5, which will appear in *Physical Review Letters*). I am the sole author of Chapter 2. Chapters 3–6 are collaborative efforts to which I contributed at least equally with my collaborators. I was a major contributor to all substantive aspects of the research in all of these chapters, except for the template placement algorithm in Section IV of Chapter 3 and for the calculation of stochastic background radiation in Section IV B of Chapter 6 (due mainly to Curt Cutler; I merely checked the numbers). The prose in these chapters is largely my own except for Chapter 5, where Lee Lindblom wrote more than I did, and Chapter 6, where he wrote as much as I did.

Each of these papers was written for experts in the field. This Introduction provides background information on the problems addressed and gives a nontechnical overview of each paper suitable for physicists in other fields.

Chapters 2–4 concern the generation and detection of gravitational waves from inspiraling compact binaries. Chapters 2 and 3 deal with the data analysis involved in the detection of inspiraling compact binaries, particularly the computational costs of a matched filtering search. Chapter 4 deals with high-order post-Newtonian calculations of waveforms from binaries composed of spinning bodies.

Chapters 5 and 6 concern gravitational waves from the Chandrasekhar-Friedman-Schutz instability acting on the r-modes of rotating neutron stars. Chapter 5 shows that this instability is not suppressed by viscosity in hot young neutron stars. In fact a rapidly rotating young neutron star radiates most of its rotational energy as gravitational waves within the first year after the supernova. Chapter 6 computes gravitational waveforms from the r-mode instability and concludes that the waves from single neutron stars in the Virgo cluster of galaxies will be detectable by "enhanced" LIGO interferometers [1], if a suitable data analysis strategy can be developed. A

stochastic background (from approximately 25 Hz to more than 1 kHz) made up of many weaker r-mode signals from neutron stars out to cosmological distances will be detectable by "advanced" LIGO [2].

I. MATCHED FILTERING SEARCH FOR INSPIRALING COMPACT BINARIES

A. Background

Inspiraling compact binaries such as the Hulse-Taylor pulsar have long been considered a staple source of gravitational waves for laser interferometers such as LIGO [3]. They are known to exist (although in uncertain numbers) [4] and to have fairly clean dynamics—i.e., waveforms which can be modeled with great precision—up to the final stages of their inspiral due to gravitational radiation reaction. However the signal strengths are expected to be so weak as to be undetectable in the presence of interferometer noise without extensive data analysis. Because the waveforms can be precisely modeled, the obvious data analysis technique to use (both to search for signals and to estimate parameters of signals once detected) is matched filtering.

Matched filtering, introduced by Wiener in the 1940s and frequently used in radar and sonar applications [5], entails cross-correlating the data stream with a set of template waveforms. If one of the templates is proportional to the signal, the cross-correlation increases the signal-to-noise ratio to the maximum value possible for any linear filtering method. In practice, of course, it is highly unlikely that any of the templates will be exactly proportional to the signal, so the goal is to make sure that at least one template resembles the signal closely enough to extract most of the optimal signal-to-noise ratio.

There are two main problems to be solved before achieving this goal. First, one must construct the right class of templates. In the case of inspiraling compact binaries,

this translates to knowing what order is needed in the post-Newtonian expansion used to generate the waveforms and then carrying out the calculations up through that order. Once the right class of templates is in hand, an algorithm is needed to place a discrete set of actual templates in the parameter space so as to assure that a signal at an arbitrary point in parameter space will be close enough to at least one template to have a sufficiently high cross-correlation with it.

The problem of finding a sufficient post-Newtonian order is now under control. Apostolatos [6] has defined the *fitting factor* FF as (effectively) the fraction of optimal signal-to-noise ratio retained when using an approximate family of templates, e.g. templates computed only up to some finite post-Newtonian order. Recently Droz and Poisson [7] have computed fitting factors for binary inspiral waveforms in the test-mass limit where the exact waveforms can be calculated from black-hole perturbation theory and then compared to post-Newtonian expansions at various orders. Droz and Poisson [7] thereby concluded that the the standard second post-Newtonian waveforms [8,9] satisfy the criterion $FF \geq 90\%$. Damour, Iyer, and Sathyaprakash [10] introduced a new class of waveforms, taking advantage of physical insight to rephrase the standard post-Newtonian expansion of the waveforms' phase evolution in a better way (similar to the way Padé approximants do better than Taylor series by including poles in the complex plane). Their version of the second post-Newtonian expansion has $FF \geq 95\%$.

The above fitting factors were computed neglecting the effects of the bodies' spins about their own axes. Most data analysis papers (and post-Newtonian wave generation papers, see Section II) neglect spin effects because (i) evolutionary models of known binary pulsars indicate that near the end of inspiral the spins will be small (spin/mass$^2 \ll 1$ in geometrized units) [11] and (ii) Apostolatos [6] found at post$^{1.5}$-Newtonian order that if the spins are parallel to the orbital angular momentum (so that the plane of the orbit does not precess), spinless templates have $FF \geq 98\%$.

He also found that if the orbit does precess, spinless templates have $FF \geq 90\%$ over most of the parameter space. However, for binaries composed of a rapidly spinning black hole (spin$\sim$mass^2) and a less massive object such as a neutron star in an orbit inclined by more than about 30 degrees to the black hole's spin, precession modulates the amplitude and phase of the waveforms so much that spinless templates are all but useless. Again, because of the small spins of known binary pulsars it is expected that few binaries live in this fairly small region of parameter space, but the gravitational waves from those that do will carry a great deal of interesting astrophysical information. The desirability of detecting such binaries motivates the work described in Section II; but now let us return to the discussion of matched filtering issues for non-precessing binaries.

The first attempt at solving the parameter-space problem was made in a series of papers by Sathyaprakash and Dhurandhar [12]. They considered at first a simple one-parameter family of waveforms. These "Newtonian" waveforms (see Section II) are described by one mass parameter, a symmetric combination of the masses of the two objects called the binary's *chirp mass.* For such waveforms, the parameter space is simply the number line and the technique for choosing the actual templates is quite simple: Place templates along the number line so that a signal at an arbitrary location along the line has a cross-correlation with the closest template that exceeds a designated minimum value (fixed by the acceptable loss of event rate).

It was clear that the techniques used by Sathyaprakash and Dhurandhar could be generalized in some way to higher-dimensional parameter spaces (which were needed since the one-parameter Newtonian waveforms were known to be inadequate [6]). But it was not clear how (for example) to deal with covariances between parameters. Such covariances were the source of a certain amount of confusion, seeming to make the template spacing depend on waveform parametrization. Also, using then-available techniques, the entire calculation had to be redone numerically and *ab initio*

for different noise curves, with no scaling laws. The early estimates of numbers of templates and computing power were somewhat chancy since they typically considered primitive noise spectra such as white noise. With the prospect of operational LIGO interferometers only a few years away it was desirable to have a systematic way of placing templates and estimating computational costs for general waveforms and noise spectra. Chapter 2 of this thesis solved this problem.

B. A geometric approach

Chapter 2 introduces a geometric approach to solving parameter-space problems. Specifically, in this chapter I define a metric on the template parameter space which quantitatively relates distance in that space to the signal-to-noise ratio obtained using a template with the wrong parameter values. The main benefits of this geometric approach are (i) one can easily compute how many templates are needed (and thence the computational cost) for any family of waveforms, noise spectrum, and coverage level; and (ii) one can place the templates in parameter space in the most efficient way possible, taking advantage of covariances between parameters to reduce the template spacing.

In Chapter 2, I use this geometric approach to calculate the numbers of templates needed, and thereby infer the computational power needed to filter the data in real time assuming (i) the "first" and "advanced" LIGO noise spectra [2], (ii) a two-parameter template family (the stars' two masses) that neglects the effects of spins (see Section II below), (iii) a search based on making a single pass through the data, (iv) template spacings that lose no more than 10% of the event rate due to coarseness of the template grid, (v) a search over masses ranging from much more than $1M_{\odot}$ down to the minimum mass of a neutron star, $0.2M_{\odot}$. In Chapter 2, I also present the (approximate) scalings of the number of templates and computational power with the parameters of the noise spectrum and the parameters of the search strategy.

My conclusions, for the above parameters, are that the first LIGO interferometers will require some tens of gigaflops (floating point operations per second) to perform data analysis at the same rate as data acquisition. This computational cost is feasible but not cheap, and therefore the real LIGO data analysis will probably use something along the lines of a hierarchical search, for instance as described by Mohanty and Dhurandhar [13]. A hierarchical search (by contrast with the single-pass search assumed above) involves using a loosely-spaced set of templates to perform a first pass through the data (at a reduced threshold signal-to-noise ratio), then following up promising candidates from the first pass with a more closely-spaced set of templates (and higher threshold to weed out false alarms). Because the geometric formalism of Chapter 2 is based on the limit of close template spacing (appropriate for a simple one-pass search), it might not be adequately accurate for the first pass of a hierarchical search.

My goal in Chapter 2 was to estimate the number of templates and computational power required to within about a factor of three. The numbers in Chapter 2 are rough estimates because I used two-parameter waveforms which are now known (and even then were suspected) to be inadequate for a real search. I used the "first post-Newtonian" waveforms (see Section II) because they were the simplest possible two-parameter family. My primary goal was to set forth the method of calculation, and secondarily to get rough estimates of the actual numbers. Because the approximate waveforms used were already a source of uncertainty at the factor-of-three level, I made several other simplifying assumptions that could cause errors of somewhat less than that.

Chapter 3 of this thesis (written with B. S. Sathyaprakash) refines the rough estimates of Chapter 2 by incorporating more up-to-date waveforms and noise spectra. We use the two-parameter (two masses), second post-Newtonian waveforms given, for example, in Reference [9]. We also use more up-to-date noise spectra for the four large- and intermediate-scale interferometers LIGO, VIRGO, GEO, and TAMA, and

correct several small factors neglected in the analysis of Chapter 2. We find that the computational power required is about five times that estimated in Chapter 2. Most of the change can be attributed to our using second post-Newtonian waveforms and a higher sampling rate than assumed in Chapter 2.

The geometric approach to template placement and estimating computational requirements, which I introduced and developed in Chapter 2, has since been used in computational cost estimates for searches for other sources of gravitational waves such as pulsars [14] and the quasinormal modes of black holes excited after a binary black-hole merger [15].

II. POST-NEWTONIAN SPIN EFFECTS IN COMPACT BINARIES

A. Background

The calculation of gravitational waveforms from inspiraling compact binaries is complicated by the fact that there is no exact solution to the field equations of general relativity for two arbitrary bodies. However, the equations of general relativity can be expanded in a "post-Newtonian" series to approximate weak-field, slow-motion effects. The lowest-order terms in the post-Newtonian series have been known for decades, but for the most part workers in the field felt that the enormous complexity of obtaining higher-order terms (comparable to the precise calculations of the gyromagnetic ratio of the electron in quantum electrodynamics) made the project not worth pursuing in the absence of experimental comparison. The situation changed with the advent of the LIGO project. Because matched filtering requires precise template waveforms, LIGO will not detect most inspiral events unless the templates include very high post-Newtonian orders [6]. Typical inspiral signals will spend of order 10^4 cycles in the LIGO frequency band, and in order to detect a signal the phase evolution of a template waveform must track the phase of the signal to well

within one cycle over that band. (To estimate parameters without bias, the tracking must be somewhat better.) Thus there has been in recent years a great deal of effort expended on pushing the post-Newtonian approximation to very high order.

Although post-Newtonian calculations tend to be quite complicated, the underlying physical and mathematical concepts are quite simple. Currently the two main approaches are those of Blanchet, Damour, and Iyer (BDI) [8] and of Will and Wiseman (WW) [9]. The BDI approach is a formal use of matched asymptotic expansions. There is one expansion (in orbital velocity v/c) which is good asymptotically close to the source and another (in deviations from a flat metric) which is good asymptotically far away. When the orbital velocity is small compared to the speed of light ($v/c \ll 1$), the domains of validity of the two expansions overlap; therefore the expansion coefficients can be matched in the overlap zone. The WW approach is more intuitive. It entails a direct integration of a retardation expansion of the Einstein equations in a particularly convenient gauge, very similar to a Green's function calculation of electromagnetic waves from a charge distribution.

Both approaches require very involved calculations (single expressions can take up nearly a full page in *Physical Review D*) even when using the simplest possible matter source, a pair of δ-functions representing point masses. Therefore, many experts have been wary of including finite-body effects such as spins which would seem to require a more complicated matter source. The first derivation of spin effects in the post-Newtonian expansion was given by Kidder, Will, and Wiseman [16]. They used a fluid ball description of the bodies to derive the lowest-order spin-orbit and spin-spin effects in the simplest case (when both spins are parallel to the orbital angular momentum so there is no precession). Precession was investigated to lowest order by Apostolatos *et al.* [17] and by Kidder [18]. Although the spinless post-Newtonian expansion has been pushed to much higher order in the years since (in the interest of producing accurate templates for matched filtering), there has been no comparable

work on spin effects. The reason is the additional complexity of fluid ball calculations, which were thought necessary to approximate spinning bodies.

In parallel to the "full post-Newtonian" expansion described above, there has been much work [19] on obtaining post-Newtonian waveforms valid to much higher orders, but only in the test-mass limit $\mu \ll M$. This is done by perturbing known solutions of the Einstein equations—most especially the Kerr spacetime, taken to represent a rotating black hole of mass M with a small mass μ in orbit around it. At leading order in μ/M, the post-Newtonian expansion has been pushed to much higher order in v/c than has been done for the full post-Newtonian expansion ($\mu \sim M$). This has been possible because the calculations for $\mu \ll M$ are somewhat more tractable (though still quite involved). By perturbing the Kerr spacetime using the traditional point-mass source for the test body, one can of course obtain spin effects due to the central body but one cannot obtain spin-spin effects or the spin-orbit contribution due to the spin of the test body. And of course one cannot thereby obtain the finite-mass contributions to any effects, which based on the known terms in the full post-Newtonian expansion are expected to be comparable to the test-mass effects.

B. "Spinning point mass" approach

Recently Mino, Shibata, and Tanaka [20] introduced a form of the stress-energy tensor (hereafter called the MST tensor) which incorporates spin effects while being formally represented as a δ-function for ease of computation. This stress-energy tensor, based on the work of Dixon in the 1970s [21], was used to extend the Kerr perturbation work to obtain higher-order spin-orbit and spin-spin effects on the phase evolution of gravitational waveforms.

Chapter 4 of this thesis (written with Hideyuki Tagoshi and Akira Ohashi) is the first use of the MST "spinning-particle" stress-energy tensor in the full post-Newtonian theory, i.e. valid for arbitrary mass ratios. In this chapter we present an

integral expression which allows one to obtain from the MST stress-energy tensor a post-Newtonian expansion of the spin-orbit contributions to any radiative multipole that enters into the post-Newtonian waveforms and luminosities. We then use this expression to calculate the lowest order spin effect that was previously unkown: a second post-Newtonian spin-orbit contribution to the amplitude (but not phase) evolution of the waveforms for spins parallel to the orbital angular momentum. We find that, as expected, the finite-mass contributions to this term are comparable to the test-mass contributions. Because the phase evolution of the waveforms is more important for data analysis than the amplitude evolution, the main value of this chapter is not its derivation of the new contribution to the wave amplitude, but rather the relatively easy methods of computation that it introduces.* These new methods will find their real payoff in future computations of spin contributions to the waves' phase.

As I write this, Tagoshi and I are discussing how to obtain the 5/2 post-Newtonian [order $(v/c)^5$] spin-orbit term in the phase evolution (in the absence of precession). This requires as a first step obtaining the equation of motion to comparable order, which we think we can do by extending the methods of Chapter 4. The next step, which needs to be completed before LIGO begins taking data, will be to compute all the higher-order precession effects that can show up in signal detection and information extraction for the few but extremely interesting binaries that have strong precessional modulation.

---

*For me, personally, there was a second major payoff from the work described in Chapter 4: It showed me that spin contributions are generally stronger in the radiative current multipoles than in the radiative mass multipoles. This disruption of the standard progression of post-Newtonian orders triggered my suspicion that the r-modes of neutron stars might be more interesting than people had thought (see Section III).

III. GRAVITATIONAL RADIATION INSTABILITY IN HOT YOUNG RAPIDLY ROTATING NEUTRON STARS

A. Background

The Chandrasekhar-Friedman-Schutz (CFS) gravitational radiation instability has been of interest to relativists since the 1970s [22]. In this instability, certain normal modes of rapidly rotating stars self-excite through gravitational radiation reaction. Sadly, for all modes of neutron stars investigated prior to this thesis, viscous damping has turned out to suppress the instability except in the most rapidly rotating young neutron stars (those that are on the verge of being torn apart by the centrifugal force anyway).

In Chapter 5 of this thesis (written with Lee Lindblom and Sharon M. Morsink) we show that for one set of modes ("r-modes") the CFS instability is very much an astrophysical reality, even in fairly slowly rotating young neutron stars. In fact it appears that the CFS instability in r-modes is responsible not only for giving young neutron stars their relatively slow rotation rates but for emitting copious amounts of gravitational radiation (of order $10^{-2}M_{\odot}c^2$ during the first year after a supernova).

The CFS instability is one of a broad class of dissipation-driven instabilities (*two-stream instabilities* such as the Kelvin-Helmholtz instability) which arise because of disagreements between observers as to which way a disturbance propagates. In this case the disagreement is between observers in a spinning star's co-rotating frame (where the internal viscosity of the neutron star lives) and in an inertial reference frame far from the star (where the emitted gravitational radiation lives). The unstable modes are those that propagate retrograde as seen by a co-rotating observer but prograde as seen by a distant, inertial observer. Because the mode is retrograde in the co-rotating frame, it is a negative perturbation of the star's angular momentum and of its energy as measured by distant inertial observers; but it is a positive perturbation

of the energy as seen by co-rotating observers. The emitted gravitational radiation lives in the distant inertial frame and, because the mode is prograde in that frame, carries off angular momentum that is positive as seen by all observers and energy that is positive as seen by the distant inertial observers but negative as seen by the co-rotating observers. Therefore, as seen by everybody, conservation of energy and angular momentum requires that radiation reaction increase the absolute values of the mode's energy and angular momentum, driving rather than damping the mode. The condition for this CFS instability is that the mode propagate in the retrograde direction on the star, but be dragged prograde by the star's rotation as seen by distant inertial observers; this happens when the mode's pattern speed (mode angular frequency ω divided by azimuthal wave number m) in the inertial frame is less than the angular velocity of the star Ω: $\omega/m < \Omega$.

The CFS instability in neutron stars has long been of interest to relativists as a potential source of gravitational waves [23]. Unlike other hypothesized sources, rotating neutron stars are very common, and any mechanism of self-exciting such a star's deviations from axisymmetry has been viewed as a potentially good candidate for observations by LIGO. The CFS instability has also been considered potentially astrophysically interesting because it could (by radiating away energy and angular momentum) naturally set an upper limit on the angular velocities (i.e., a lower limit on the periods) of young neutron stars [24]. This comes from the fact that gravitational radiation is much stronger at higher angular velocities, and thus a star would spin down to the point where viscosity suppresses the instability.

Unfortunately, for the past twenty years almost all neutron-star modes which were found to be formally susceptible to the CFS instability turned out to be stabilized by viscosity [25]. The sole exception was a group of f-modes (fundamental pulsation modes) with high azimuthal wave number, where the instability survived only at very high angular velocities (over 90% of the breakup value). Thus the minimum neutron-

star period set by the f-modes was not much greater than the Kepler period at which the star loses material due to centrifugal force, and the instability was still not very interesting astrophysically—though gravitational-wave theorists did hope to find a small population of young neutron stars spinning down and radiating gravitational waves via the f-modes. Part of the trouble was that the modes people studied had frequencies (in the inertial frame) much greater than the angular velocity of the star, which meant that very high wave numbers m were needed for the mode to be formally unstable. However, modes with high wave numbers are much more strongly sheared and thus more subject to viscous damping.

B. The r-modes and their influence on the evolution of a young neutron star

The r-modes are so designated because they have nonzero frequency only in rotating stars. The restoring force on the r-modes is the Coriolis force, so their frequencies are in fact proportional to (and comparable to) the angular velocity of the star. Sometimes the r-modes are called axial modes, because in the slow rotation limit the fluid displacement is an axial vector (proportional to a magnetic-type vector spherical harmonic) rather than a polar vector as for other modes. The r-modes are unlike other stellar normal modes not only because of their parity and their relatively low frequencies, but also because they move fluid elements around nearly on equipotential surfaces with little change in density (analogous to large-scale Rossby waves in the Earth's oceans and atmosphere).

In 1997 while cataloguing all the modes of neutron stars, Nils Andersson discovered that in the absence of viscosity *all* of the r-modes of *all* rotating neutron stars are subject to the CFS instability [26]. That is, modes which are retrograde in the corotating frame but prograde in an inertial frame can be found for all azimuthal wave numbers at all angular velocities. Although throughout 1997 no one had computed the viscous timescales—and, it turned out, no one had properly computed the gravi-

tational radiation timescales—Andersson's discovery generated considerable interest by itself. The fact that the r-mode instability persists even at low wave numbers (where shear viscosity is less important) led the experts to suspect that it might be damped less than the instabilities of other modes. The instability of the r-modes even in the limit of slow rotation also led the experts to suspect that the r-modes might be slightly more effective at spinning down young neutron stars than the other modes previously investigated. Both suspicions proved correct—much more so than anyone expected.

Throughout 1997 interest in the r-modes was widespread but not very intense, and experts in the field were slow to properly calculate the gravitational radiation and viscous timescales. There were two reasons. First, the fact that all the neutron-star modes investigated for twenty years had proved stable in the presence of viscosity (with the modest exception of the f-modes) led the experts to be pessimistic that any modes would prove unstable enough to be astrophysically interesting. Thus, although the tools for doing the simple viscosity calculation were available, the experts put off the r-mode problem to work on other projects. Second, the experts roughly estimated the time scale for the r-modes to grow, making the standard assumption that mass-multipole waves are dominant, and obtained timescales discouragingly long because the r-modes have very small density perturbations. It was known that in principle the current multipoles would also radiate and produce radiation reaction. However, calculations of such effects had been confined to the specialized post-Newtonian binary literature (e.g. [8]), where decades of relativity lore taught that they were high-order corrections to the mass multipole radiation. Due to the believed low payoff of a current-multipole calculation for the r-modes and the perception by the broader relativity community of the post-Newtonian literature as opaque and obscure, the current multipoles were neglected.

I was lucky enough to walk into this problem with the one missing piece, the

ability to calculate current multipoles. On the first night of the GR15 meeting (in Pune, India, December 1997) when most of the experts in the relativistic stellar pulsation community were gathered at dinner to talk about the r-modes, I happened to sit at the same table. Over dinner, Bernard Schutz speculated that for the r-modes, because their density perturbations were small compared to their velocity perturbations, current multipoles might prove as important as the mass multipoles. He urged the experts to overcome their fears of the impenetrable post-Newtonian literature and investigate further, going so far as to goad Nils Andersson with a bet. At the time I was certainly no expert on the r-modes—I knew very little about fluid dynamics or stellar pulsations, and most of the talk went over my head. But I was lucky enough to have the one missing piece—fortuitously, I had recently finished a calculation (Chapter 4 of this thesis) of post-Newtonian effects in spinning binaries which had involved current multipoles, and therefore they held no fear or mystery for me. Knowing little about r-modes but something about current multipoles, I did my first calculation (of which mode numbers would contribute to which multipoles, knowing only the angular dependences of the perturbations) at the dinner table while the speculation and debate went on around me. When I returned to Caltech and had the chance to look up the r-mode literature and learn the dependence of the density and velocity perturbations on the star's angular velocity, I refined that calculation. I found that the current multipoles were in fact the dominant effect and that the gravitational radiation was stronger than previously suspected by several orders of magnitude. Fortunately Lee Lindblom, one of the dinner guests at GR15 and an expert on stellar pulsations for over twenty years, had just arrived at Caltech for his annual four-month stay, so I could benefit from his wealth of expertise on the subject. I showed him my gravitational radiation results and he quickly calculated viscous timescales. Thus we launched a very fruitful collaboration.

Chapter 5 of this thesis (written with Lee Lindblom and Sharon M. Morsink) is

the first computation of viscous timescales and the first proper computation of gravitational radiation timescales for the r-modes. We demonstrate that for a reasonable model of a young neutron star the gravitational radiation timescale is orders of magnitude shorter than the viscous timescales—and thus the modes are unstable in fact as well as in principle—even at angular velocities a small fraction of the Kepler angular velocity (at which the star breaks up due to centrifugal force). The instability persists for about a year after the formation of the neutron star, until it has spun down to a fraction of its angular velocity and cooled to the superfluid transition temperature. We find, using the viscosity of hot neutron fluid, that the minimum period for stability of the r-modes is about 13 times the Kepler period at the star's surface (about $13 \times 1.5 = 17$ms). However, this number should not be believed to more than about a factor of two due to several approximations we made (see below).

The viscous damping mechanisms considered in Chapter 5 are the standard bulk and shear viscous processes for hot neutron fluid (see the references in Chapter 5 for further discussion). The bulk viscosity comes from the disturbance in the β-equilibrium of a fluid element subjected to a density perturbation. That is, some of the protons and electrons are combined to neutrons in the compression phase and vice versa in the rarefaction phase. Neutrinos are produced in the process and quickly escape from the star, thereby taking energy out of the mode. (Presumably at very high temperatures the neutrinos scatter several times before escaping, heating the star with some of their energy, but the net result is still to take energy out of the mode.) This process dominates the viscosity at very high temperatures such as those found in the first few minutes after a supernova. The temperature dependence of the bulk viscosity is very steep, and as the star cools below 10^{10}K the lower-temperature shear viscosity due to neutron-neutron scattering becomes important. As the hot neutron fluid cools to about 10^9K, it becomes a superconducting superfluid, and the main viscous damping mechanism is believed to become mutual friction [27], whereby

electrons scatter off of ordinary neutron fluid vortices containing strong magnetic fields due to proton supercurrents. No calculation for mutual-friction damping of the r-modes has yet been done, but based on previous experience with other modes it is expected to completely suppress the CFS instability at temperatures below the superfluid transition temperature $T_c \simeq 1 \times 10^9$K. This is consistent with the known rapid rotation rates of old, cold millisecond pulsars.

There are several important effects neglected or given short shrift in Chapter 5. Much of this neglect is due to space limitations (Chapter 5 will appear in *Physical Review Letters*). Here I shall give brief descriptions of some of the effects left out, and make hand-waving arguments as to why they should not qualitatively change our picture of the instability (although they will certainly quantitatively change the timescales somewhat).

Two obvious viscous mechanisms mentioned but given little discussion in Chapter 5 are magnetic fields and crust formation. The r-modes do not wrap magnetic fields around the star in the same way as the post-supernova collapse and boil; they simply shake the fluid and its embedded field lines back and forth at frequencies up to about 1 kHz. Any shaking of the field lines due to a shear mode could in principle carry off a lot of energy by coupling to the magnetosphere. However, the magnetosphere plasma frequencies are typically 10 kHz or more, even using the corotation charge density as a lower limit [28]. Therefore the transmission coefficient for 1 kHz oscillations of the stellar matter to get out into the magnetosphere is quite low [29].

Crust formation seems a bit more difficult to treat. A crust should begin forming near the surface of the star when the core fluid cools to approximately 10^{10}K [30], which is about the same temperature at which the quadrupolar r-mode becomes unstable. Prior to submitting Chapter 5 for publication, we tried one simple test: we simply turned the mode off in the outer layers, i.e. at densities low enough for the crust to form, and found that this had little effect on the instability. Since then

I have done slightly better. The maximum elastic energy in a well-established crust is of order 10^{44}ergs [29] at a breaking strain of order 10^{-2}, and while the crust is forming the power being fed into the r-mode by gravitational radiation reaction is of order 10^{49}erg/s. Therefore the r-mode should easily shear away any incipient crust, presumably melting the material in the process. Since the power being fed into the r-mode in this regime is greater than the neutrino luminosity by which the entire neutron star cools (see Figure 6.3), converting even a small fraction of the mode's power into heat should be sufficient to re-melt the outer layers without overcoming the mode's instability.

In quickly performing the calculations that became Chapter 5, we also neglected a number of non-dissipative effects such as rapid rotation, nonlinear hydrodynamics, and relativistic gravity (beyond what was needed to generate gravitational radiation). We naively expect full general relativity to change the results by a factor of order the gravitational redshift—i.e., about unity. More important are the rapid rotation and nonlinear hydrodynamics issues, which are coupled at some level. The expressions and symmetries we use for the r-modes are valid only in the slow-rotation limit. They are also valid only as long as the mode is a small perturbation of the rigidly rotating equilibrium configuration. At some point, the star is no longer describable as a linear superposition of an r-mode and a rigidly rotating equilibrium fluid, and nonlinear hydrodynamics is needed. For instance, it is possible that the growing mode causes the star to evolve into some highly nonspherical fluid configuration analogous to the Maclaurin spheroids. We make a crude attempt at describing such a situation in Chapter 6 (see below). Again, this would be an interesting research problem which we expect to quantitatively modify but not qualitatively negate the results of Chapter 5.

The biggest challenge (so far) to the results obtained in Chapter 5 is the discovery of a very fast young pulsar in the Large Magellanic Cloud [31]. This pulsar has a 16ms period and an apparent age of 5000 years. Its braking index has not yet been

measured, but assuming a value comparable to that in other young pulsars, one can deduce an initial period of about 7ms. If true, the 7ms period certainly modifies the simple model given in Chapter 5 but does not completely invalidate the result. It could indicate that some other damping mechanism comes into play before the star cools to 10^9K; for instance, if the critical temperature T_c for superfluidity is about 2×10^9K rather than 10^9K and mutual friction suppresses the instability below T_c, that would change the minimum period to 7ms. Several other effects neglected in Chapter 5 could be significant in this regime because the star has spun down by a large factor and thus the gravitational radiation (which depends strongly on angular velocity) has become much weaker. However our r-mode spindown result is very robust, and still interesting even if the minimum period is 7ms rather than the 17ms that we estimated for $T_c = 1 \times 10^9$K.

C. Gravitational waves from the r-modes

Chapter 6 of this thesis (written with Lee Lindblom, Curt Cutler, Bernard F. Schutz, Alberto Vecchio, and Nils Andersson) computes gravitational waveforms and wave strengths from young neutron stars spinning down due to the r-mode instability and discusses the detectability of the waves by ground-based interferometers. We conclude that the r-mode instability could be detectable by enhanced LIGO interferometers out to the Virgo cluster if suitable data analysis techniques can be devised. It could also be detected by advanced LIGO interferometers as a stochastic background made up of many weaker signals from neutron stars out to cosmological distances.

In chapter 6, we construct a simple phenomenological model for the evolution of a small initial r-mode perturbation under the influence of gravitational radiation and viscous damping, and examine the effect of the r-mode evolution on the total angular momentum of the star for various phenomenological parameters. We model the star as an r-mode with a certain amplitude, linearly superposed on a rigidly

rotating equilibrium configuration with some angular velocity (and simple polytropic equation of state). We evolve the r-mode amplitude and stellar angular velocity by imposing conservation of energy and angular momentum. Of course once the mode grows too large it can no longer be treated as a small perturbation on a rigidly rotating equilibrium. We expect, based on the example of Maclaurin spheroids, that nonlinear hydrodynamical effects cause the mode to saturate at some amplitude of order unity, which we include (along with the initial r-mode amplitude) as a phenomenological parameter. Nonlinear effects should also change the mode frequencies to some extent, but we have not modeled this.

We find that the gravitational waveforms from a neutron star in the Virgo cluster rise quickly (on a timescale of minutes) to a strain of about 10^{-24} independent of the size of the inital perturbation. Thereafter the waves decrease in amplitude and frequency for about a year until effects not included in our simple model (such as superfluidity) presumably damp the r-mode. This happens after it has dwindled to a gravitational-wave strain of less than 10^{-26} at a gravitational-wave frequency of about 120 Hz. The gravitational-wave signal is long-lived and highly monochromatic in two senses: (i) the "spindown age" $f\,dt/df$ is longer than the duration of the signal, and more importantly (ii) the signal is coherent and lasts long enough to be significantly affected by the Doppler shift due to the Earth's daily (and other) motions. Such signals are logical candidates for the data analysis techniques long used by radio astronomers to look for pulsars and analyzed in the context of gravitational waves by Brady *et al.* [14]. These pulsar search techniques center around the simple method of Fourier transforming long stretches of data (after some significant corrections) and looking for peaks.

There are several serious complications to such a Fourier transform search. To begin with, any integration time longer than a substantial fraction of a day must take into account the time-varying Doppler shift of the signal induced by the rotation

(and other motions) of the Earth. This Doppler shift depends on the position of the source on the sky. If the position is not known (an "all-sky search") the data must be corrected (barycentered) for a large number of points on the sky. This requires a great deal of computational power [14]. In addition, the Fourier transform must correct for the (unknown) spin-induced frequency evolution of the source itself in the frame of the solar system barycenter. Both types of frequency shifts must be compensated for in the data so that the power of the signal is not spread across several frequency bins in the Fourier transform (thereby degrading the signal-to-noise ratio).

If the position of the r-mode source is known, as it likely will be due to electromagnetic observations of the supernova, one still must search over the star's spindown parameters (a "directed spindown search"). This search may be daunting due to the rapidity of the spindown (spindown age about six times the actual age, which in turn is less than one year compared to 40 years or longer in all such gravitational-wave searches previously contemplated [14]). The low spindown age necessitates a large number of spindown parameter values, which in turn sets a limit on the coherent integration time possible as well as on the number of points in parameter space which can be tested (analogous to the matched filtering issues discussed in Section I). Unfortunately, even with a computing budget of teraflops it is impossible for a directed search to achieve more than a fairly small fraction—at most of order 10%—of the optimal signal-to-noise ratio [32]. This number is obtained by optimizing the search sensitivity for a fixed computational budget, varying the total integration time and varying the stacking strategy (in which one incoherently adds the power spectra of shorter Fourier transforms to gain integration time at the cost of lesser sensitivity). Some kind of hierarchical search (see Section I) is possible, but not expected to gain much. Since we calculate the optimal signal-to-noise ratio at the Virgo cluster to be about 7 for enhanced LIGO, it is necessary to develop data analysis techniques that can do better than those currently in the literature in order to detect this interesting

source of gravitational waves.

The r-mode instability is an interesting source of gravitational waves not only as well-defined, relatively strong signals, but as a stochastic background of weak contributions from objects out to cosmological distances. The data analysis involved in searching for stochastic backgrounds (typically believed to arise from fluctuations in the early universe) amounts to cross-correlating the "noise" between two interferometers and is computationally quite inexpensive [33]. The detectable gravitational-wave energy density is determined by the noise in the two interferometers and the separation between them. For the two 4-km advanced LIGO interferometers at Livingston and Hanford, the detectable signal at 95% confidence (5% false alarm probability) corresponds to a gravitational-wave energy density, in a bandwidth equal to frequency $f \sim 70$Hz, a few times 10^{-10} of that needed to close the universe ($\Omega_{\rm gw} \sim \text{few} \times 10^{-10}$). (Allen [33] used a slightly bad fit to the advanced LIGO noise spectrum thereby obtaining a different estimate of the detectable $\Omega_{\rm gw}$.) In Chapter 6 we find that the r-mode background energy density will be about 10^{-9} times closure in the band around 70Hz, making it detectable by advanced LIGO with 95% confidence. For enhanced LIGO interferometers there is as yet no careful estimate of the detectable $\Omega_{\rm gw}$, but we crudely estimate it to be about 15 times the advanced LIGO value, making the r-mode background undetectable by enhanced interferometers.

---

[1] B. Barish *et al.*, LIGO Advanced Research and Development Proposal, Caltech/MIT, 1996 (unpublished).

[2] A. Abramovici *et al.*, Science **256**, 325 (1992).

[3] K. S. Thorne, in *Black Holes and Relativistic Stars,* edited by R. M. Wald (University of Chicago Press, Chicago, in press; gr-qc/9706079); and references therein.

[4] E. S. Phinney, Astrophys. J. **380**, L17 (1991); R. Narayan, T. Piran, and A. Shemi, Astrophys. J. **379**, L17 (1991).

[5] C. W. Helstrom, *Statistical Theory of Signal Detection,* 2nd edition (Pergamon Press, Oxford, 1968).

[6] T. A. Apostolatos, Phys. Rev. D **52**, 605 (1995).

[7] S. Droz and E. Poisson, Phys. Rev. D **56**, 4449 (1997).

[8] L. Blanchet, T. Damour, and B. R. Iyer, Phys. Rev. D **51**, 5360 (1995).

[9] C. M. Will and A. G. Wiseman, Phys. Rev. D **54**, 4813 (1996).

[10] T. Damour, B. R. Iyer, and B. S. Sathyaprakash, Phys. Rev. D **57**, 885 (1998).

[11] L. Blanchet, T. Damour, B. R. Iyer, C. M. Will, and A. G. Wiseman, Phys. Rev. Lett. **74**, 3515 (1995).

[12] B. S. Sathyaprakash and S. V. Dhurandhar, Phys. Rev. D **44**, 3819 (1991); S. V. Dhurandhar and B. S. Sathyaprakash, Phys. Rev. D **49**, 1707 (1994); B. S. Sathyaprakash, Phys. Rev. D **50**, R7111 (1994).

[13] S. D. Mohanty and S. V. Dhurandhar, Phys. Rev. D **54**, 7108 (1996); S. D. Mohanty, Phys. Rev. D **57**, 630 (1998).

[14] P. R. Brady, T. Creighton, C. Cutler, and B. F. Schutz, Phys. Rev. D **57**, 2101 (1998).

[15] É. É. Flanagan and S. A. Hughes, Phys. Rev. D **57**, 4535 (1998).

[16] L. E. Kidder, C. M. Will, and A. G. Wiseman, Phys. Rev. D **47**, R4183 (1993).

[17] T. A. Apostolatos, C. Cutler, G. J. Sussman, and K. S. Thorne, Phys. Rev. D **49**, 6274 (1994).

[18] L. E. Kidder, Phys. Rev. D **52**, 821 (1995).

[19] Y. Mino, M. Sasaki, M. Shibata, H. Tagoshi, and T. Tanaka, Prog. Theor. Phys. Suppl. **128**, 1 (1997).

[20] Y. Mino, M. Shibata, and T. Tanaka, Phys. Rev. D **53**, 622 (1996).

[21] W. G. Dixon, in *Isolated Gravitating Systems in General Relativity,* edited by J. Ehlers (North-Holland, Amsterdam, 1979), p. 156; and references therein.

[22] S. Chandrasekhar, Phys. Rev. Lett. **24**, 611 (1970); J. L. Friedman and B. F. Schutz, Astrophys. J. **222**, 281 (1978).

[23] K. S. Thorne, in *300 Years of Gravitation,* edited by S. W. Hawking and W. Israel (Cambridge University Press, Cambridge, England, 1987), p. 330; and references therein.

[24] J. L. Friedman, Phys. Rev. Lett. **51**, 11 (1983).

[25] L. Lindblom, in *Relativistic Astrophysics,* edited by H. Riffert, H. Ruder, H.-P. Nollert, and F. W. Hehl (Vieweg Verlag, Wiesbaden, 1997), p. 155; and references therein.

[26] N. Andersson, to appear in Astrophys. J. (gr-qc/9706075).

[27] L. Lindblom and G. Mendell, Astrophys. J. **444**, 804 (1995).

[28] P. Goldreich and W. H. Julian, Astrophys. J. **157**, 869 (1969).

[29] O. Blaes, R. Blandford, P. Goldreich, and P. Madau, Astrophys. J. **343**, 839 (1989).

[30] S. L. Shapiro and S. Teukolsky, *Black Holes, White Dwarfs, and Neutron Stars: The Physics of Compact Objects* (Wiley, New York, 1983); and references therein.

[31] F. E. Marshall, E. V. Gotthelf, W. Zhang, J. Middleditch, and Q. D. Wang, submitted to Astrophys. J. Lett. (astro-ph/9803214).

[32] P. R. Brady and T. Creighton, in preparation.

[33] B. Allen, in *Relativistic Gravitation and Gravitational Radiation,* edited by J.-P. LaSota

and J.-A. Marck (Cambridge University Press, Cambridge, 1997), p. 373; and references therein.

Chapter 2 Gravitational waves from inspiraling compact binaries: Choice of template spacing

Appeared in Phys. Rev. D **53**, 6749 (1996)

Gravitational waves from inspiraling, compact binaries will be searched for in the output of the LIGO/VIRGO interferometric network by the method of "matched filtering"—i.e., by correlating the noisy output of each interferometer with a set of theoretical waveform templates. These search templates will be a discrete subset of a continuous, multiparameter family, each of which approximates a possible signal. The search might be performed *hierarchically*, with a first pass through the data using a low threshold and a coarsely-spaced, few-parameter template set, followed by a second pass on threshold-exceeding data segments, with a higher threshold and a more finely spaced template set that might have a larger number of parameters. Alternatively, the search might involve a single pass through the data using the larger threshold and finer template set. This paper extends and generalizes the Sathyaprakash-Dhurandhar (S-D) formalism for choosing the discrete, finely-spaced template set used in the final (or sole) pass through the data, based on the analysis of a single interferometer. The S-D formalism is rephrased in geometric language by introducing a metric on the continuous template space from which the discrete template set is drawn. This template metric is used to compute the loss of signal-to-noise ratio and reduction of event rate which result from the coarseness of the template grid. Correspondingly, the template spacing and total number $\mathcal{N}$ of templates are expressed, via the metric, as functions of the reduction in event rate. The theory is developed for a template family of arbitrary dimensionality (whereas the original S-D formalism was restricted to a single nontrivial dimension). The theory is then applied to a simple post^1-Newtonian template family with two nontrivial dimen-

sions. For this family, the number of templates $\mathcal{N}$ in the finely-spaced grid is related to the spacing-induced fractional loss $\mathcal{L}$ of event rate and to the minimum mass $M_{\rm min}$ of the least massive star in the binaries for which one searches by $\mathcal{N} \sim 2 \times 10^5 (0.1/\mathcal{L})(0.2\ M_\odot/M_{\rm min})^{2.7}$ for the first LIGO interferometers and by $\mathcal{N} \sim 8 \times 10^6 (0.1/\mathcal{L})(0.2\ M_\odot/M_{\rm min})^{2.7}$ for advanced LIGO interferometers. This is several orders of magnitude greater than one might have expected based on Sathyaprakash's discovery of a near degeneracy in the parameter space, the discrepancy being due to this paper's lower choice of $M_{\rm min}$ and more stringent choice of $\mathcal{L}$. The computational power $\mathcal{P}$ required to process the steady stream of incoming data from a single interferometer through the closely-spaced set of templates is given in floating-point operations per second by $\mathcal{P} \sim 3 \times 10^{10} (0.1/\mathcal{L})(0.2\ M_\odot/M_{\rm min})^{2.7}$ for the first LIGO interferometers and by $\mathcal{P} \sim 4 \times 10^{11} (0.1/\mathcal{L})(0.2\ M_\odot/M_{\rm min})^{2.7}$ for advanced LIGO interferometers. This will be within the capabilities of LIGO-era computers, but a hierarchical search may still be desirable to reduce the required computing power.

I. INTRODUCTION

Compact binary star systems are likely to be an important source of gravitational waves for the broadband laser interferometric detectors now under construction [1], as they are the best understood of the various types of postulated gravity wave sources in the detectable frequency band and their waves should carry a large amount of information. Within our own galaxy, there are three known neutron star binaries whose orbits will decay completely under the influence of gravitational radiation reaction within less than one Hubble time, and it is almost certain that there are many more as yet undiscovered. Current estimates of the rate of neutron star/neutron star

(NS/NS) binary coalescences [2,3] based on these (very few) known systems project an event rate of three per year within a distance of roughly 200 Mpc; and estimates based on the evolution of progenitor, main-sequence binaries [4] suggest a distance of as small as roughly 70 Mpc for three events per year. These distances correspond to a signal strength which is within the target sensitivities of the LIGO and VIRGO interferometers [5,6]. However, to find the signals within the noisy LIGO/VIRGO data will require a careful filtering of the interferometer outputs. Because the predicted signal strengths lie so close to the level of the noise, it will be necessary to filter the interferometer data streams in order to detect the inspiral events against the background of spurious events generated by random noise.

The gravitational waveform generated by an inspiraling compact binary has been calculated using a combination of post-Newtonian and post-Minkowskian expansions [7,8] to post^2-Newtonian order by the consortium of Blanchet, Damour, Iyer, Will, and Wiseman [9], and will be calculated to post^3-Newtonian order long before the LIGO and VIRGO interferometers come on-line (c. 2000). Because the functional form of the expected signal is so well-known, it is an ideal candidate for matched filtering, a venerable and widely known technique which is laid out in detail elsewhere [10] and briefly summarized here.

The matched filtering strategy is to compute a cross-correlation between the interferometer output and a template waveform, weighted inversely by the noise spectrum of the detector. The signal-to-noise ratio is defined as the value of the cross-correlation of the template with a particular stretch of data divided by the rms value of the cross-correlation of the template with pure detector noise. If the signal-to-noise ratio exceeds a certain threshold, which is set primarily to control the rate of false alarms due to fluctuations of the noise, a detection is registered. If the functional form of the template is identical to that of the signal, the mean signal-to-noise ratio in the presence of a signal is the highest possible for any linear data processing technique,

which is why matched filtering is also known as optimal filtering.

In practice, however, the template waveforms will differ somewhat from the signals. True gravitational-wave signals from inspiraling binaries will be exact solutions to the Einstein equations for two bodies of non-negligible mass, while the templates used to search for these signals will be, at best, finite-order approximations to the exact solutions. Also, true signals will be characterized by many parameters (e.g. the masses of the two objects, their spins, the eccentricity and orientation of the orbit...), some of which might be neglected in construction of the search templates. Thus, the true signals will lie somewhat outside the submanifold formed by the search templates in the full manifold of all possible detector outputs (see Fig. 2.1).

Apostolatos [11] has defined the "fitting factor" FF to quantitatively describe the closeness of the true signals to the template manifold in terms of the reduction of the signal-to-noise ratio due to cross-correlating a signal lying outside the manifold with all the templates lying inside the manifold. If the fitting factor of a template family is unity, the signal lies in the template manifold. If the fitting factor is less than unity, the signal lies outside the manifold, and the fitting factor represents the cross-correlation between the signal and the template nearest it in the template manifold.

Even if the signal were to lie within the template manifold, it would not in general correspond to any of the actual templates used to search the data. The parameters describing the search templates (masses, spins, etc.) can vary continuously throughout a finite range of values. The set of templates characterized by the continuously varying parameters is of course infinite, so the interferometer output must be cross-correlated with a finite subset of the templates whose parameter values vary in discrete steps from one template to the next. This subset (the "discrete template family") has measure zero on the manifold of the full set of possible templates (the "continuous template family"), so the template which most closely matches a signal will generally lie in between members of the discrete template family (again, see Fig. 2.1). The mis-

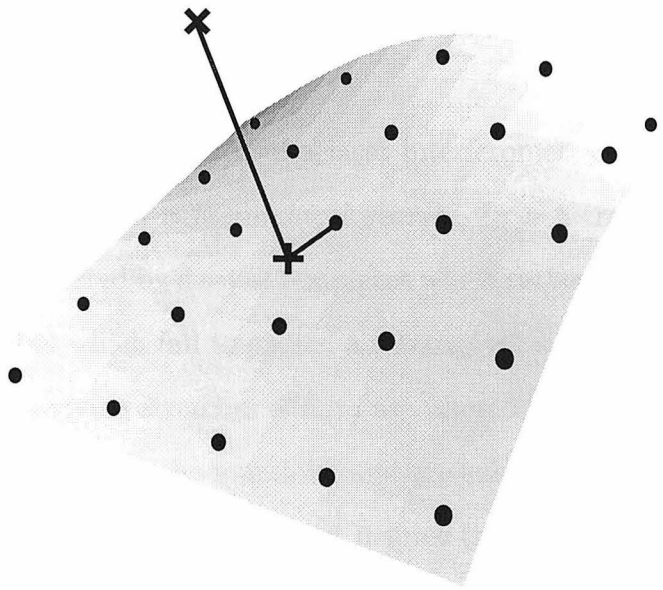

FIG. 2.1. A schematic depiction of the manifold formed by the continuous template family, here represented as a two-dimensional surface lying within a three-dimensional space. The discrete template family, shown by the dots, resides within this manifold. The $\times$ indicates the location of an actual signal, which because it is an exact solution to the Einstein equations does not lie within the manifold. The + marks the spot in the manifold which is closest to (has the highest inner product with) the signal. In general, this location falls in between the actual discrete templates.

match between the signal and the nearest of the discrete templates will cause some reduction in the signal-to-noise ratio and therefore in the observed event rate, as some signals which would lie above the threshold if cross-correlated with a perfectly matched filter are driven below the threshold by the mismatch. Thus the spacing between members of the discrete template family must be chosen so as to render acceptable the loss in event rate, without requiring a prohibitive amount of computing power to numerically perform the cross-correlations of the data stream with all of the discrete templates.

The high computational demands of a laser interferometric detector may in fact make it desirable to perform a *hierarchical search.* In a hierarchical search, each stretch of data is first filtered by a set of templates which rather sparsely populates the manifold, and stretches which fail to exceed a relatively low signal-to-noise threshold are discarded. The surviving stretches of data are filtered by a larger set of templates which more densely populates the manifold, and are subjected to a higher threshold. The sparseness of the first-pass template set insures that most of the data need only be filtered by a small number of templates, while the high threshold of the final pass reduces the false alarm rate to an acceptable level.

Theoretical foundations for choosing the discrete set of templates from the continuous family were laid by Sathyaprakash and Dhurandhar for the case of white noise in Ref. [12], and for (colored) power-recycling interferometer noise in Ref. [13]. Both papers used a simplified (so-called "Newtonian") version of the waveform which can be characterized by a single parameter, the binary's "chirp mass" $\mathcal{M}$. Recently, Sathyaprakash [14] began consideration of an improved, "post-Newtonian" set of templates characterized by two mass parameters. He found that, by a judicious choice of the two parameters, the spacing between templates can be made constant in both dimensions of the intrinsic parameter space. Sathyaprakash's parameters also make it obvious (by producing a very large spacing in one of the dimensions) that a two-

parameter set of templates can be constructed which, if it does not populate the manifold too densely, need not be much more numerous than the one-parameter set of templates used in Refs. [12,13].

In this paper I shall recast the S-D formalism in geometric language which, I believe, simplifies and clarifies the key ideas. I shall also generalize the S-D formalism to an arbitrary spectrum of detector noise and to a set of template shapes characterized by more than one parameter. This is necessary because, as Apostolatos [11] has shown, no one-parameter set of templates can be used to filter a post-Newtonian signal without causing an unacceptably large loss of signal-to-noise ratio.

In one respect, my analysis will be more specialized than that of the S-D formalism. My geometric analysis requires that the templates of the discrete set be spaced very finely in order that certain analytical approximations may be made, while the numerical methods of Sathyaprakash and Dhurandhar are valid even for a large spacing between templates (as would be the case in the early stages of a hierarchical search). The small spacing approximation is justified on the grounds that at some point, even in a hierarchical search, the data must be filtered by many closely spaced templates in order to detect a reasonable fraction (of order unity) of the binary inspirals occurring in the universe within range of the LIGO/VIRGO network.

The rest of this paper is organized as follows: In Sec. II, I develop my generalized, geometric variant of the S-D formalism. I then apply this formalism to the general problem of detection of gravitational waves from inspiraling binaries, and develop general formulas for choosing a discrete template family from a given continuous template family. In Sec. III, I detail an example of the use of my formalism, choosing discrete templates from a continuous template family which describes nonspinning, circularized binaries to post^1-Newtonian order in the evolution of the waveform's phase. I also estimate the computing power required for a single-pass (non-hierarchical) search using this discrete template family, and compare to the pre-

vious work of Sathyaprakash [14]. Finally, in Sec. IV, I summarize my results and suggest future directions for research on the choice of discrete search templates.

II. THEORY OF MISMATCHED FILTERING

In this section, a geometric, multiparameter variant of the S-D formalism is developed. Unless otherwise stated, the following conventions and definitions are assumed:

Following Cutler and Flanagan [15], we define the inner product between two functions of time $a(t)$ and $b(t)$ (which may be templates or interferometer output) as

$$\begin{aligned}\langle a|b\rangle &\equiv 2\int_0^\infty df \frac{\tilde{a}^*(f)\tilde{b}(f)+\tilde{a}(f)\tilde{b}^*(f)}{S_h(f)} \\ &= 4\Re\left[\int_0^\infty df \frac{\tilde{a}^*(f)\tilde{b}(f)}{S_h(f)}\right].\end{aligned} \tag{2.2.1}$$

Here $\tilde{a}(f)$ is the Fourier transform of $a(t)$,

$$\tilde{a}(f) \equiv \int_{-\infty}^{\infty} dt\ e^{i2\pi ft} a(t), \tag{2.2.2}$$

and $S_h(f)$ is the detector's noise spectrum, defined below.

The interferometer output $o(t)$ consists of noise $n(t)$ plus a signal $\mathcal{A}s(t)$, where $\mathcal{A}$ is a dimensionless, time-independent amplitude and $s(t)$ is normalized such that $\langle s|s\rangle = 1$. Thus, $\mathcal{A}$ describes the strength of a signal and $s(t)$ describes its shape.

Waveform templates are denoted by $u(t;\boldsymbol{\mu},\boldsymbol{\lambda})$, where $\boldsymbol{\lambda}$ is the vector of "intrinsic" or "dynamical" parameters characterizing the template shape and $\boldsymbol{\mu}$ is the vector of "extrinsic" or "kinematical" parameters describing the offsets of the waveform's endpoint. Examples of intrinsic parameters λ^i are the masses and spins of the two objects in a compact binary; examples of extrinsic parameters μ^i are the time of a compact binary's final coalescence t_0 and the phase of the waveform at coalescence Φ_0.

Templates are assumed to be normalized such that $\langle u(\boldsymbol{\mu},\boldsymbol{\lambda})|u(\boldsymbol{\mu},\boldsymbol{\lambda})\rangle = 1$ for all $\boldsymbol{\mu}$ and $\boldsymbol{\lambda}$.

Expectation values of various quantities over an infinite ensemble of realizations of the noise are denoted by E[ ].

The interferometer's strain spectral noise density $S_h(f)$ is the one-sided spectral density, defined by

$$\mathrm{E}[\tilde{n}(f_1)\tilde{n}^*(f_2)] = \frac{1}{2}\delta(f_1 - f_2)S_h(f_1) \tag{2.2.3}$$

for positive frequencies and undefined for negative frequencies. The noise is assumed to have a Gaussian probability distribution.

Newton's gravitational constant G and the speed of light c are set equal to one.

A. Formalism

In developing our formalism, we begin by defining the signal-to-noise ratio. For any single template $u(t)$ of unit norm, the cross-correlation with pure noise $\langle n|u\rangle$ is a random variable with mean zero and variance unity (cf. Sec. II.B. of Ref. [15], wherein it is shown that $\mathrm{E}[\langle n|a\rangle\langle n|b\rangle] = \langle a|b\rangle$). The signal-to-noise ratio of a given stretch of data $o(t)$, after filtering by $u(t)$, is defined to be

$$\rho \equiv \frac{\langle o|u\rangle}{\text{rms } \langle n|u\rangle} = \langle o|u\rangle. \tag{2.2.4}$$

This ratio is the statistic which is compared to a predetermined threshold to decide if a signal is present.

If the template u is the same as the signal s, it optimally filters the signal, and the corresponding (mean) optimal signal-to-noise ratio is

$$\mathrm{E}[\rho] = \mathrm{E}[\langle n + \mathcal{A}u|u\rangle] = \mathcal{A}. \tag{2.2.5}$$

If the template u used to filter the data is not exactly the same as the signal s, the mean signal-to-noise ratio is decreased somewhat from its optimal value:

$$\mathrm{E}[\rho] = \mathrm{E}[\langle n + \mathcal{A}s|u\rangle] = \mathcal{A}\langle s|u\rangle. \tag{2.2.6}$$

The inner product $\langle s|u\rangle$, which is bounded between zero and one, is the fraction of the optimal $\mathrm{E}[\rho]$ retained in the mismatched filtering case, and as such is a logical measure of the effectiveness of the template u in searching for the signal shape s.

Now suppose that we search for the signal with a family of templates specified by an extrinsic parameter vector $\boldsymbol{\mu}$ and an intrinsic parameter vector $\boldsymbol{\lambda}$. Let us denote the values of the parameters of the actual templates by $(\boldsymbol{\mu}_{(k)}, \boldsymbol{\lambda}_{(k)})$. For example, $\mu^1_{(k)}$ might be the value of the time t_0 of coalescence for the kth template in the family, and $\mu^2_{(k)}$ might be the phase of the kth template waveform at coalescence.

The search entails computing, via fast Fourier transforms (FFT's), all the inner products $\langle o|u(\boldsymbol{\mu}_{(k)}, \boldsymbol{\lambda}_{(k)})\rangle$ for $k = 1, 2, \ldots$ In these numerical computations, the key distinction between the extrinsic parameters $\boldsymbol{\mu}$ and the intrinsic parameters $\boldsymbol{\lambda}$ is this: One explores the whole range of values of $\boldsymbol{\mu}$ very quickly, automatically, and efficiently for a fixed value of $\boldsymbol{\lambda}$; but one must do these explorations separately for each of the $\boldsymbol{\lambda}_{(k)}$. In this sense, dealing with the extrinsic parameters is far easier and more automatic than dealing with the intrinsic ones [16].

As an example (for further detail see Sec. 16.2.2 of Schutz [17]), for a given stretch of data one explores *all* values of the time of coalescence ($t_0 \equiv \mu^1$) of a compact binary simultaneously (for fixed values of the other template parameters) via a single FFT. If we write the Fourier transform (for notational simplicity) as a continuous integral rather than a discrete sum, we get

$$\langle o|u(\boldsymbol{\mu}_{(k)}, \boldsymbol{\lambda}_{(k)})\rangle \quad = \int_0^\infty df \; \frac{e^{i2\pi f t_0}}{S_h(f)} \tilde{o}^*(f)\tilde{u}(f; \text{other } \boldsymbol{\mu}_{(k)}, \boldsymbol{\lambda}_{(k)}). \tag{2.2.7}$$

The discrete FFT yields the discrete analog of the function of t_0 as shown above, an array of numbers containing the values of the Fourier transform for all values of t_0.

Because, for fixed $\boldsymbol{\lambda}_{(k)}$, the extrinsic parameters $\boldsymbol{\mu}$ are dealt with so simply and quickly in the search, throughout this paper we shall focus primarily on a template family's intrinsic parameters $\boldsymbol{\lambda}$, which govern the shape of the template. Correspondingly, we shall adopt the following quantity as our measure of the effectiveness

with which a particular template shape—i.e. a particular vector $\boldsymbol{\lambda}_{(k)}$ of the intrinsic parameters—matches the incoming signal:

$$\max_{\mu} \langle s|u(\boldsymbol{\mu}, \boldsymbol{\lambda}_{(k)})\rangle. \tag{2.2.8}$$

Here the maximization is over all continuously varying values of the extrinsic parameters. Then the logical measure of the effectiveness of the entire discrete family of templates in searching for the signal shape is

$$\max_{k} [\max_{\mu} \langle s|u(\boldsymbol{\mu}, \boldsymbol{\lambda}_{(k)})\rangle], \tag{2.2.9}$$

which is simply (2.2.8) maximized over all the discrete template shapes.

In order to focus on the issue of discretization of the template parameters rather than on the inadequacy of the continuous template family, let us assume that the signal shape s is identical to some template. The discussion of the preceding paragraphs suggests that in discussing the discretization of the template parameters we will want to make use of the *match* between two templates $\tilde{u}(f; \boldsymbol{\mu}, \boldsymbol{\lambda})$ and $\tilde{u}(f; \boldsymbol{\mu}+\Delta\boldsymbol{\mu}, \boldsymbol{\lambda}+\Delta\boldsymbol{\lambda})$ which we will define as

$$M(\boldsymbol{\lambda}, \Delta\boldsymbol{\lambda}) \equiv \max_{\mu, \Delta\mu} \langle u(\boldsymbol{\mu}, \boldsymbol{\lambda})|u(\boldsymbol{\mu} + \Delta\boldsymbol{\mu}, \boldsymbol{\lambda} + \Delta\boldsymbol{\lambda})\rangle. \tag{2.2.10}$$

This quantity, which is known in the theory of hypothesis testing as the *ambiguity function,* is the fraction of the optimal signal-to-noise ratio obtained by using a template with intrinsic parameters $\boldsymbol{\lambda}$ to filter a signal identical in shape to a template with intrinsic parameters $\boldsymbol{\lambda} + \Delta\boldsymbol{\lambda}$.

Using the match (2.2.10) it is possible to quantify our intuitive notion of how "close" two template shapes are to each other. Since the match clearly has a maximum value of unity at $\Delta\boldsymbol{\lambda} = 0$, we can expand in a power series about $\Delta\boldsymbol{\lambda} = 0$ to obtain

$$M(\boldsymbol{\lambda}, \Delta\boldsymbol{\lambda}) \approx 1 + \frac{1}{2}\left(\frac{\partial^2 M}{\partial\Delta\lambda^i \partial\Delta\lambda^j}\right)_{\Delta\lambda^k=0} \Delta\lambda^i \Delta\lambda^j. \tag{2.2.11}$$

This suggests the definition of a metric

$$g_{ij}(\boldsymbol{\lambda}) = -\frac{1}{2}\left(\frac{\partial^2 M}{\partial\Delta\lambda^i\partial\Delta\lambda^j}\right)_{\Delta\lambda^k=0} \tag{2.2.12}$$

so that the *mismatch* $1 - M$ between two nearby templates is equal to the square of the proper distance between them:

$$1 - M = g_{ij}\Delta\lambda^i\Delta\lambda^j. \tag{2.2.13}$$

Having defined a metric on the intrinsic parameter space, we can now use it to calculate the spacing of the discrete template family required to retain a given fraction of the ideal event rate. Schematically, we can think of the templates as forming a lattice in the N-dimensional intrinsic parameter space whose unit cell is an N-dimensional hypercube with sides of proper length dl. The worst possible case (lowest E[ρ]) occurs if the point $\tilde{\boldsymbol{\lambda}}$ describing the signal is exactly in the middle of one of the hypercubes. If the templates are closely spaced, i.e. $dl \ll 1$, such a signal has a squared proper distance

$$g_{ij}\Delta\lambda^i\Delta\lambda^j = N(dl/2)^2 \tag{2.2.14}$$

from the templates at the corners of the hypercube.

We define the *minimal match* MM to be the match between the signal and the nearest templates in this worst possible case, i.e. the fraction of the optimal signal-to-noise ratio retained by a discrete template family when the signal falls exactly "in between" the nearest templates. This minimal match is the same quantity that Dhurandhar and Sathyaprakash in Ref. [13] denote as κ^{-1}; but since it is the central quantity governing template spacing it deserves some recognition in the form of its own name. Our choice of name closely parallels the term "fitting factor" FF, which Apostolatos introduced in Ref. [11] to measure the similarity between actual signals and a continuous template family.

The minimal match, which is chosen by the experimenter based upon what he or she considers to be an acceptable loss of ideal event rate, will determine our choice

of spacing of the discrete template parameters and therefore the number of discrete templates in the family. More specifically, the experimenter will choose some desired value of the minimal match MM; and then will achieve this MM by selecting the templates to reside at the corners of hypercubes with edge dl given by

$$MM = 1 - N(dl/2)^2. \tag{2.2.15}$$

The number of templates in the resulting discrete template family will be the proper volume of parameter space divided by the proper volume per template dl^N, i.e.

$$\mathcal{N} = \frac{\int d^N\boldsymbol{\lambda}\sqrt{\det \|g_{ij}\|}}{\left(2\sqrt{(1-MM)/N}\right)^N}. \tag{2.2.16}$$

B. Inspiraling Binaries Detected by LIGO

The formalism above applies to the detection of any set of signals which have a functional form that depends on a set of parameters which varies continuously over some range. We now develop a more explicit formula for the metric, given an analytical approximation to the LIGO noise curve and a particular class of inspiraling binary signals.

We approximate the "initial" and "advanced" benchmark LIGO noise curves by the following analytical fit to Fig. 7 of Ref. [5]:

$$S_h(f) = \begin{cases} \frac{1}{5}S_0\{(f/f_0)^{-4} + 2[1 + (f/f_0)^2]\}, & f > f_s \\ \infty, & f < f_s, \end{cases} \tag{2.2.17}$$

where f_0 is the "knee frequency" or frequency at which the interferometer is most sensitive (which is determined by the reflectivities of the mirrors and is set by the experimenters to the frequency where photon shot noise begins to dominate the spectrum) and S_0 is a constant whose value is not important for our purposes. This spectrum describes photon shot noise in the "standard recycling" configuration of

the interferometer (second term) superposed on thermal noise in the suspension of the test masses (first term), and it approximates seismic noise by setting S_h infinite at frequencies below the "seismic-cutoff frequency" f_s.

Throughout the rest of this paper, the "first LIGO noise curve" will refer to (2.2.17) with $f_s = 40$ Hz and $f_0 = 200$ Hz, and the "advanced LIGO noise curve" will refer to (2.2.17) with $f_s = 10$ Hz and $f_0 = 70$ Hz. These numbers are chosen to closely fit Fig. 7 of Ref. [5] for the first LIGO interferometers and for the advanced LIGO benchmark. In this paper, when various quantities (such as the number of discrete templates) are given including a scaling with f_0, this indicates how the quantity changes while f_0 is varied but f_s/f_0 is held fixed.

At this point it is useful to define the moments of the noise curve (2.2.17), following Poisson and Will [18], as

$$I(q) \equiv S_h(f_0) \int_{f_s/f_0}^{f_c/f_0} dx \frac{x^{-q/3}}{S_h(x\ f_0)}$$
$$= \int_{f_s/f_0}^{f_c/f_0} dx \frac{5x^{-q/3}}{x^{-4} + 2(1+x^2)}, \tag{2.2.18a}$$
$$J(q) \equiv I(q)/I(7). \tag{2.2.18b}$$

The upper limit of integration f_c denotes the coalescence frequency or high-frequency cutoff of whatever template we are dealing with, which very roughly corresponds to the last stable circular orbit of a test particle in a non-spinning black hole's Schwarzschild geometry.

For both first and advanced LIGO noise curves, the majority of inspiraling binary search templates will occupy regions of parameter space for which f_c is many times f_0. Because we will always be dealing with $I(q)$ for $q > 0$, and because the noise term in the denominator of the integrand in Eq. (II B) rises as f^2 for $f \gg f_0$, we can simplify later calculations by approximating $f_c = \infty$ in the definition of the moments.

To illustrate the metric formalism, we shall use templates based on a somewhat simplified version of the post-Newtonian expansion. Since the inner product (2.2.1)

has negligible contributions from frequencies at which the integrand oscillates rapidly, it is far more important to get the phase of $\tilde{u}(f)$ right than it is to get the amplitude dependence. Therefore, we adopt templates based on the "restricted" post-Newtonian approximation in which one discards all multipolar components except the quadrupole, but keeps fairly accurate track of the quadrupole component's phase (for more details see Secs. II.C. and III.A. of Ref. [15]). Applying the stationary phase approximation to that quadrupolar waveform, we obtain

$$\tilde{u}(f;\boldsymbol{\lambda},\boldsymbol{\mu}) = f^{-7/6}\exp\ i\left[-\frac{\pi}{4} - \Phi_0 + 2\pi f t_0 + \Psi(f;\boldsymbol{\lambda})\right], \tag{2.2.19}$$

up to a multiplicative constant which is set by the condition $\langle u|u\rangle = 1$ [19].

The function Ψ, describing the phase evolution in (2.2.19), is currently known to post^2-Newtonian order for the case of two nonspinning point masses in a circular orbit about each other as

$$\begin{aligned}\Psi(f;M,\eta) = \frac{3}{128}\eta^{-1}(\pi Mf)^{-5/3}\Big[1 + \frac{20}{9}\Big(\frac{743}{336} + \frac{11}{4}\eta\Big)(\pi Mf)^{2/3} - 16\pi(\pi Mf) \\ +10\Big(\frac{3058673}{1016064} + \frac{5429}{1008}\eta + \frac{617}{144}\eta^2\Big)(\pi Mf)^{4/3}\Big]\end{aligned} \tag{2.2.20}$$

(cf. Eq. (3.6) of Ref. [18]). Here the mass parameters have been chosen to be M, the total mass of the system, and η, the ratio of the reduced mass to the total mass.

The actual amplitude $\mathcal{A}$ of a waveform is proportional to $1/R$, where R is the distance to the source; and this lets us find the relation between minimal match and event rate which we will need in order to wisely choose the minimal match. Assuming that compact binaries are uniformly distributed throughout space on large distance scales, this means that the rate of events with a given set of intrinsic parameters and with an amplitude greater than $\mathcal{A}$ is proportional to $1/\mathcal{A}^3$. Setting a signal-to-noise threshold ρ_0 is equivalent to setting a maximum distance $R_0 \propto 1/\mathcal{A}$ to which sources with a given set of intrinsic parameters can be detected. Thus, if we could search for signals with the entire continuous template family, we would expect the observed

event rate to scale as $1/\rho_0^3$. This ideal event rate is an upper limit on what we can expect with a real, discrete template family.

We can obtain a lower bound on the observed event rate by considering what happens if all signals conspire to have parameters lying exactly in between the nearest search templates. In this case, all events will have reduced signal-to-noise ratios of MM times the optimal signal-to-noise ratio $\mathcal{A}$. This is naively equivalent to optimally filtering with a threshold of ρ_0/MM, so a pessimistic guess is

$$\text{event rate} \propto \left(\frac{MM}{\rho_0}\right)^3 \tag{2.2.21}$$

for a fixed rate of false alarms. Note that the fraction of false dismissals *due to template spacing* scales as $1 - MM^3$, independently of the threshold ρ_0 (assuming $\rho_0 \gg 1$). This is because the scaling of absolute event rate with $\mathcal{A}$ is independent of $\mathcal{A}$, as discussed in the previous paragraph.

In real life, ρ_0 is affected by the total number of discrete templates and by the minimal match of the discrete template family. This can be seen by the fact that the signal-to-noise ratio,

$$\rho \equiv \max_k [\max_\mu \langle o|u(\boldsymbol{\mu}, \boldsymbol{\lambda}_{(k)})\rangle], \tag{2.2.22}$$

is the maximum of a number of random variables. The covariance matrix of these variables will be determined by the minimal match, and will itself determine the probability distribution of ρ (in the absence of a signal) which is used to set the threshold ρ_0 in order to keep the false alarm rate below a certain level. However, since these effects are fairly small at high signal-to-noise ratios (such as those to be used by LIGO) and the issue of choosing thresholds is a problem worthy of its own paper [20], we will use (2.2.21) for the rest of this paper.

For this two-parameter template family, the formula for the match (2.2.10) can be simplified somewhat by explicitly performing the maximization over the extrinsic parameters $\boldsymbol{\mu}$ and $\Delta\boldsymbol{\mu}$. Since the integrand in the inner product (2.2.1) depends on

$\boldsymbol{\mu}$ and $\Delta\boldsymbol{\mu}$ as exp $i[2\pi f\Delta t_0 - \Delta\Phi_0]$, there is no dependence on $\boldsymbol{\mu}$ but only on $\Delta\boldsymbol{\mu}$. Maximizing over $\Delta\Phi_0$ is easy: instead of taking the real part of the integral in the inner product (2.2.1), we take the absolute value.

To maximize over Δt_0 we go back a step. Let us define $\lambda^0 \equiv t_0$, and consider the $(N+1)$-dimensional space formed by λ^0 and λ^j. We expand the inner product between adjacent templates to quadratic order in $\Delta\lambda^\alpha$ to get a preliminary metric $\gamma_{\alpha\beta}$, where the Greek indices range from 0 to N (Latin indices range from 1 to N):

$$\gamma_{\alpha\beta}(\boldsymbol{\lambda}) = -\frac{1}{2}\left[\frac{\partial^2}{\partial\Delta\lambda^\alpha\partial\Delta\lambda^\beta}\left\{\frac{\left|\int_0^\infty df\,\frac{f^{-7/3}}{S_h(f)}\exp\ i[2\pi f\Delta t_0 + \Delta\Psi(f;\lambda^j,\Delta\lambda^j)]\right|}{\int_0^\infty df\,\frac{f^{-7/3}}{S_h(f)}}\right\}\right], \tag{2.2.23}$$

evaluated at $\Delta\lambda^\alpha = 0$. Here $\Delta\Psi \equiv \Psi(f;\lambda^j + \Delta\lambda^j) - \Psi(f;\lambda^j)$ [21].

We define the moment functional $\mathcal{J}$ such that, for a function a,

$$\mathcal{J}[a] = \frac{1}{I(7)}\int_{f_s/f_0}^{f_c/f_0} dx\frac{x^{-7/3}}{S_h(x\ f_0)}a(x), \tag{2.2.24}$$

and thus

$$\mathcal{J}\left[\sum_n a_n x^n\right] = \sum_n a_n J(7-3n). \tag{2.2.25}$$

We also define the quantities ψ_α such that

$$\psi_0 \equiv 2\pi f, \quad \psi_j \equiv \frac{\partial\Delta\hat{\Psi}}{\partial\Delta\lambda^j}, \tag{2.2.26}$$

where the derivative is evaluated at $\Delta\lambda^j = 0$ and $\hat{\Psi}$ is the part of Ψ in Eq. (2.2.19) that is frequency dependent (any non-frequency-dependent, additive parts of Ψ are removed when we take the absolute value in the maximized inner product). Evaluation of the derivative in Eq. (2.2.23) then shows that, in the limit $f_c/f_0 \to \infty$,

$$\gamma_{\alpha\beta} = \frac{1}{2}\left(\mathcal{J}[\psi_\alpha\psi_\beta] - \mathcal{J}[\psi_\alpha]\mathcal{J}[\psi_\beta]\right). \tag{2.2.27}$$

Finally, we minimize $\gamma_{\alpha\beta}\Delta\lambda^\alpha\Delta\lambda^\beta$ with respect to Δt_0 (i.e., we project $\gamma_{\alpha\beta}$ onto the subspace orthogonal to t_0) and thereby obtain the following expression for the metric of our continuous template family:

$$g_{ij} = \gamma_{ij} - \frac{\gamma_{0i}\gamma_{0j}}{\gamma_{00}}. \tag{2.2.28}$$

By taking the square root of the determinant of this metric and plugging it into Eq. (2.2.16), we can compute the number of templates $\mathcal{N}$ that we need in our discrete family as a function of our desired minimal match MM, or equivalently of the loss of ideal event rate.

III. EXAMPLE: CIRCULARIZED NONSPINNING BINARIES TO POST^1-NEWTONIAN ORDER

Although the phase of the inspiraling binary signal has recently been calculated to post^2-Newtonian order [9], it is useful to calculate the number of templates that would be required in a universe where the waveforms evolve only to post^1-Newtonian order and all binaries are composed of nonspinning objects in circular orbits. There are several reasons for this exercise.

1. Spin effects are expected to be significant only for a small fraction of sources. Blanchet et al. [9] estimate very small spin-orbit and spin-spin phase modulation terms for typical neutron star binaries based on models of evolution for currently known binary pulsars. Apostolatos [11] has shown that templates with no spin-related terms perform quite well when searching for "signals" with spin-induced phase modulation but no amplitude modulation, corresponding approximately to a favorable orientation of the spin axes. He has also shown that amplitude modulation due to spin-orbit precession can indeed be a significant effect, but only for large spins and certain unfavorable orientations of the axes. Therefore

consideration of a spinless family of templates is quite sufficient for a rough estimate of the computing power required to perform a search that will overlook a small fraction of binary inspiral events due to mismatched filtering.

2. We assume circular orbits because gravitational radiation reaction circularizes most eccentric orbits on a timescale much less than the lifetime of a compact binary [22].

3. The phase of the templates is truncated at post^1-Newtonian order for simplicity. Although Apostolatos has demonstrated in Ref. [11] that post^1-Newtonian templates will not have a large enough fitting factor to be useful, consideration of such a set is a first step toward obtaining an adequate set of templates—and it is a particularly important step since the metric coefficients will turn out to be constant over the template manifold.

A. Calculation of the 2-Dimensional Metric

Having chosen as the continuous template family the set of post^1-Newtonian, circular, spinless binary waveforms, we must now choose the discrete templates from within this continuous family. The first step is to calculate the coefficients of the metric on the two-dimensional dynamical parameter space.

It is convenient to change the mass parameterization from the variables (M, η) to the Sathyaprakash variables [14]

$$\tau_1 = \frac{5}{256}\eta^{-1}M^{-5/3}(\pi f_0)^{-8/3}, \tag{2.3.1}$$

$$\tau_2 = \frac{5}{192}(\eta M)^{-1}\left(\frac{743}{336}+\frac{11}{4}\eta\right)(\pi f_0)^{-2}. \tag{2.3.2}$$

Note that τ_1 and τ_2 are simply the Newtonian and post^1-Newtonian contributions to the time it takes for the carrier gravitational wave frequency to evolve from f_0 to infinity. The advantage of these variables is that the metric coefficients in (τ_1, τ_2)

coordinates are constant (in the limit $f_c \gg f_0$) for all templates. This is because the phase of the waveform $\tilde{u}(f)$ is linear in the Sathyaprakash variables, and so the integral in the definition of the match (2.2.10) depends only on the displacement $(\Delta\tau_1, \Delta\tau_2)$ between the templates, not on the location (τ_1, τ_2) of the templates in the dynamical parameter space.

The dynamical parameter-dependent part of the templates' phase is given by [Eq. (2.2.20) truncated to first post-Newtonian order and reexpressed in terms of (τ_1, τ_2) using Eqs. (2.3.1) and (2.3.2)]

$$\Psi(f; \tau_1, \tau_2) = \frac{6}{5}\pi f_0 (f/f_0)^{-5/3}\tau_1 + 2\pi f_0 (f/f_0)^{-1}\tau_2, \tag{2.3.3}$$

and it is easy to read off ψ_1 and ψ_2 [Eq. (2.2.26)] as the coefficients of τ_1 and τ_2 [23]. By inserting these ψ_j into Eq. (2.2.25), the relevant moment functionals can be expressed in terms of the moments of the noise:

$$\begin{aligned}
\mathcal{J}[\psi_0] &= 2\pi f_0 \; J(4), \\
\mathcal{J}[\psi_1] &= 2\pi f_0 \; \tfrac{3}{5} J(12), \\
\mathcal{J}[\psi_2] &= 2\pi f_0 \; J(10), \\
\mathcal{J}[\psi_0^2] &= (2\pi f_0)^2 \; J(1), \\
\mathcal{J}[\psi_0\psi_1] &= (2\pi f_0)^2 \; \tfrac{3}{5} J(9), \\
\mathcal{J}[\psi_0\psi_2] &= (2\pi f_0)^2 \; J(7), \\
\mathcal{J}[\psi_1^2] &= (2\pi f_0)^2 \; \tfrac{9}{25} J(17), \\
\mathcal{J}[\psi_1\psi_2] &= (2\pi f_0)^2 \; \tfrac{3}{5} J(15), \\
\mathcal{J}[\psi_2^2] &= (2\pi f_0)^2 \; J(13).
\end{aligned} \tag{2.3.4}$$

We can compute the needed moments of the noise by numerically evaluating the integrals (II B). By setting the upper limit of integration to infinity, i.e. by approximating f_c/f_0 as infinite for all templates under consideration, we find that the moments have the constant values given in Table 2.1; and therefore the moment functionals (2.3.4) have the constant values given in Table 2.2. Inserting these values into

TABLE 2.1. Numerical values of the moments of the noise in the limit $f_c/f_0 \to \infty$, for the noise curves of the first LIGO interferometers ($f_s/f_0 = 1/5$) and advanced LIGO interferometers ($f_s/f_0 = 1/7$).

Noise moment	First LIGO value	Advanced LIGO value
J(1)	1.27	1.26
J(4)	0.927	0.919
J(7)	1 (exact)	1 (exact)
J(9)	1.24	1.26
J(10)	1.44	1.49
J(12)	2.13	2.31
J(13)	2.69	3.03
J(15)	4.67	5.80
J(17)	8.88	12.7

Eqs. (2.2.27) and (2.2.28) yields, for the coordinates ($\lambda^0 = t_0$, $\lambda^1 = \tau_1$, $\lambda^2 = \tau_2$), the 3-metric and 2-metric

$$\gamma_{\alpha\beta} = (2\pi f_0)^2 \begin{pmatrix} +0.208 & -0.220 & -0.168 \\ . & +0.784 & +0.481 \\ . & . & +0.309 \end{pmatrix} \text{ and} \tag{2.3.5}$$

$$g_{ij} = (2\pi f_0)^2 \begin{pmatrix} 0.552 & 0.304 \\ . & 0.173 \end{pmatrix} \tag{2.3.6}$$

for the first LIGO noise curve, and

$$\gamma_{\alpha\beta} = (2\pi f_0)^2 \begin{pmatrix} +0.209 & -0.257 & -0.183 \\ . & +1.320 & +0.712 \\ . & . & +0.407 \end{pmatrix} \text{ and} \tag{2.3.7}$$

TABLE 2.2. Numerical values of the moment functionals, under the same assumptions as in Table 2.1.

Moment functional	First LIGO value	Advanced LIGO value
$\mathcal{J}[\psi_0]$	$(2\pi f_0)0.927$	$(2\pi f_0)0.919$
$\mathcal{J}[\psi_1]$	$(2\pi f_0)1.28$	$(2\pi f_0)1.38$
$\mathcal{J}[\psi_2]$	$(2\pi f_0)1.44$	$(2\pi f_0)1.49$
$\mathcal{J}[\psi_0^2]$	$(2\pi f_0)^2 1.27$	$(2\pi f_0)^2 1.26$
$\mathcal{J}[\psi_0\psi_1]$	$(2\pi f_0)^2 0.743$	$(2\pi f_0)^2 0.756$
$\mathcal{J}[\psi_0\psi_2]$	$(2\pi f_0)^2$ (exact)	$(2\pi f_0)^2$ (exact)
$\mathcal{J}[\psi_1^2]$	$(2\pi f_0)^2 3.20$	$(2\pi f_0)^2 4.56$
$\mathcal{J}[\psi_1\psi_2]$	$(2\pi f_0)^2 2.80$	$(2\pi f_0)^2 3.48$
$\mathcal{J}[\psi_2^2]$	$(2\pi f_0)^2 2.69$	$(2\pi f_0)^2 3.03$

$$g_{ij} = (2\pi f_0)^2 \begin{pmatrix} 1.01 & 0.486 \\ . & 0.246 \end{pmatrix} \tag{2.3.8}$$

for the advanced LIGO noise curve (where the dots denote terms obtained by symmetry).

We shall also estimate the errors in the metric coefficients due to the approximation $f_c/f_0 \to \infty$: The moment integrals defined in Eq. (II B) can be rewritten as

$$\int_{f_s/f_0}^{\infty} dx \frac{5x^{-q/3}}{x^{-4} + 2(1+x^2)} - \int_{f_c/f_0}^{\infty} dx \frac{5x^{-q/3}}{x^{-4} + 2(1+x^2)},$$

where the first integral is the expression used in the above metric coefficients and the second is the correction due to finite f_c/f_0. The second integral can be expanded to lowest order in f_0/f_c as

$$\frac{5}{2(1+q/3)}(f_0/f_c)^{1+q/3},$$

and from this the errors in the moments (and therefore in the metric coefficients) due to approximating f_c as infinite are estimated to be less than or of order ten percent for the first LIGO interferometers and one percent for the advanced LIGO interferometers over most of the relevant volume of parameter space. Since the two-parameter, post[1]-Newtonian continuous template family is known to be inadequate for the task of searching for real binaries, these errors are small enough to justify our use of the $f_c \to \infty$ approximation in this exploratory analysis.

B. Number of Search Templates Required

Since the metric coefficients are constant in this analysis, the formula for the required number of templates [Eq. (2.2.16)] reduces to

$$\mathcal{N} = \frac{\sqrt{\det \|g_{ij}\|}}{2(1 - MM)} \int d\tau_1 \, d\tau_2. \tag{2.3.9}$$

The square root of the determinant of the metric is given by $(2\pi f_0)^2$ 0.108 for the advanced LIGO noise curve and by $(2\pi f_0)^2$ 0.058 for the initial LIGO noise curve, so once we have decided on the range of parameters we deem astrophysically reasonable we will have a formula for $\mathcal{N}$ as a function of MM.

The most straightforward belief to cherish about neutron stars is that they all come with masses greater than a certain minimum $M_{\rm min}$, which might be set to 0.2 $M_\odot$ (based on the minimum mass that any neutron star can have [24]) or 1.0 $M_\odot$ (based on the observed masses of neutron stars in binary pulsar systems [25]). In terms of the variables (M, η) the constraint $M_1 > M_{\rm min}$ and $M_2 > M_{\rm min}$ is easily expressed as

$$\frac{1}{2} M (1 - \sqrt{1 - 4\eta}) > M_{\rm min},$$

but in terms of the Sathyaprakash variables [Eqs. (2.3.1) and (2.3.2)] the expression becomes rather unwieldy to write down. However, see Fig. 2.2 for a plot of the allowed region in (τ_1, τ_2) coordinates.

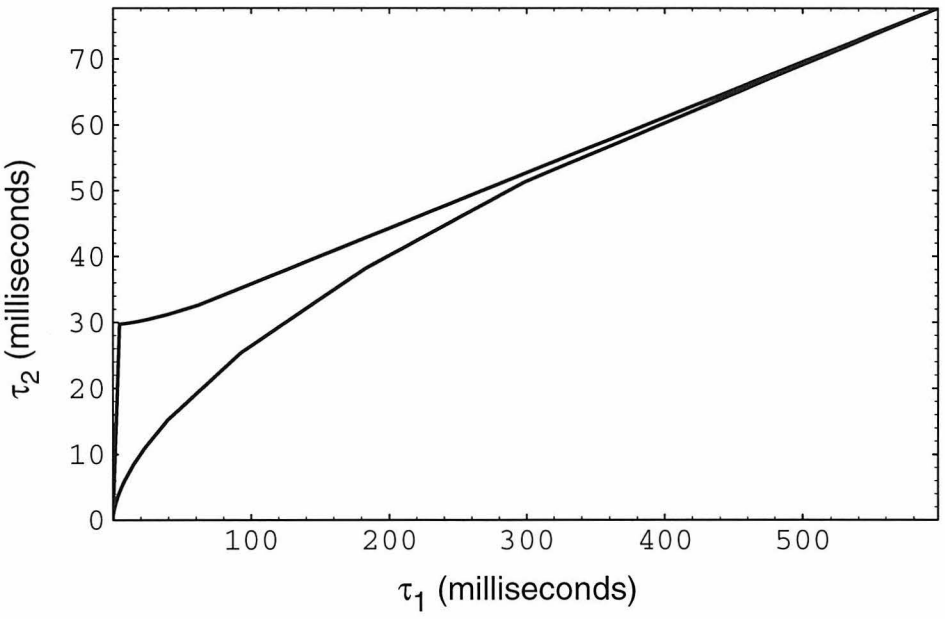

FIG. 2.2. The two-dimensional region of parameter space inhabited by binaries composed of objects more massive than 1 $M_{\odot}$. τ_1 and τ_2 are expressed (in milliseconds) for $f_0 = 200$ Hz, but the shape of the region does not change with f_0. The upper boundary of the wedge is set by $M_{\rm min}$. The left-hand boundary is set by $M_{\rm max}$, but is essentially identical to the τ_2 axis for $M_{\rm max}$ greater than a few solar masses. The region below the wedge corresponds to $\eta > 1/4$, which is *a priori* impossible.

For this reason we have found it convenient to use a Monte Carlo integration routine [26] to evaluate the coordinate volume integral $\int d\tau_1\ d\tau_2$. The Monte Carlo approach becomes especially attractive when evaluating the proper volume integral $\int d\tau_1\ d\tau_2\ \sqrt{\det\ \|g_{ij}\|}$ for cases where the integrand is allowed to vary—and in fact may itself have to be evaluated numerically, as will be the case for a post^2-Newtonian set of templates. The integral has numerical values of 0.18 and 24 seconds^2 for initial and advanced LIGO interferometer parameters, respectively, assuming a $M_{\rm min}$ of 0.2 $M_\odot$ and arbitrarily large $M_{\rm max}$. The integral can be shown (numerically) to scale roughly as $f_0^{-4.5}$ (independent of f_0) and as $M_{\rm min}^{-2.7}$ for $M_{\rm min}$ ranging from 0.2 to 1.0 solar masses (the dependence on $M_{\rm max}$ is negligible for any value greater than a few solar masses).

Inserting the above numbers into Eq. (2.3.9), we find that

$$\mathcal{N} \simeq 2.7 \times 10^5 \left(\frac{1-MM}{0.03}\right)^{-1} \left(\frac{M_{\rm min}}{0.2\ M_\odot}\right)^{-2.7} \left(\frac{f_0}{200\ {\rm Hz}}\right)^{-2.5} \tag{2.3.10}$$

for the first LIGO noise curve and

$$\mathcal{N} \simeq 8.4 \times 10^6 \left(\frac{1-MM}{0.03}\right)^{-1} \left(\frac{M_{\rm min}}{0.2\ M_\odot}\right)^{-2.7} \left(\frac{f_0}{70\ {\rm Hz}}\right)^{-2.5} \tag{2.3.11}$$

for the advanced LIGO noise curve. The fiducial value of MM has been chosen as 0.97 to correspond to an event rate of roughly 90 percent of the ideal event rate [cf. Eq. (2.2.21)]. In terms of the template-spacing-induced fractional loss $\mathcal{L}$ of event rate, the number of templates required is

$$\mathcal{N} \simeq 2.4 \times 10^5 \left(\frac{\mathcal{L}}{0.1}\right)^{-1} \left(\frac{M_{\rm min}}{0.2\ M_\odot}\right)^{-2.7} \left(\frac{f_0}{200\ {\rm Hz}}\right)^{-2.5} \tag{2.3.12}$$

for the first LIGO noise curve and

$$\mathcal{N} \simeq 7.6 \times 10^6 \left(\frac{\mathcal{L}}{0.1}\right)^{-1} \left(\frac{M_{\rm min}}{0.2\ M_\odot}\right)^{-2.7} \left(\frac{f_0}{70\ {\rm Hz}}\right)^{-2.5} \tag{2.3.13}$$

for the advanced LIGO noise curve. (For a minimum mass of 1.0 $M_\odot$, these numbers reduce to 3.1×10^3 and 9.9×10^4, respectively.)

The thirtyfold increase in the number of templates between the initial LIGO and advanced LIGO noise curves is due to the lowering of the seismic frequency f_s. If f_s is lowered, a given signal evolves a greater number of cycles in the interferometer bandwidth. Therefore the filtered signal-to-noise ratio is sensitive to smaller changes in the signal parameters, and the discrete template spacing must be tightened to compensate—resulting in a larger number of templates. A factor of two in the increase is due to the difference in the *shape* of the noise curve (f_s/f_0 changes from 1/5 to 1/7); the remainder is due to the scaling with f_0 (or, equivalently, f_s) as f_s/f_0 is held fixed, which is shown in the previous four equations.

C. Template Spacing

With the aid of the metric coefficients given in Eqs. (2.3.6) and (2.3.8), it is a simple task to select the locations of the templates and the spacing between them.

Because the metric coefficients form a constant 2×2 matrix, we can easily find the eigenvectors $\boldsymbol{e}_{x_1}$ and $\boldsymbol{e}_{x_2}$ of $\|g_{ij}\|$ and use them as axes to lay out a grid of templates. The numerical values are

$$\begin{aligned} \boldsymbol{e}_{x_1} &= 0.874\boldsymbol{e}_{\tau_1} + 0.485\boldsymbol{e}_{\tau_2}, \\ \boldsymbol{e}_{x_2} &= -0.485\boldsymbol{e}_{\tau_1} + 0.874\boldsymbol{e}_{\tau_2} \end{aligned} \tag{2.3.14}$$

for the first LIGO noise curve and

$$\begin{aligned} \boldsymbol{e}_{x_1} &= 0.899\boldsymbol{e}_{\tau_1} + 0.437\boldsymbol{e}_{\tau_2}, \\ \boldsymbol{e}_{x_2} &= -0.437\boldsymbol{e}_{\tau_1} + 0.899\boldsymbol{e}_{\tau_2} \end{aligned} \tag{2.3.15}$$

for the advanced LIGO noise curve. The infinitesimal proper distance is given in terms of the eigen-coordinates as $E_1(dx_1)^2 + E_2(dx_2)^2$, where E_1 and E_2 are the eigenvalues of the metric.

Therefore we simply use Eq. (2.2.15) to obtain the template spacings

$$dx_j = \sqrt{\frac{2(1-MM)}{E_j}}, \quad j = 1, 2. \tag{2.3.16}$$

We find that the eigenvalues of the metrics (2.3.6) and (2.3.8) are $(2\pi f_0)^2$ times 0.721 and 0.00427 (first LIGO), and $(2\pi f_0)^2$ times 1.25 and 0.00984 (advanced LIGO). Therefore the template spacings are given by

$$dx_1 = 0.22 \text{ ms} \left(\frac{1-MM}{0.03}\right)^{1/2} \left(\frac{f_0}{200 \text{ Hz}}\right)^{-1},$$
$$dx_2 = 2.9 \text{ ms} \left(\frac{1-MM}{0.03}\right)^{1/2} \left(\frac{f_0}{200 \text{ Hz}}\right)^{-1} \tag{2.3.17}$$

for the first LIGO noise curve and by

$$dx_1 = 0.49 \text{ ms} \left(\frac{1-MM}{0.03}\right)^{1/2} \left(\frac{f_0}{70 \text{ Hz}}\right)^{-1},$$
$$dx_2 = 5.6 \text{ ms} \left(\frac{1-MM}{0.03}\right)^{1/2} \left(\frac{f_0}{70 \text{ Hz}}\right)^{-1} \tag{2.3.18}$$

for the advanced LIGO noise curve. Figure 2.3 shows the locations of some possible templates superposed on a contour plot of the match with the template in the center of the graph.

D. Computing Power Requirements

Drawing on the previous work of Schutz [17] concerning the mechanics of fast-Fourier-transforming the data, we can estimate the CPU power required to process the interferometer output on-line through a single-pass (non-hierarchical) search involving $\mathcal{N}$ templates.

Although the data will be sampled at a rather high rate (tens of kHz), frequencies above some upper limit $f_u \simeq 4f_0$ can be thrown away (in Fourier transforming the data) with only negligible effects on the signal-to-noise ratio. This lowers the effective frequency of sampling to $2f_u$ (the factor of two is needed so that the Nyquist frequency is f_u), and thereby considerably reduces the task of performing the inner-product integrals. If the length of the array of numbers required to store a template is F and that required to store a given stretch of data is D, the number of floating point operations required to process that data stretch through $\mathcal{N}$ filters is

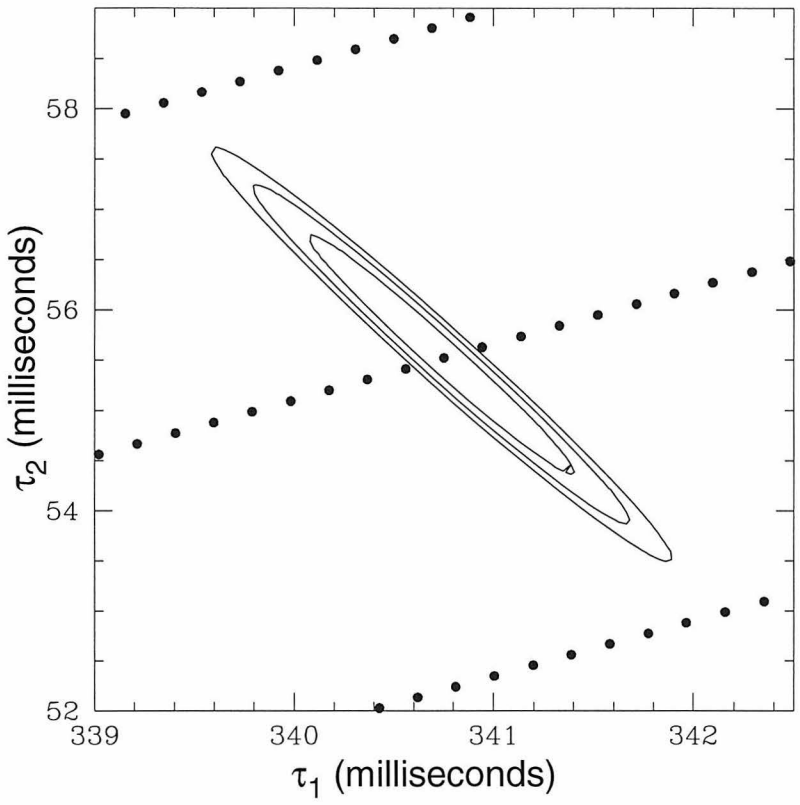

FIG. 2.3. Locations of various discrete templates for the first LIGO interferometers are shown by dots. The contours indicate the value of the match between a template located at (τ_1, τ_2) and the template located in the center of the figure. The contours are drawn at match values of 0.97, 0.98, and 0.99. Templates are placed along the principal axes of the elliptical contours. However, in order to make the ellipses visible the figure had to be stretched horizontally, distorting the contours and making the axes appear non-orthogonal.

$$N_{\mathrm{f.o.}} \simeq D\mathcal{N}(16 + 3\log_2 F) \tag{2.3.19}$$

[cf. Eq. (16.37) of Schutz [17], with the fractional overlap between data segments x chosen as roughly 1/15].

Actually, F varies from filter to filter, but most of the search templates occupy regions of parameter space where the mass is very low—and thus the storage size of the template,

$$F \simeq 2 f_u \tau_1 (f_0/f_s)^{8/3}, \tag{2.3.20}$$

is very large [27]. The longest filter is the one computed for two stars of mass M_{min}, so by inserting $\eta = 1/4$ and $M = 2M_{\mathrm{min}}$ into Eq. (2.3.1) and combining with Eq. (2.3.20), we find that we can make a somewhat pessimistic estimate of the computational cost by using

$$F \simeq 2^{24} \left(\frac{M_{\mathrm{min}}}{0.2\ M_\odot}\right)^{-5/3} \left(\frac{f_s}{10\ \mathrm{Hz}}\right)^{-8/3} \left(\frac{f_0}{70\ \mathrm{Hz}}\right). \tag{2.3.21}$$

The required CPU power $\mathcal{P}$ for an on-line search is obtained by dividing Eq. (2.3.19) by the total duration of the data set,

$$T_{\mathrm{tot}} \simeq D/(2f_u),$$

to find that

$$\mathcal{P} \simeq 2\mathcal{N} f_u (16 + 3\log_2 F). \tag{2.3.22}$$

Combining Eq. (2.3.22) with Eqs. (2.3.10) and (2.3.11) gives us

$$\mathcal{P} \simeq 30\ \mathrm{Gflops} \left(\frac{\mathcal{L}}{0.1}\right)^{-1} \left(\frac{M_{\mathrm{min}}}{0.2\ M_\odot}\right)^{-2.7} \left(\frac{f_0}{200\ \mathrm{Hz}}\right)^{-1.5} \tag{2.3.23}$$

for an on-line search by the first LIGO interferometers and

$$\mathcal{P} \simeq 400\ \mathrm{Gflops} \left(\frac{\mathcal{L}}{0.1}\right)^{-1} \left(\frac{M_{\mathrm{min}}}{0.2\ M_\odot}\right)^{-2.7} \left(\frac{f_0}{70\ \mathrm{Hz}}\right)^{-1.5} \tag{2.3.24}$$

for the advanced LIGO interferometers.

Although the estimates in the paragraph above are not to be believed beyond a factor of order unity, the magnitude of the numbers shows that a hierarchical search strategy may be desirable to keep the computing power requirements at a reasonable level for non-supercomputing facilities. That is, the data would first be filtered through a more widely spaced (low minimal match) set of templates with a relatively low signal-to-noise threshold, and only the segments which exceed this preliminary threshold would be analyzed with the finely spaced (high minimal match) templates.

The metric-based formalism of this paper only holds for the finely spaced set of templates used in the final stage of the hierarchical search; the template spacing used in the earlier stages of the search will have to be chosen using more complex methods such as those of Sathyaprakash and Dhurandhar [12,13].

E. Comparison With Previous Results

The only previous analysis of the problem of choosing the discrete search templates from the two-parameter, restricted post^1-Newtonian continuous template family is that of Sathyaprakash [14], in which he found that the entire volume of parameter space corresponding to $M_{\rm min} = 1\ M_\odot$ could be covered by a set of templates which vary only in $\tau_1 + \tau_2$—thereby reducing the effective dimensionality of the mass parameter space to one. This implied a value of $\mathcal{N}$ similar to that obtained in the one-parameter (Newtonian template) analysis of Dhurandhar and Sathyaprakash in Ref. [13].

It is not possible to fairly compare my value for $\mathcal{N}$ to the values given by Dhurandhar and Sathyaprakash in Table II of Ref. [13] due to our differing assumptions concerning the sources and the desirable level of the minimal match. Therefore I will compare the assumptions.

Dhurandhar and Sathyaprakash typically consider a minimal match of 0.8 or 0.9 rather than 0.97, This would lead to a loss of thirty to fifty percent of the ideal event rate [cf. Eq. (2.2.21)]. If the current "best estimates" of inspiraling binary event rates [2,3] are correct, the ideal event rate for LIGO and VIRGO will not be more than about one hundred per year even when operating at the "advanced interferometer" noise levels, and the loss of up to half of these events would be unacceptable.

From Eqs. (2.3.23) and (2.3.24) it can be seen that the dependence of $\mathcal{N}$ on $M_{\rm min}$ is the most important factor influencing the computing power requirement. The two-parameter analysis of Sathyaprakash [14] uses a value for $M_{\rm min}$ of 1 $M_\odot$, which is based on the statistics of (electromagnetically-) known binary pulsars. However, because there is no known, firm physical mechanism that prevents neutron stars from forming with masses between 0.2 and 1 $M_\odot$, LIGO and VIRGO should use a discrete template family with $M_{\rm min} = 0.2\ M_\odot$. After all, laser interferometer gravitational wave detectors are expected to bring us information about astronomical objects as yet unknown.

During the late stages of completion of this paper, a paper by Balasubramanian, Sathyaprakash, and Dhurandhar appeared [28] which applies differential geometry to the problem of detecting compact binary inspiral events and extracting source parameters from them. That paper applies the tools of differential geometry primarily to the problem of parameter measurement rather than that of signal detection, and so does not develop the geometrical formalism as far as is done in Sec. II of this paper. The metric constructed in Ref. [28] is identical to the information matrix which was suggested for use in the construction of a closely-spaced discrete template family in the authors' previous work [13]. While this is quite useful for parameter measurement, it neglects maximization over kinematical parameters and thus is not very useful for the construction of search templates. Also, the assumptions about MM and $M_{\rm min}$ are no different from those made in previous work up to and including Ref. [14], and

so the result for $\mathcal{N}$ is no different.

The main difference between the results of Ref. [28] and previous analyses by the same authors—and therefore the most important part of the preprint as far as the detection problem is concerned—is the introduction of the possibility of choosing search templates to lie outside the manifold of the continuous template family. Using an *ad hoc* example, the authors show that such a placement of templates can result in a spacing roughly double that between discrete templates chosen from the manifold formed by the continuous template family. My analysis in this paper does not consider this possibility, but the formalism of Sec. II can easily be extended to investigate this problem in the future.

IV. CONCLUSIONS

A. Summary of Results

This paper has presented a method for semi-analytically calculating the number of templates required to detect gravity waves from inspiraling binaries with LIGO as a function of the fraction of event rate lost due to the discrete spacing of the templates in the binary parameter space. This method, based on differential geometry, emphasizes that ultimately a finer template spacing is required than has previously been taken as typical in the literature, in order to retain a reasonable fraction of the event rate. This paper details the first calculation of this kind that uses post-Newtonian templates and a noise curve which takes into account the coloration of noise in the detector due to both standard recycling photon shot noise and thermal noise in the suspension of the test masses.

The result is that it is possible to search the data for binaries containing objects more massive than 0.2 $M_{\odot}$ thoroughly enough to lose only ~ 10 percent of the ideal event rate without requiring a quantum leap in computing technology. The computa-

tional cost of such a search, conducted on-line using a single pass through the data, is roughly 20 Gflops for the first LIGO interferometers (ca. 2000) and 270 Gflops for the advanced LIGO interferometers (some years later). Due to the nature of the approximations made in this paper, these numbers should not be believed to any greater precision than a factor of order unity; but they are certainly good order-of-magnitude estimates. These numbers are feasible (or very nearly feasible) even for a present-day supercomputing facility, but a hierarchical search strategy (using as its first stage a widely-spaced set of templates similar to that analyzed by Sathyaprakash [14]) may be desirable to reduce the cost.

B. Future Directions

There are several issues in this area which remain open for further investigation. Generally speaking, they fall into two categories characterized by pursuit of two different but complementary goals: obtaining an estimate of computing requirements to a precision better than the factor of unity achieved by the rough estimate of this paper, and reducing those computing requirements by using different algorithms to cover the templates' parameter space.

1. A thorough investigation of hierarchical search strategies is in order: How should the threshold and the minimal match of the first stage be set in order to minimize the CPU power required while keeping the false alarm and false dismissal rates at acceptable levels? How would non-Gaussian noise statistics affect the first stage threshold and minimal match? Would a hierarchical search benefit by using more than two stages? How is the threshold affected by the minimal match when the approximation of high signal-to-noise ratio can no longer be made?

2. The formalism of this paper should be applied to choose discrete templates from a better continuous template family than the one considered here. The best two-parameter templates will be based on the highest post-Newtonian order computations that have been performed for circularized, spinless binaries, augmented perhaps by terms of still higher order from the theory of perturbations of Schwarzschild or Kerr spacetime. I plan to soon apply my geometric formalism to the post$^{2.5}$-Newtonian templates which are currently the best available.

3. In order to detect some of the more interesting signals, it will be necessary to consider templates with more than two intrinsic parameters. Apostolatos has shown in Ref. [11] that when the objects comprising the binary are no longer constrained to have negligible spins, large volumes of the resulting five-dimensional parameter space are very poorly detected by spinless templates. It remains to be seen how many sources are expected by astrophysicists to populate those regions of parameter space, although current estimates [9] place the number at a small fraction of compact binaries. It would also be wise to consider the effect of an eccentricity parameter, since binaries formed by close capture (which may be common in globular clusters) would not be guaranteed to have circularized orbits.

4. The fact that the waveform templates are close but not exact solutions to the general relativistic two-body problem (i.e. the fitting factor of even the best continous template family will be slightly less than unity) will change this paper's estimates of computing power somewhat. Clearly, the spacing between templates must be tightened to some degree in order to compensate for the imperfection, but a more detailed analysis of this correction has not yet been done.

5. The effect of non-quadrupolar harmonics of the gravitational wave on the construction of search templates should be considered. These harmonics have been ignored in previous analyses of detection and even of parameter measurement, but they may have a noticeable effect when a very low loss of ideal event rate is desired.

6. Finally, a systematic investigation of the optimal choice of search templates outside the continuous template family is in order. This problem has been addressed in a preliminary way in Ref. [28], but is deserving of further scrutiny, especially since it relates to item 4 above.

ACKNOWLEDGMENTS

My thanks to Theocharis Apostolatos and Éanna Flanagan for helping me get started. I am most indebted to Kip Thorne for his guidance and his patience in reviewing the manuscript. This work was supported in part by my NSF graduate fellowship and in part by NSF grant PHY-9424337.

---

[1] K. S. Thorne, in *300 Years of Gravitation*, ed. S. W. Hawking and W. Israel (Cambridge University Press, Cambridge, England, 1987), p. 330.

[2] E. S. Phinney, Astrophys. J. **380**, L17 (1991).

[3] R. Narayan, T. Piran, and A. Shemi, Astrophys. J. **379**, L17 (1991).

[4] For example, A. V. Tutukov and L. R. Yungelson, Mon. Not. Roy. Astron. Soc. **260**, 675 (1993).

[5] A. Abramovici, W. E. Althouse, R. W. P. Drever, Y. Gürsel, S. Kawamura, F. J. Raab, D. Shoemaker, L. Sievers, R. E. Spero, K. S. Thorne, R. E. Vogt, R. Weiss, S. E. Whitcomb, and M. E. Zucker, Science **256**, 325 (1992).

[6] C. Bradaschia, E. Calloni, M. Cobal, R. Del Fasbro, A. Di Virgilio, A. Giazotto, L. E. Holloway, H. Kautzky, B. Michelozzi, V. Montelatici, D. Pascuello, and W. Velloso, in *Gravitation 1990*, Proceedings of the Banff Summer Institute, ed. R. Mann and P. Wesson (World Scientific, Singapore, 1991).

[7] L. Blanchet and T. Damour, Phys. Rev. D **51**, 5360 (1995).

[8] C. M. Will and A. G. Wiseman, Phys. Rev. D **54**, 4813 (1996).

[9] L. Blanchet, T. Damour, B. R. Iyer, C. M. Will, and A. G. Wiseman, Phys. Rev. Lett. **74**, 3515 (1995).

[10] See, e.g., N. Wiener, *The Extrapolation, Interpolation and Smoothing of Stationary Time Series with Engineering Applications* (Wiley, New York, 1949) or L. A. Wainstein and V. D. Zubakov, *Extraction of Signals from Noise* (Prentice-Hall, London, 1962).

[11] T. A. Apostolatos, Phys. Rev. D **52**, 605 (1995).

[12] B. S. Sathyaprakash and S. V. Dhurandhar, Phys. Rev. D **44**, 3819 (1991).

[13] S. V. Dhurandhar and B. S. Sathyaprakash, Phys. Rev. D **49**, 1707 (1994).

[14] B. S. Sathyaprakash, Phys. Rev. D **50**, R7111 (1994).

[15] C. Cutler and É. É. Flanagan, Phys. Rev. D. **49**, 2658 (1994).

[16] Note the terms "intrinsic" and "extrinsic" are meant with regard *to the shape of the waveform*, not to the source itself. Consider, for example, the direction angles of a source on the celestial sphere. These parameters are clearly not intrinsic to the binary itself—it does not care how it is oriented with respect to the Earth. These parameters

are not intrinsic to the waveform either, if the signal is of short duration—they simply change the overall phase of the signal, and can be lumped together with the coalescence phase. But they *are* intrinsic to the shape of the waveform if the signal lasts long enough to be significantly modulated by the Doppler effect of the interferometer's motion with respect to the solar system barycenter. In the former case (typical of stellar-mass objects detected by LIGO) the direction angles are very easily handled in the analysis; in the latter (typical of binaries detected by LISA) they are intrinsic to the waveform and must be treated with great care, as is the case for long-term, all-sky pulsar searches.

[17] B. F. Schutz, in *The Detection of Gravitational Radiation*, ed. D. Blair (Cambridge University Press, Cambridge, England,1989).

[18] E. Poisson and C. M. Will, Phys. Rev. D **52**, 848 (1995).

[19] Note that the Φ_0 used here is the coalescence phase of the *waveform*. In the restricted post-Newtonian approximation, this is twice the coalescence phase of the *orbit* ϕ_0, which is used by Cutler and Flanagan in Ref. [15].

[20] S. D. Mohanty and S. V. Dhurandhar, Phys. Rev. D **54**, 7108 (1996). Also L. S. Finn, in preparation.

[21] This $(N+1)$-dimensional metric $\gamma_{\alpha\beta}$ is related to the Fisher information matrix, which was used by Dhurandhar and Sathyaprakash in the appendix of Ref. [13] to compute the template spacing analytically in the small-spacing limit. However, in taking the absolute value to maximize over $\Delta\Phi_0$, we have lost some dependence on the dynamical (intrinsic) template parameters, so our γ-metric is not even the projection of the information matrix onto the subspace perpendicular to Φ_0. This lets us tolerate a greater mismatch between the templates' dynamical parameters than was possible before maximization, thereby reducing the total number of templates required.

[22] P. C. Peters, Phys. Rev. **136**, B1224 (1964).

[23] The ψ_j given here are different from those given in Eq. (13a-3) of Ref. [14] because Sathyaprakash does not use t_0 and Φ_0 as kinematical parameters, but rather the time and phase at which the quadrupole part of the waveform reaches a frequency of f_0.

[24] S. L. Shapiro and S. A. Teukolsky, *Black Holes, White Dwarfs, and Neutron Stars: The Physics of Compact Objects* (Wiley, New York, 1983).

[25] J. H. Taylor, Rev. Mod. Phys. **66**, 711 (1994).

[26] Numerical integrations were performed with the aid of Mathematica [S. Wolfram, *Mathematica: A System for Doing Mathematics by Computer* (Addison-Wesley, Redwood City, California, 1988)] and with a Monte Carlo code based on Numerical Recipes [W. H. Press, S. A. Teukolsky, W. T. Vetterling, and B. P. Flannery, *Numerical Recipes: The Art of Scientific Computing* (Cambridge University Press, Cambridge, England, 1992)].

[27] The storage size of the template is equal to the effective sampling frequency $2f_u$ times the duration of the template waveform. In the restricted post-Newtonian approximation, the duration of a binary chirp waveform template is equal to the time it takes for the gravitational wave frequency to sweep from the seismic frequency f_s up to infinity. Since $\tau_1 \propto f_0^{-8/3}$ is the dominant (Newtonian) contribution to the time it takes the gravitational wave frequency to sweep from f_0 up to infinity, the duration of a waveform template is roughly $\tau_1(f_0/f_s)^{8/3}$. Thus we obtain Eq. (2.3.20).

[28] R. Balasubramanian, B. S. Sathyaprakash, and S. V. Dhurandhar, Phys. Rev. D **53**, 3033 (1996).

Chapter 3 Matched filtering of gravitational waves from inspiraling compact binaries: Computational cost and template placement

Written with B. S. Sathyaprakash

To be submitted to Phys. Rev. D

This paper is an extension of the analysis described in Chapter 2: We estimate the number of templates, computational power, and storage required for a one-step, on-line search for gravitational waves from inspiraling compact binaries, using a discrete family of two-parameter templates that are based on a post-Newtonian analysis of spinless binaries in circular orbits. The main differences between this chapter and Chapter 2 are that here we (i) do the calculations for the GEO600, TAMA, and VIRGO noise spectra, as well as the initial, enhanced, and advanced LIGO noise spectra; (ii) use higher order (second post-Newtonian) template waveforms, and (iii) use a more realistic estimate of the sampling rate needed by each interferometer. We find that in a search for inspiral waves from binaries whose smaller object has minimum mass $m_{\rm min} = 0.2M_\odot$, with template spacing fine enough that no more than 10% of the signals are lost due to finite spacing, the initial LIGO interferometers will require about 1.4×10^{11} flops (floating point operations per second) to keep up with the incoming data; this is 5 times higher than estimated in Chapter 2, in part because of the higher sampling rate and in part because of the improved family of templates. Enhanced LIGO, GEO600, and TAMA will require similar computational power (refer to Tables 3.2–3.4 for details). Advanced LIGO will require 1.1×10^{12} flops, and initial VIRGO will require 3.9×10^{12} flops to take full advantage of its target noise spectrum. As was shown in Chapter 2, the computational power required scales roughly as $m_{\rm min}^{-8/3}$. Since this scaling is slightly disturbed by the curvature of the parameter space at second post-Newtonian order, we provide in Tables 3.2–3.4 estimates for a search with $m_{\rm min} = 1M_\odot$. We also sketch and discuss

an algorithm for placing the templates in the parameter space.

I. INTRODUCTION

Close binary systems composed of compact objects (such as black holes and neutron stars) are expected to be an important source of gravitational waves for broad-band laser interferometers such as LIGO, VIRGO, GEO, and TAMA [1–4]. The orbit of a compact binary decays under the influence of gravitational radiation reaction, emitting a gravitational wave signal that increases in amplitude and "chirps" upward in frequency as the objects spiral in toward each other just before their final coalescence. According to current astronomical lore [5–7], the rate of coalescences should be about three per year within 200 to 300 Mpc [5] of the Earth for neutron-star–neutron-star binaries, and within 400 Mpc to 1 Gpc for black-hole–black-hole binaries. Signals from inspiraling compact binaries at these distances are strong enough to be detected by "enhanced" LIGO and VIRGO interferometers [8], but only if aided by a nearly optimal signal-processing technique. Fortunately, the distinctive frequency chirp has been calculated to a remarkable degree of precision using a variety of approximations to the general relativistic two-body problem (e.g. [9,10]). Because the functional form of the chirp is quite well-known, a search for inspiral signals in noisy data is ideally suited to matched filtering.

Matched filtering [11] has long been known to be the optimal linear signal-processing technique and is well-discussed in the literature (e.g. [12]); therefore we will only briefly summarize it here. In the frequency domain, a matched filter is a best-guess template of the expected signal waveform divided by the interferometer's spectral noise density. The interferometer output is cross-correlated with the matched filter at different time delays to produce a filtered output. The signal-to-noise ratio,

defined as the ratio of the actual value of the filtered output to its rms value in the presence of pure noise, is compared to a predetermined threshold to decide if a signal is present in the noise. If the signal from which the matched filter was constructed is present, it contributes coherently to the cross-correlation, while the noise contributes incoherently and thus is reduced relative to the signal. Also, the weighting of the cross-correlation by the inverse of the spectral noise density emphasizes those frequencies to which the interferometer is most sensitive. Consequently, signals thousands of cycles long whose unfiltered amplitude is only a few percent of the rms noise can be detected.

A matched filtering search for inspiraling compact binaries can be computationally intensive due to the variety of possible waveforms. Although the inspiral signals are all expected to have the same functional form, this form depends on several parameters—the masses of the two objects, their spins, the eccentricity of their orbit, etc.—some of them quite strongly. A filter constructed from a waveform template with any given parameter vector may do a very poor job of detecting a signal with another parameter vector. That is, the difference in parameter vectors can lead to a greatly reduced cross-correlation between the two wave forms; and in general, the greater the difference, the more the cross-correlation is reduced. Because the parameter vector of a signal is not known in advance, it is necessary to filter the data with a family of templates located at various points in parameter space—e.g., placed on a lattice—such that any signal will lie close enough to at least one of the templates to have a good cross-correlation with that template.

There are several questions that must be answered in order to determine the feasibility of a matched filtering search strategy and, if feasible, to implement it. Which parameters significantly affect the waveform? How should the spacing of the template parameters (lattice points) be chosen? Is there a parametrization that is in some sense "preferred" by the template waveforms? How many templates are needed

to cover a given region of interest in the parameter space, and how much computing power and memory will it cost to process the data through them? In the case of inspiraling compact binaries, the full general-relativistic waveforms are not exactly known, but are instead approximated (e.g., using the post-Newtonian scheme); and we must also ask, what approximation to the true waveforms is good enough?

All of these questions have been addressed in recent years, at least at some level. The current state of affairs is summarized by the following brief review of the literature:

The standard measure for deciding what class of waveforms is good enough is the *fitting factor* (FF) introduced by Apostolatos [13]. The fitting factor is effectively the fraction of optimal signal-to-noise-ratio obtained when filtering the data with an approximate family of templates. Because binaries are (on large scales) uniformly distributed in space and because the signal strength scales inversely with distance, the fraction of event rate retained is approximately FF^3. Therefore it has become conventional to regard $FF = 97\%$—i.e., 10% loss of event rate—as a reasonable goal. Using the standard post-Newtonian expansion in the test-mass case (i.e., when one body is much less massive than the other so the waveforms can be computed with arbitrarily high precision using the "Teukolsky formalism"), Droz and Poisson [14] found that 2PN signals had fitting factors of 90% or higher. Damour, Iyer, and Sathyaprakash [15] have devised a new way of rearranging the usual post-Newtonian expansion to take advantage of physical intuition in much the same way that Padé approximants are better than Taylor series. They find fitting factors of 95% or higher for the 2PN templates. Research underway by L. Blanchet, T. Damour, B. Iyer, C. Will, and A. Wiseman will lead to 3PN templates that should easily achieve $FF > 97\%$.

Several people [16,13,17] have shown that it is insufficient to use templates that depend on just one shape parameter (the "chirp mass," which governs the rate of

frequency sweep at Newtonian-quadrupole order). To achieve $FF > 90\%$ one must include the masses of both objects as template parameters, as was done in the above 2PN analyses by Droz and Poisson, and by Damour, Iyer and Sathyaprakash, and as is being done in the forthcoming 3PN templates.

Apostolatos [13,24] showed that for binaries whose bodies spin rapidly but with spins orthogonal to the orbital plane so there is no precession, neglecting the spin parameters (i.e., using two-mass-parameter waveforms based on the theory of spinless binaries) degraded the fitting factors by less than 2%. With precession the situation is much more complicated, and data analysis algorithms are as yet poorly developed: It is clear that there are interesting corners of parameter space (most especially a neutron star in a substantially nonequatorial, precessing orbit around a much heavier rapidly spinning black hole) in which the two-mass-parameter, spinless waveforms give $FF \ll 90\%$; to search for such binaries will require waveforms with three or more parameters. However, the 2PN (or 3PN) two-mass-parameter waveforms do appear to cover adequately a significant portion of the parameter space for precessing binaries [13].

Sathyaprakash [18] showed that in computations with the two-mass-parameter waveforms, the best coordinates to use on the parameter space are not the two masses, but rather the inspiral times from some fiducial location to final merger, as computed at Newtonian and first post-Newtonian order.

Sathyaprakash and Dhurandhar [19–21] developed a criterion for choosing a discrete family of templates within the template space, for use in data analysis—i.e., a criterion for putting a discrete grid on the templates' parameter space; and they did a numerical implementation of their criterion for a one-parameter (Newtonian) family of templates and for simple noise models. Owen [22] (chapter 2 of this thesis), building on the work of Sathyaprakash and Dhurandhar, defined the concept of the *minimal match* as a measure of how well a discrete set of templates covers the parameter space;

this minimal match is an analog of Apostolatos' [13] fitting factor. Owen then defined a metric on the parameter space, from which one can semi-analytically deduce the template spacing needed to achieve a desired minimal match, and can deduce the total number of templates needed and the computational requirements to keep up with the data, for any family of waveforms and any interferometer noise spectrum. Owen combined his metric-based formalism with computational counting procedures from Schutz [23] to estimate the computational requirements for LIGO searches based on two-mass-parameter 1PN templates. These estimates were confirmed by Apostolatos [24] using a numerical method in the vein of (but more sophisticated than) the previous work of Sathyaprakash and Durandhar [19–21]. Apostolatos also showed that a search for precessing binaries that fully covers all the nooks and crannies of the precessional parameter space, using currently available templates and techniques, is prohibitively costly.

Mohanty and Dhurandhar [25,26] have studied hierarchical search strategies. Such strategies reduce computational costs by making a first pass through the data with a coarsely-spaced template grid and a low signal-to-noise threshold to identify candidate signals. Each candidate flagged by the first pass is examined more closely with a second, finely-spaced grid of templates and a higher threshold to weed out false alarms. Such strategies can reduce the total computational requirements by roughly a factor 10.

The purpose of this paper is to refine and update the analyses by Owen [22] (Chapter 2 of this thesis) for the 2-mass-parameter, spinless templates that are likely to be used in most of LIGO's binary-inspiral searches. This refinement is needed because the kilometer-scale interferometers will begin taking data in about 2 years (preliminary, engineering run); people are even now designing software to implement the simplest matched filtering search algorithm [27]; and in the context of these implementations, the factor of 3 accuracy attempted in Ref. [22] is no longer adequate. The

numbers that are derived in this paper should establish a reliable baseline to which more sophisticated search strategies (e.g., hierarchical searches) can be compared.

The substantial differences between this paper and Ref. [22] (Chapter 2) are that we now (i) approximate the phase evolution of the inspiral waveform to 2PN rather than 1PN order; (ii) give results for the noise spectra of several more interferometers; and (iii) use a better estimate of the sampling frequency needed for each interferometer. We assume the following fiducial search: a minimal match of 97% (corresponding to 10% loss of event rate due to coarse parameter space coverage), second post-Newtonian waveforms, and templates made for objects of minimum mass $m_{\rm min} = 0.2 M_\odot$ and up.

Our results for the computational requirements are given in Tables 3.2–3.4. Those tables show that the initial LIGO interferometers need about 1.5 times as many templates and 5 times as much computational power as was estimated in Ref. [22] (Chapter 2). These increases result mainly from using 2PN waveforms rather than the (clearly inadequate) 1PN, and from a using a higher sampling rate (as, it turns out, is required to keep time-step discretization error from compromising the 97% minimal match). GEO600 requires slightly more templates and power than LIGO because of its flatter noise spectrum, and TAMA requires slightly less because its sensitivity is limited to higher frequencies where there are fewer cycles. Initial VIRGO, with its extremely broad and flat spectrum, requires about the same as advanced LIGO. We conclude that even if VIRGO achieves its putative low-frequency sensitivity, it will be unable to take advantage of that sensitivity with matched filtering because of the large number of templates required.

The rest of this paper is organized as follows. In Sec. II we analyze the application of matched filtering to a search for inspiraling binaries and summarize the method of Ref. [22] (Chapter 2) which uses differential geometry to answer important questions about such a search. We use this method in Sec. III to estimate the computational

costs and other requirements of a matched-filtering binary search for LIGO, VIRGO, GEO, and TAMA. In Sec. IV we illustrate a detailed example of a template placement algorithm, and in Sec. V we summarize our results and conclusions.

II. FORMALISM

This Section summarizes material previously presented in [22] with several incremental improvements. We begin by introducing some notation.

The Fourier transform of a function $h(t)$ is denoted by $\tilde{h}(f)$, where

$$\tilde{h}(f) \equiv \int_{-\infty}^{\infty} dt\, e^{i2\pi ft} h(t). \tag{3.2.1}$$

Complex conjugation is denoted by an asterisk.

We write the interferometer output $h(t)$ as the sum of noise $n(t)$ and signal $\mathcal{A}s(t)$, where we have separated the signal into a dimensionless, time-independent amplitude $\mathcal{A}$ and a "shape" function $s(t)$ which is defined to have unit norm [see Eq. (3.2.4) below].

The strain power spectral noise density of an interferometer is denoted by $S_h(f)$. We use the one-sided spectral density, defined by

$$\mathrm{E}[\tilde{n}(f_1)\tilde{n}^*(f_2)] = \frac{1}{2}\delta(f_1 - f_2) S_h(|f_1|), \tag{3.2.2}$$

where E[ ] denotes the expectation value over an ensemble of realizations of the noise.

We use geometrized units, i.e. Newton's gravitational constant G and the speed of light c have values of unity.

A. Matched filtering

First we flesh out the Introduction's brief description of matched filtering. In the simplest idealization of matched filtering, the filtered signal-to-noise ratio is defined by

$$\frac{S}{N} \equiv \frac{\langle h, u \rangle}{\text{rms } \langle n, u \rangle}. \tag{3.2.3}$$

Here u is the template waveform used to filter the data stream h, and the inner product

$$\langle a, b \rangle \equiv 4\,\text{Re}\left[\int_0^\infty df\, \frac{\tilde{a}^*(f)\,\tilde{b}(f)}{S_h(f)}\right] \tag{3.2.4}$$

is the noise-weighted cross-correlation between a and b (cf. [28]). The denominator of (3.2.3) is equal to $\sqrt{\langle u, u \rangle}$, the norm of u (see Sec. II B of Ref. [28] for a proof). Because the norm of u cancels out of (3.2.3), we can simplify our calculations without loss of generality by considering all templates to have unit norm.

When searching for a parametrized family of signals the situation is somewhat more complicated. The parameter values of the signals are not known in advance; therefore one must filter the data through many templates constructed at different points in the parameter space. To develop a strategy for searching the parameter space, one must know how much the SNR is reduced by using a template whose parameter values differ from those of the signal. Neglecting fluctuations due to the noise, the fraction of the optimal SNR obtained by using the wrong parameter values is given by the *ambiguity function*,

$$A(\boldsymbol{\lambda}, \boldsymbol{\Lambda}) \equiv \langle u(\boldsymbol{\lambda}),\, u(\boldsymbol{\Lambda}) \rangle \tag{3.2.5}$$

(see, e.g., Chs. XIII and X of Ref. [12]). Here $\boldsymbol{\lambda}$ and $\boldsymbol{\Lambda}$ are the parameter vectors of the signal and template (it doesn't matter which is which). The ambiguity function, as its name implies, is a measure of how distinguishable two waveforms are with respect to the matched filtering process. It can be regarded as an inner product on the waveform parameter space and is fundamental to the theory of parameter estimation [29].

For the purposes of a search for inspiraling compact binaries, the ambiguity function isn't quite what is needed. This is because the test statistic (for a given set of parameter values $\boldsymbol{\theta}$) is not given by Eq. (3.2.3), but rather by

$$\max_{\phi_c,t_c} \frac{\langle h, u(\boldsymbol{\theta}) \exp[i(2\pi f t_c - \phi_c)]\rangle}{[\text{rms } \langle n, u(\boldsymbol{\theta})\rangle]}. \tag{3.2.6}$$

Here ϕ_c and t_c are respectively the coalescence time and coalescence phase (see Chapter 2). We separate these parameters out from the rest: $\boldsymbol{\lambda} = (\phi_c, t_c, \boldsymbol{\theta})$, where $\boldsymbol{\theta}$ is the vector of *intrinsic parameters* that determine the shape of the waveform and ϕ_c and t_c are *extrinsic parameters* (see Chapter 2). The practical difference is that maximization over the extrinsic parameters is performed automatically by Fourier transforming, taking the absolute value, and looking for peaks. The use of Eq. (3.2.6) as a detection statistic suggests the definition of a modified ambiguity function known as the *match* [22]

$$M(\boldsymbol{\theta}_1, \boldsymbol{\theta}_2) \equiv \max_{\phi_c,t_c} \langle u(\boldsymbol{\theta}_1), u(\boldsymbol{\theta}_2) \exp[i(2\pi f t_c - \phi_c)]\rangle, \tag{3.2.7}$$

where the templates u are assumed to have unit norm. The use of this match function rather than the ambiguity function takes into account the fact that a search can benefit from systematic errors in the extrinsic parameters.

B. Applications of differential geometry

The match (3.2.7) can be regarded as an inner product on the space of template shapes and intrinsic template parameters, and correspondingly Owen [22] has defined a metric on this space:

$$g_{ij}(\boldsymbol{\theta}) \equiv -\frac{1}{2} \left. \frac{\partial^2 M(\boldsymbol{\theta}, \boldsymbol{\Theta})}{\partial\Theta^i \partial\Theta^j} \right|_{\Theta^i=\theta^i}. \tag{3.2.8}$$

The metric (3.2.8) is derived from the match (3.2.7) in the same way the information matrix Γ_{ij} is derived from the ambiguity function [29], and plays a role in signal detection similar to that played by the information matrix in parameter estimation. The g_{ij} can be derived by expanding $M(\boldsymbol{\theta}, \boldsymbol{\Theta})$ about $\boldsymbol{\Theta} = \boldsymbol{\theta}$, or equivalently by projecting Γ_{ij} on the subspace orthogonal to ϕ_c and t_c.

The g_{ij} can be used to approximate the match in the regime $1 - M \ll 1$ by

$$M(\boldsymbol{\theta}, \boldsymbol{\theta} + \Delta\boldsymbol{\theta}) \simeq 1 - g_{ij}\Delta\theta^i\Delta\theta^j, \tag{3.2.9}$$

which is simply another way of writing the Taylor expansion of $M(\boldsymbol{\theta}, \boldsymbol{\theta} + \Delta\boldsymbol{\theta})$ about $\Delta\boldsymbol{\theta} = 0$. (The first derivative term vanishes because M takes its maximum value of unity at $\Delta\boldsymbol{\theta} = 0$.) We find that the quadratic approximation (3.2.9) is good typically for $M \simeq 0.95$ or greater, though this depends on the waveform and noise spectrum used. Experience [27] suggests that the quadratic approximation generally underestimates the true match; and thus the spacings and numbers of templates we calculate using Eq. (3.2.9) err on the safe side.

In the limit of close template spacing, Eq. (3.2.9) leads to a simple, analytical way of placing templates on a lattice. We discuss this in some detail in Sec. IV, but for now turn our attention to the use of the quadratic approximation in calculating the number of templates needed for a lattice.

C. Computational costs

If the number $\mathcal{N}$ of templates needed to cover a region of interest is large, it is well approximated by the ratio of the proper volume of the region of interest to the proper volume per template ΔV,

$$\mathcal{N} = (\Delta V)^{-1} \int d^D\theta \sqrt{\det \|g_{ij}\|}, \tag{3.2.10}$$

where D is the dimension of the parameter space [22]. Equation (3.2.10) overestimates $\mathcal{N}$ when not in the limit $\Delta V \to 0$ ($\mathcal{N} \to \infty$). The reason is template *spill over,* i.e. the fact that in any real algorithm for laying out templates, those on the boundaries of the region of interest will to some extent cover regions just outside. This effect is small in the limit of many templates because it goes as the surface-to-volume ratio of the region of interest.

The proper volume per template, ΔV, depends on the packing algorithm used, which in turn depends on the number D of dimensions (see Sec. IV). For $D = 2$, the optimal packing is a hexagonal lattice, and thus

$$\Delta V = \frac{3\sqrt{3}}{2}(1 - MM), \tag{3.2.11}$$

where MM is the *minimal match* parameter described in Chapter 2. There is no packing scheme which is optimal for all D, but it is always possible (though inefficient) to use a hypercubic lattice, for which

$$\Delta V = (2\sqrt{(1 - MM)/D})^D. \tag{3.2.12}$$

For inspiraling compact binaries, Ref. [22] has spelled out a detailed prescription for obtaining the g_{ij} needed to evaluate the proper integral, given any noise spectrum and any restricted post-Newtonian waveform. See Sec. III for the details of our implementation of this prescription.

Once $\mathcal{N}$ has been found it is a relatively straightforward matter to calculate the CPU power and storage required to process all the templates in an on-line search.

The interferometer data stream is broken up for processing into segments of D samples (real numbers), such that $D \gg F$ where F is the length (in real numbers) of the longest filter. See Schutz [23] for a discussion of the optimization of D/F taking into account the fact that successive data segments must overlap by at least F to avoid circular correlations in the Fourier transform. Using the operation count for a fast Fourier transform given by Prince (private communication), filtering the data segment through $\mathcal{N}$ templates of length F requires

$$\mathcal{N} D(16 + 2.5 \log_2 F) \tag{3.2.13}$$

floating point operations. Note that Prince's operation count is slightly less than that of Schutz. If we take the sampling frequency to be $2f_u$ (see Sec. III and Table 3.1), the computational power required to keep pace with data acquisition is

$$\mathcal{P} \simeq \mathcal{N} f_u (32 + 5 \log_2 F) \tag{3.2.14}$$

flops (floating point operations per second). For more details on our implementation see Sec. III.

III. COMPUTATIONAL COST USING RESTRICTED 2PN TEMPLATES

Using the geometric formalism summarized in Sec. II, we calculate the number $\mathcal{N}$ of templates required to cover a region of interest as a function of the minimal match. We then use this number to calculate the computational cost of filtering a single interferometer's output through all these templates in an on-line search.

A. Functional form of the templates

We construct our waveform templates using two intrinsic parameters based on the masses of the binary's components. Inspiral waveforms in principle can be strongly affected by several other parameters: spins of the two components, orbital eccentricity, and several angles describing the orientation of the binary with respect to the interferometer. However, it is believed that two-parameter templates will be adequate to search for most binaries for the following reasons.

(i) Based on models of the evolution of currently known binary pulsars, it is expected [9] that typical NS-NS binaries will have spins of negligible magnitude ($\text{spin}/\text{mass}^2 \ll 1$). Apostolatos [24] has shown that, even if the magnitudes of the spins are large, their effect on S/N is small (reduces FF by less than 2% if the orbit and the spin vectors do not precess). He has also shown that precession will not reduce FF below 90% except in the relatively small region of parameter space containing binaries with a neutron star orbiting a more massive, rapidly rotating ($\text{spin}/\text{mass}^2 \sim 1$) black hole with orbital angular momentum inclined by more than about 30 degrees to the black hole's spin.

(ii) It has long been known [30] that gravitational radiation reaction circularizes all but the most eccentric orbits on a time scale much smaller than the lifetime of the binary if the progenitor system was the same binary. This may not be true, however, in the case of close binaries formed by capture in densely populated environments, e.g. galactic nuclei.

(iii) The angles make no difference in our analysis because we use the *restricted post-Newtonian* approximation [28], in which the phase evolution of the inspiral waveform is followed to a high post-Newtonian order but the amplitude is only followed to lowest order. In this approximation, the combined effect of the angles is to multiply the waveform by a constant amplitude and phase factor, which does not affect the choice of search templates. Presently it is believed [28] that the restricted post-Newtonian approximation will be good enough for data analysis of ground-based interferometers.

The standard post-Newtonian expansion of the waveform phase is given as a function of mass parameters based on the standard astronomical choices M (total mass) and μ (reduced mass). In order to clearly isolate test-mass terms (i.e., those that remain when one body is much less massive than the other), the variable $\eta = \mu/M$ is typically used instead of μ. In terms of M and η, the second post-Newtonian waveform phase is given by

$$\Psi(f) = -\frac{3}{128\eta}\left[(\pi M f)^{-5/3} + \frac{20}{9}\left(\frac{743}{336} + \frac{11}{4}\eta\right)(\pi M f)^{-1} \right.$$
$$\left. -16\pi(\pi M f)^{-2/3} + 10\left(\frac{3\,058\,673}{1\,016\,064} + \frac{5\,429}{1\,008}\eta + \frac{617}{144}\eta^2\right)(\pi M f)^{-1/3}\right] \qquad (3.3.1)$$

[derived from Eq. (3.6) of Ref. [31]]. However, M and η are inconvenient parameters for our purposes because, when they are used as the parameter-space coordinates, the values of the metric components vary strongly over parameter space, making calculations difficult and prone to numerical error. In earlier analyses [18,29,22] it was found more convenient to use as parameters the Newtonian and 1PN *chirp times*

$$\tau_0 = \frac{5}{256}(\pi M f_0)^{-5/3}\eta^{-1}, \tag{3.3.2a}$$

$$\tau_1 = \frac{5}{192}(\pi M f_0)^{-1}\left(\frac{743}{336\eta} + \frac{11}{4}\right), \tag{3.3.2b}$$

which are respectively the Newtonian and 1PN contributions to the time it takes the gravitational-wave frequency to (formally) evolve from f_0 to infinity. The chirp times are more convenient than the usual mass parameters because, when they are chosen as parameter-space coordinates, at 1PN order the metric components are constant. Assuming the post-Newtonian expansion has reasonable convergence properties, one would expect the metric components in these coordinates to remain nearly constant at higher post-Newtonian orders (and indeed we find this is so). However, at higher than 1PN order one cannot write the waveform phase analytically in terms of τ_0 and τ_1. To remedy this, following a suggestion of Mohanty [26], we base our second parameter on the 1.5PN chirp time $\tau_{1.5}$. More specifically, we introduce new dimensionless coordinates in parameter space. We define

$$\theta^1 = 2\pi f_0 \tau_0 = \frac{5}{128}(\pi M f_0)^{-5/3}\eta^{-1}, \tag{3.3.3a}$$

$$\theta^2 = 2\pi f_0 \tau_{1.5} = \frac{\pi}{4}(\pi M f_0)^{-2/3}\eta^{-1}, \tag{3.3.3b}$$

which can be inverted to obtain

$$M = \frac{5}{32\pi^2 f_0}\frac{\theta^2}{\theta^1}, \tag{3.3.4a}$$

$$\eta = \left[\frac{16\pi^5}{25}\frac{(\theta^1)^2}{(\theta^2)^5}\right]^{1/3}. \tag{3.3.4b}$$

This choice of (θ^1, θ^2) lets us write the waveform phase analytically while keeping the metric components from varying too strongly; therefore it is convenient for calculating numbers of templates (see below). However, for other purposes (τ_0, τ_1) are just as convenient, and to be consistent with the literature we will use them.

B. Noise spectra

In this paper we consider the noise spectra of the four large- and intermediate-scale interferometer projects, LIGO, VIRGO, GEO600, and TAMA. For LIGO we analyze three noise spectra corresponding to three interferometer configurations, the "first interferometers" [1] (which are planned to perform a gravitational-wave search in 2002–2003), the "enhanced interferometers" [8] (which are likely to be carrying out searches in the mid 2000's), and the "advanced interferometers" [1] (which are thought representative of the type of detector that might operate a few years after the enhanced ones). For convenience we abbreviate these respectively as LIGO I, LIGO II, and LIGO III. We also analyze the VIRGO and GEO noise spectra recently provided in Refs. [2,3]. There is no TAMA noise spectrum in the literature; therefore we rely on data provided by M.-K. Fujimoto and bundled with GRASP [27].

For many reasons—not least of which is the convenience of our colleagues—it is desirable to have simple analytical fits to the noise power spectral densities used. Kip Thorne and Scott Hughes (private communications) have provided us with fits to LIGO I and LIGO III respectively, and a fit to LIGO II was derived in Ref. [34]. We have constructed our own fits to the remaining noise spectra listed in the previous paragraph. All of these analytical fits to the noise spectra are tabulated in Table 3.1.

The shape of each noise spectrum determines natural low- and high-frequency cutoffs for the matched filtering integrals. The low-frequency cutoff f_s is the defined as frequency above which 99% of S^2/N^2 is obtained; we call this the *seismic frequency* and denote it with a subscript s because it is typically near the frequency at which seismic noise causes the noise power spectral density $S_h(f)$ to begin rising sharply. Because integration below this frequency contributes little to the detectability of signals and costs much in terms of total number of templates and computational resources, we assume the templates to begin with gravitational-wave frequency f_s.

TABLE 3.1. Analytical fits to noise power spectral densities $S_h(f)$ of the interferometers treated in this paper. Here S_0 is the minimum value of $S_h(f)$, and f_0 is the frequency at which the minimum value occurs. For our purposes $S_h(f)$ can be treated as infinite below the seismic frequency f_s. The high-frequency cutoff f_u is chosen so that the loss of signal-to-noise ratio due to finite sampling rate $2f_u$ is 0.75% (see text). Here S_0 is given in Hz^{-1}, f_0 and f_s in Hz, and f_u in kHz.

Interferometer	Fit to noise power spectral density	S_0	f_0	f_s	f_u
LIGO I	$S_0/3\ [(f_0/f)^4 + 2(f/f_0)^2]$	8.0×10^{-46}	175	40	2.6
LIGO II	$S_0/11\ \left\{2(f_0/f)^{9/2} + 9/2[1 + (f/f_0)^2]\right\}$	7.9×10^{-48}	110	25	1.8
LIGO III	$S_0/5\ \{(f_0/f)^4 + 2[1 + (f/f_0)^2]\}$	2.3×10^{-48}	75	12	1.25
VIRGO	$S_0/4\ [260(f_s/f)^5 + 2(f_0/f) + 1 + (f/f_0)^2]$	1.4×10^{-45}	500	20	6.0
GEO600	$S_0/5\ \left[4(f_0/f)^{3/2} - 2 + 3(f/f_0)^2\right]$	6.6×10^{-45}	210	40	2.9
TAMA	$S_0/32\ \{(f_0/f)^5 + 13(f_0/f) + 9[1 + (f/f_0)^2]\}$	2.4×10^{-44}	400	75	6.7

The high-frequency cutoff f_u, as pointed out by Éanna Flanagan (private communication), needs to be high enough that the S/N degradation due to discrete time steps is less than that due to discrete choices of the templates' intrinsic parameters. Quantitatively, this requires that

$$\gamma_{00}/(2f_u)^2 < 1 - MM, \tag{3.3.5}$$

where γ_{00} is the time-time component of the metric before t_c is projected out [see Eq. (2.2.23)]. At any post-Newtonian order we have $\gamma_{00} = 1/2\,[J(1) - J(4)^2]$ [see Eq. (2.2.27)] and thus

$$f_u > \pi f_0 \sqrt{\frac{J(1) - J(4)^2}{2(1 - MM)}}. \tag{3.3.6}$$

We have chosen f_u to be double the right-hand side of this expression so that the loss due to sampling is 1/4 the loss due to discrete values of intrinsic parameters. There is probably a more clever way of optimizing f_u, but this is a first cut.

C. Number of templates and computational cost

We now proceed with the calculation of the number of templates needed to perform a single-pass, on-line search for gravitational-wave signals of the form in Eq. (3.3.1). for the noise spectra in Table 3.1. The prescription is essentially the same as in [22].

The first task is to obtain the intrinsic-parameter metric. We rewrite the waveform phase at 2PN order as

$$\begin{aligned}\Psi = &\frac{3}{5}\theta^1\left(\frac{f}{f_0}\right)^{-5/3} + \left[\frac{11\pi}{12}\frac{\theta^1}{\theta^2} + \frac{743}{2016}\left(\frac{25}{2\pi^2}\right)^{1/3}(\theta^1)^{1/3}(\theta^2)^{2/3}\right]\left(\frac{f}{f_0}\right)^{-1} \\ &-\frac{3}{2}\theta^2\left(\frac{f}{f_0}\right)^{-2/3} + \left[\frac{617\pi^2}{384}\frac{\theta^1}{(\theta^2)^2} + \frac{5429}{5376}\left(\frac{25\pi}{2}\right)^{1/3}\left(\frac{\theta^1}{\theta^2}\right)^{1/3}\right. \\ &\left.+\frac{15\,293\,365}{10\,838\,016}\left(\frac{5}{4\pi^4}\right)^{1/3}\frac{(\theta^2)^{4/3}}{(\theta^1)^{1/3}}\right]\left(\frac{f}{f_0}\right)^{-1/3}. \end{aligned} \tag{3.3.7}$$

We take the parameter-space gradient of the waveform phase,

$$\psi_i = \frac{\partial}{\partial\theta^i}\Psi(f), \tag{3.3.8}$$

by differentiating Eq. (3.3.7). The expressions are straightforward to obtain, but too lengthy and cumbersome to display here. The three-parameter metric (see Chapter 2) is given by

$$\gamma_{\alpha\beta} = \frac{1}{2}(\mathcal{J}[\psi_\alpha\psi_\beta] - \mathcal{J}[\psi_\alpha]\mathcal{J}[\psi_\beta]), \tag{3.3.9}$$

where $\mathcal{J}$ is the moment functional [22]

$$\mathcal{J}[a(f)] = \langle f^{-7/3}, a(f)\rangle / \int_0^\infty df\,\frac{f^{-7/3}}{S_h(f)}. \tag{3.3.10}$$

By inspection of Eq. (3.3.8) we see that $\gamma_{\alpha\beta}$ can be expanded in the form

$$\gamma_{\alpha\beta} = \sum_p a_p J(p), \tag{3.3.11}$$

where the moments of the noise are defined by

$$J(p) = \int_0^\infty df\,\frac{f^{-p/3}}{S_h(f)}. \tag{3.3.12}$$

We project out the coalescence time t_c to obtain

$$g_{ij} = \gamma_{ij} - \gamma_{0i}\gamma_{0j}/\gamma_{00}. \tag{3.3.13}$$

Next, we obtain the proper volume

$$V = \int d^2\theta \sqrt{\det \|g_{ij}\|} \tag{3.3.14}$$

of the region of interest. The boundaries of this region are set by the range of masses $[m_{\rm min}, m_{\rm max}]$ of the individual objects in binaries. It turns out that only $m_{\rm min}$ has a strong influence on V [22]. In the case of constant $\det g$ (which holds for 1PN waveforms), V can be obtained analytically using the coordinates (τ_0, τ_1) [27]. Beyond 1PN order in the waveform, the intrinsic parameter space is not flat, and thus the calculation of V is slightly more difficult. Since high precision is not needed, we take a Monte Carlo integral; in order to make the integrand as nearly constant as possible we use the metric tensor transformation law to switch to (τ_0, τ_1) (because in these coordinates the metric components are constant or nearly so). Finally, to obtain the number of templates we divide the proper volume V by the proper volume per template ΔV. For a hexagonal lattice, this is given by Eq. (3.2.11). The resulting values of $\mathcal{N}$ calculated for the noise spectra given in Table 3.1 are shown in Table 3.2.

These numbers are easily translated into the computational costs shown in Tables 3.3 and 3.4 using Eq. (3.2.14). To a good approximation, the length of the longest filter is given by

$$\begin{aligned} F &\simeq 2 f_u \tau_0 (f_0/f_s)^{8/3} \\ &= \frac{5}{32} f_u (\pi f_s)^{-8/3} (2 m_{\rm min})^{-5/3}. \end{aligned} \tag{3.3.15}$$

The storage required for all of the templates is then roughly given by

$$\mathcal{S} \simeq \mathcal{N} F. \tag{3.3.16}$$

Approximate scaling laws can be obtained as follows. The coordinate volume (using τ_0 and τ_1) of the region of interest goes as $f_0\tau_0 \times f_0\tau_1 \sim m_{\rm min}^{-8/3} f_0^{-8/3}$. At 1PN

order (where parameter space is flat) the proper volume scales likewise; therefore at higher post-Newtonian orders where the metric components are nearly constant in the (τ_0, τ_1) coordinates this scaling nearly holds. Inserting the dependence of the proper volume per template on the minimal match (3.2.11), we obtain

$$\mathcal{N} \sim (1 - MM)^{-1} m_{\rm min}^{-8/3} f_0^{-8/3}. \tag{3.3.17}$$

Taking Eq. (3.2.14), neglecting the weak logarithmic dependence, and noting that f_u is proportional to f_0, we find that

$$\mathcal{P} \sim (1 - MM)^{-1} m_{\rm min}^{-8/3} f_0^{-5/3}. \tag{3.3.18}$$

Multiplying the number of templates $\mathcal{N}$ by the length of each template F, the storage scales as

$$\mathcal{S} \sim (1 - MM)^{-1} m_{\rm min}^{-13/3} f_0^{-8/3} f_s^{-5/3}. \tag{3.3.19}$$

Note that the above scaling laws implicitly assume that f_0 or f_s is varied while holding the overall shape of the noise spectrum fixed, and thus are not reliable only for fairly small changes in f_0 or f_s.

IV. A TEMPLATE PLACEMENT ALGORITHM

In this Section we deal with the actual placement of the templates in the parameter space. The parameter space is shown in Fig. 3.1a in terms of the masses and in Fig. 3.1b in terms of chirp times τ_0 and τ_1, for searches in which the the maximum total mass of the system is 100 $M_\odot$ and the lower-cutoff in the mass of each component star is 0.2, 0.5 or $1.0 M_\odot$. The bottom line in Fig. 3.1a corresponds to binaries of equal mass ($\eta = 1/4$) with the right most point corresponding to lowest mass binaries and the left most to greatest mass binaries of our search. There are no binaries in the region below this line as the parameter η exceeds $1/4$ there, which is unphysical. The

TABLE 3.2. Numbers of templates $\mathcal{N}$ required to cover parameter space down to the stated $m_{\min}$ with a hexagonal grid at a minimal match of 0.97 using restricted post-Newtonian templates whose phase Ψ is accurate up to the indicated post-Newtonian order.

	$m_{\min} = 0.2M_\odot$			$m_{\min} = 1M_\odot$
Interferometer	1PN	1.5PN	2PN	2PN
LIGO I	1.8×10^5	4.3×10^5	3.7×10^5	8.4×10^3
LIGO II	8.0×10^5	1.5×10^6	1.3×10^6	3.1×10^4
LIGO III	4.4×10^6	6.1×10^6	5.3×10^6	1.3×10^5
VIRGO	2.3×10^6	4.6×10^6	4.0×10^6	9.2×10^5
GEO600	3.2×10^5	7.5×10^5	6.4×10^5	1.5×10^4
TAMA	3.9×10^4	1.3×10^5	1.1×10^5	2.4×10^3

TABLE 3.3. Computational costs obtained from the numbers of templates given in Table 3.2 assuming 2PN templates and both masses $> 0.2M_\odot$. F is the length of the longest template in real numbers.

Interferometer	$\log_2 F$	CPU power (flops)	Storage (reals)
LIGO I	22	1.4×10^{11}	1.6×10^{12}
LIGO II	23	3.4×10^{11}	1.1×10^{13}
LIGO III	26	1.1×10^{12}	3.6×10^{14}
VIRGO	26	3.9×10^{12}	2.7×10^{14}
GEO600	22	2.6×10^{11}	2.7×10^{12}
TAMA	21	1.0×10^{11}	2.3×10^{11}

TABLE 3.4. Same as Table 3.3 but for masses $> 1M_{\odot}$.

Interferometer	$\log_2 F$	CPU power (flops)	Storage (reals)
LIGO I	18	2.7×10^9	2.2×10^9
LIGO II	20	7.4×10^9	3.3×10^{10}
LIGO III	22	2.3×10^{10}	5.5×10^{11}
VIRGO	22	7.8×10^{11}	3.9×10^{12}
GEO600	18	5.3×10^9	3.9×10^9
TAMA	17	1.9×10^9	3.1×10^8

top and the left lines are determined by the minimum mass of component stars $m_{\rm min}$ and maximum total mass of the system, $M_{\rm max}$, respectively. Given the minimum mass of the component stars and the maximum total mass the parameter space of binaries is completely fixed. The area of the parameter space (and the corresponding number of templates required) is a sharp function of the lower-cutoff in the masses of the component stars and increases, as we have seen, as $m_{\rm min}^{-8/3}$.

The shape of the parameter space is rather complicated and attention needs to be paid in the placement of templates so that the inevitable *spill over* (see below) is minimal. Our implementation of the filter placement is motivated by the following astrophysical consideration: The observed neutron stars are all of roughly equal mass [32]. It is therefore to be expected that many inspiral signals will come from equal mass binaries. Consequently, we optimize filter placement for equal mass binaries. This is achieved by beginning our template placement along the $\eta = 1/4$ line [33]. Now, the span of each template is taken to be the largest rectangle (in a coordinate system in which the metric is locally diagonal) that can be inscribed inside the minimal match ellipse (we take $MM = 97\%$). Note that in Fig. 3.2 the spans do not appear rectangular because they are sheared by transforming from the locally diagonal coordinates to the (τ_0, τ_1) coordinates. We begin with the leftmost

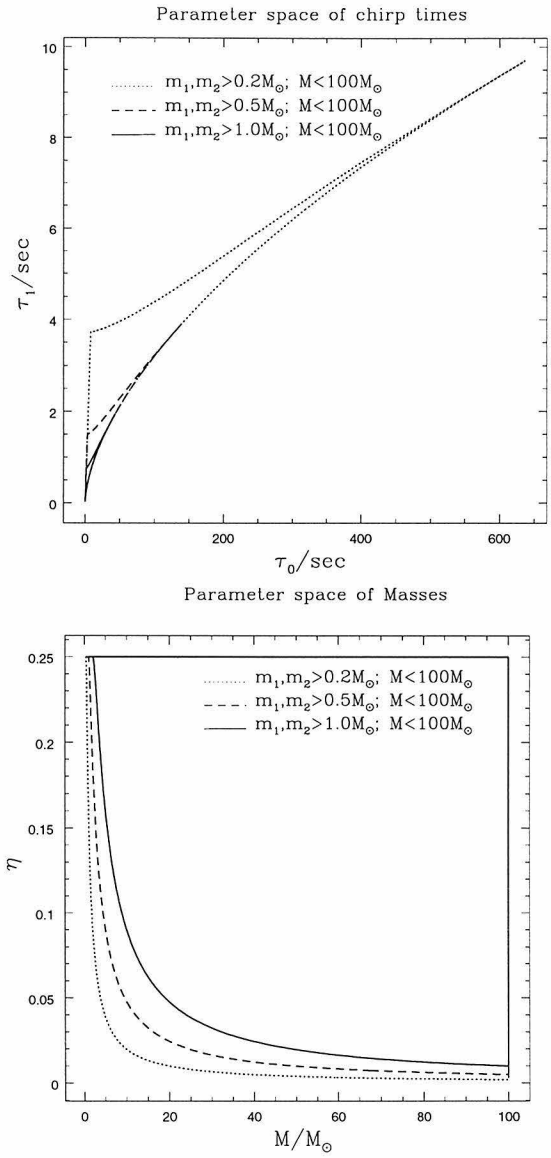

FIG. 3.1. The parameter space of search in terms of (a) masses of the component stars and (b) chirp times, for different values of the lower mass limits.

point on the bottom edge of the parameter space of Fig. 3.1, corresponding to the most massive binary of our search with the shortest chirp time. Such a system will, of course, consist of equal mass bodies and therefore our starting point is on the $\eta = 1/4$ curve. The next template is placed on the $\eta = 1/4$ curve at that location where the left edge of its rectangle touches the right edge of the previous template's rectangle. In a sense this is a straightforward generalization of placement of filters discussed in Ref. [22] along grid lines that are not necessarily straight. This optimal translation of templates is most easily done in a coordinate system in which the metric is locally diagonal.

Let (x_0, x_1) denote such a coordinate system (found by diagonalizing the two-dimensional matrix g_{ij}) and let $f(x_0, x_1) = 0$ denote a curve in the two-dimensional x_0–x_1 plane along which templates are to be placed. For instance, $\eta = 1/4$ in Fig. 3.1 is one such curve. A convenient point to begin is the point $(x_0^{(1)}, x_1^{(1)})$ at one end of the curve. In Fig. 3.2 we have sketched an arbitrary curve together with the first template and its span. The span of a template, for minimal matches close to 1, is an ellipse. However, its effective span, when setting up a lattice of templates, is only an inscribed polygon such as a rectangle or an irregular hexagon. In the following discussion we consider the span to be a rectangle and hence we will be setting up a rectangular lattice. By choosing a hexagonal lattice, the number of templates can be reduced by a maximum factor of $1/\sqrt{2}$ but the reduction is much less when the curve along which templates need to be placed is parallel to neither x_0 nor x_1 axis.

Given the 'local' distance between templates $(dx_0^{(1)}, dx_1^{(1)})$ we can get two points on the curve $f(x_0, x_1) = 0$ which are simultaneous solutions of $\{f(x_0, x_1) = 0, \quad x_0 = x_0^{(1)} + dx_0^{(1)}\}$ and $\{f(x_0, x_1) = 0, \quad x_1 = x_1^{(1)} + dx_1^{(1)}\}$, respectively. In order to cover the parameter space without leaving any 'holes' it is obvious that the next template should be placed at the point that is nearer to the first template. This is how one obtains the nearest neighbour of a template.

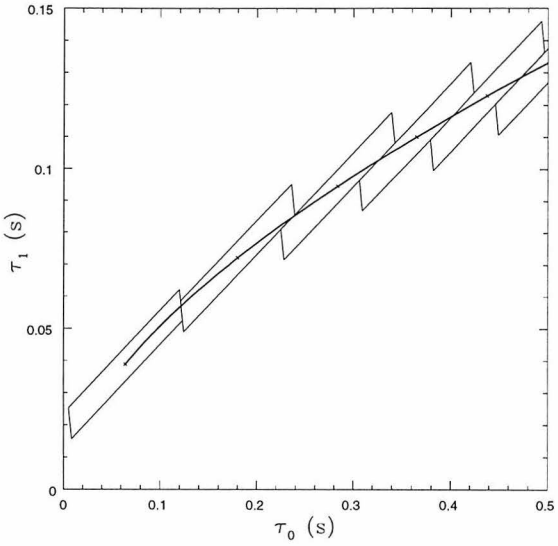

FIG. 3.2. Illustration of optimal translation of a template along an arbitrary curve.

Returning to our problem of placing templates in the parameter space of chirp times, we move along the $\eta = 1/4$ line till the binary of longest chirp time is reached. The set of templates chosen on the $\eta = 1/4$ curve form the base, on top of which we construct layers to fill the parameter space.

V. CONCLUSIONS

In this paper we have discussed the problem of optimally placing templates in a binary inspiral signal search. It is now recognized that a substantial reduction in computational cost can be achieved by carrying out a hiearchical search [25,26]. For a two-step hierarchical search strategy, in the first step a sparsely filled family of templates is used, with a threshold lower than what is acceptable based on the expected number of false alarms. Those events which cross this trigger threshold are further examined with a finer grid of templates chosen around the template that triggered the event. In such a hierarchical search, templates chosen in the first step will essentially be the same for each data segment. However, templates in the second step need to be changed from one data segment to the next, depending on which

templates from the coarse grid family produces an 'event'. It is in the case of a coarse grid that our analytical algorithm for template placement and analytical estimates of computational requirements fail and must be replaced by numerical methods that are very computationally expensive. But generating filters corresponding to the first step of the hierarchical search is more or less a one-time job. A finer grid is to be chosen quite frequently (essentially each time a possible event is selected in the first step) and in this case, fortunately, the analytical techniques discussed in this paper are quite accurate and one does not have to follow the time consuming numerical placement of templates.

For our templates we have used the restricted post^2-Newtonian waveform. We have made accurate (to within 10%) estimates of the computational costs of an on-line search of the inspiral waveform for all the long-baseline interferometeric detectors now under construction. We have addressed several important issues such as: (i) the density of templates in the parameter space, (ii) the set of parameters most suitable for easy placement of templates, (iii) the number of templates and computational resources needed to analyze the data on-line, (iv) distance up to which a given detector can 'detect' inspiral signals and the corresponding expected event rate, etc.

There are still several important assumptions made in this work: We have not treated the problem of searching the corners of parameter space where the precessing binaries live. Although requiring some effort to seek out, these systems could prove quite informative and astrophysically interesting. Also, we have used a crude relation between the minimal match and fraction of event rate lost. This could be improved by some statistical analysis such as begun by Mohanty [26]. Finally, our estimates assume that the optimal Wiener filter is employed in the data processing. It is important to explore the efficacy of non-linear filtering techniques as well as other powerful and novel data processing algorithms such as wavelets and time-frequency analysis, that have proven to be effective in a variety of other situations.

ACKNOWLEDGMENTS

Both authors were partially supported by NSF Grant PHY-9424337. BJO was also supported by the NSF graduate program. We are indebted to Bruce Allen, Kent Blackburn, Albert Lazzarini, Tom Prince, and Kip Thorne for fruitful conversations.

---

[1] A. Abramovici *et al.*, Science **256**, 325 (1992).

[2] B. Caron *et al.*, Class. Quantum Grav. **14**, 1461 (1997).

[3] H. Lück *et al.*, Class. Quantum Grav. **14**, 1471 (1997).

[4] K. Tsubono, in *Gravitational Wave Experiments* (World Scientific, Singapore, 1995), p. 112.

[5] R. Narayan, T. Piran, and A. Shemi, Astrophys. J. **379**, L17 (1991); E. S. Phinney, Astrophys. J. **380**, L17 (1991). In the intervening years two camps of astronomers have sprung up, some estimating lower event rates (based on statistics of the few known binary pulsars) and some higher (based on theoretical evolutions of progenitor populations), but their estimates have begun to converge again on the 1991 numbers. See [6] and [7] for recent examples of the high-rate and low-rate camps, respectively.

[6] S. F. P. Zwart and H. N. Spreeuw, Astron. Astrophys. **312**, 670 (1996).

[7] E. P. J. van den Heuvel and D. R. Lorimer, Mon. Not. R. Astron. Soc. **283**, L67 (1996); I. H. Stairs *et al.*, astro-ph/9712296.

[8] B. Barish *et al.*, LIGO Advanced Research and Development Proposal, Caltech/MIT, 1996 (unpublished).

[9] L. Blanchet, T. Damour, B. R. Iyer, C. M. Will, and A. G. Wiseman, Phys. Rev. Lett.

74, 3515 (1995).

[10] H. Tagoshi, M. Shibata, T. Tanaka, and M. Sasaki, Phys. Rev. D **54**, 1439 (1996).

[11] Some physicists are in the habit of calling this optimal filtering method simply "Wiener filtering." However, in the larger signal processing community, "Wiener filtering" refers to an altogether different technique. In order to avoid confusion we call this method "matched filtering."

[12] C. W. Helstrom, *Statistical Theory of Signal Detection*, 2nd edition (Pergamon Press, London, 1968).

[13] T. A. Apostolatos, Phys. Rev. D **52**, 605 (1995).

[14] S. Droz and E. Poisson, Phys. Rev. D **56**, 4449 (1997).

[15] T. Damour, B. R. Iyer and B. S. Sathyaprakash, Phys. Rev. D **57**, 885 (1998).

[16] R. Balasubramanian and S. V. Dhurandhar, Phys. Rev. D **50**, 6080 (1994).

[17] A. Królak, K. D. Kokkotas, and G. Schäfer, Phys. Rev. D **52**, 2089 (1995).

[18] B. S. Sathyaprakash, Phys. Rev. D **50**, R7111 (1994).

[19] B. S. Sathyaprakash and S. V. Dhurandhar, Phys. Rev. D **44**, 3819 (1991).

[20] B. S. Sathyaprakash and S. V. Dhurandhar, J. Comput. Phys. **109**, 215 (1993).

[21] S. V. Dhurandhar and B. S. Sathyaprakash, Phys. Rev. D **49**, 1707 (1994).

[22] B. J. Owen, Phys. Rev. D **53**, 6749 (1996).

[23] B. F. Schutz, in *The Detection of Gravitational Radiation,* edited by D. Blair (Cambridge University Press, Cambridge, England, 1991), p. 406.

[24] T. A. Apostolatos, Phys. Rev. D **54**, 2421 (1996).

[25] S. D. Mohanty and S. V. Dhurandhar, Phys. Rev. D **54**, 7108 (1996).

[26] S. D. Mohanty, Phys. Rev. D **57**, 630 (1998).

[27] B. Allen, "GRASP: a data analysis package for gravitational wave detection," version 1.6.2. Available on request from the URL http://www.ligo.caltech.edu/LIGO_web/Collaboration/lsc_interm.html.

[28] C. Cutler and É. É. Flanagan, Phys. Rev. D **49**, 2658 (1994).

[29] R. Balasubramanian, B. S. Sathyaprakash and S. V. Dhurandhar, Phys. Rev. D **53**, 3033 (1996); **54**, 1869(E) (1996).

[30] P. C. Peters, Phys. Rev. **136**, B1224 (1964).

[31] E. Poisson and C. M. Will, Phys. Rev. D **52**, 848 (1995).

[32] J. H. Taylor, Rev. Mod. Phys. **66**, 711 (1994).

[33] In the development of a numerical code that generates templates, care should be exercised in placing filters along the $\eta = 1/4$ line. Normally, the routines use chirp times τ_0 and τ_1 to generate templates. As remarked in the text there are no binaries below this line and even slight numerical errors in specifying the values of τ_0 and τ_1 such that the point in question lies below the equal mass binary line will cause the numerical code to crash.

[34] B. J. Owen, L. Lindblom, C. Cutler, B. F. Schutz, A. Vecchio, and N. Andersson, submitted to Phys. Rev. D (gr-qc/9804044).

Chapter 4 Nonprecessional spin-orbit effects on gravitational waves from inspiraling compact binaries to second post-Newtonian order

Written with Hideyuki Tagoshi and Akira Ohashi

Appeared in Phys. Rev. D **57**, 6168 (1998)

We derive all second post-Newtonian (2PN), non-precessional effects of spin-orbit coupling on the gravitational wave forms emitted by an inspiraling binary composed of spinning, compact bodies in a quasi-circular orbit. Previous post-Newtonian calculations of spin-orbit effects (at 1.5PN order) relied on a fluid description of the spinning bodies. We simplify the calculations by introducing into post-Newtonian theory a δ-function description of the influence of the spins on the bodies' energy-momentum tensor. This description was recently used by Mino, Shibata, and Tanaka (MST) in Teukolsky-formalism analyses of particles orbiting massive black holes, and is based on prior work by Dixon. We compute the 2PN contributions to the wave forms by combining the MST energy-momentum tensor with the formalism of Blanchet, Damour, and Iyer for evaluating the binary's radiative multipoles, and with the well-known 1.5PN order equations of motion for the binary. Our results contribute at 2PN order only to the amplitudes of the wave forms. The secular evolution of the wave forms' phase—the quantity most accurately measurable by LIGO—is not affected by our results until 2.5PN order, at which point other spin-orbit effects also come into play. We plan to evaluate the entire 2.5PN spin-orbit contribution to the secular phase evolution in a future paper, using the techniques of this paper.

I. INTRODUCTION

Inspiraling compact binaries are one of the main classes of gravitational wave source to be targeted by the coming generation of ground-based laser interferometers such as LIGO, VIRGO, GEO600, and TAMA [1]. There are two reasons for this. First, binary coalescences are expected to occur fairly often within detection range

of "enhanced" interferometers [2]. Astronomical lore estimates several neutron-star–neutron-star coalescences per year within 200 Mpc [3,4] and a similar rate of black-hole–black-hole coalescences within 200 Mpc to 1 Gpc [4–6]. Second, the signal from the final moments of inspiral is characterized by a complicated phase evolution containing detailed information about the physical parameters of the binary, such as the masses of the bodies and their spins about their own axes [1].

Because inspiral signals have such a complicated structure, and because they last many cycles within the frequency bands of ground-based interferometers, they are ideal candidates for the use of matched filtering [7]. Matched filtering, a signal-processing technique well-studied in the context of radar, can be used both to search for signals in noisy data and to estimate parameters once a signal is found. Matched filtering essentially entails cross-correlating noisy interferometer data with a set of theoretical template wave forms. If a template wave form is a good approximation to the signal wave form, the cross-correlation enhances the signal-to-noise ratio. In the context of matched filtering, a good approximation means (roughly speaking) one in which the phase evolution of the template matches that of the signal to within a half cycle out of the total spent in an interferometer's band. Because signals are expected to last up to tens of thousands of cycles in the bands of some interferometers, the templates must match any possible signal to a correspondingly high degree of precision.

Currently there is no exact solution to the generic two-body problem in general relativity. Thus, inspiral wave-form templates are constructed using approximation schemes which must be carried out to high precision to be useful for matched filtering. These approximation schemes can be broadly grouped into two categories, the post-Newtonian approach and the black-hole perturbation approach.

The post-Newtonian approach is the longtime standard for gravitational wave generation. It involves expanding the Einstein equations and equations of motion

in powers of the binary's orbital velocity v/c and gravitational potential $GM/rc^2 \sim (v/c)^2$, where the order in GM/rc^2 is referred to as the post-Newtonian (PN) order. Concurrently, the gravitational wave forms and luminosity are expanded in terms of time derivatives of symmetric, trace-free (STF) radiative multipoles, which are expressed as integrals of the matter source and gravitational fields. The radiative multipoles are combined with post-Newtonian equations of motion to yield explicit expressions for the wave forms, including the secular evolution of orbital phase and frequency due to radiation reaction. Recent summaries of the two main versions of the post-Newtonian approach are given by Blanchet, Damour, and Iyer [8] and by Will and Wiseman [9]. The post-Newtonian expansion of the wave forms of a binary currently has been carried out to 2.5PN order [10] [i.e., to $O(v/c)^5$ beyond leading order radiation reaction and $O(v/c)^5$ beyond Newtonian gravity in all non-radiation reaction effects] in the case where the two bodies orbit in a quasicircular fashion and do not spin about their own axes. (By "quasicircular" we mean orbits that are circular aside from gradual inspiral due to gravitational radiation reaction.)

In the case where the bodies do spin, there are three types of spin effects to be considered. Effects of the first type, due to precession of the plane of the orbit, modulate the amplitude and frequency of the gravitational radiation in a complicated, non-monotonic fashion. Secular or dissipative effects, due to radiation reaction, contribute to the (monotonic) phase and frequency evolution of the orbit; and non-dissipative effects contribute directly to the amplitudes of the various harmonics of orbital frequency in the wave forms, without affecting their phase evolution. All three types of effects can be further divided into spin-orbit contributions (i.e., terms involving one spin only) and spin-spin contributions (interactions between spins). Precessional effects were first extensively investigated by Apostolatos *et al.* [11] and by Kidder [12], and were found to complicate matters considerably. Therefore, like most other treatments of spin, ours will investigate the case where there is no precession—i.e., the

spins are parallel or antiparallel to the orbital angular momentum—leaving precession for future studies.

Non-precessional spin effects have been evaluated by Kidder, Will, and Wiseman [13,12] only to lowest order: 1.5PN for dissipative (and 1PN for non-dissipative) spin-orbit effects, and 2PN for spin-spin effects.* The main reason for the discrepancy in progress between the spinning and nonspinning cases is the form of the matter source used in the Einstein equations. In the nonspinning case one can write the energy-momentum tensor as a Dirac δ-function, which greatly simplifies the calculations. In order to derive spin effects, however, Refs. [13,12] treated the bodies as uniformly rotating balls of perfect fluid. The perfect fluid energy-momentum tensor was integrated over a finite spatial volume, which made the multipole integrals much more cumbersome than in the δ-function case and introduced additional complications in the definition of the binary's center of mass. The net result was that spin calculations at a given post-Newtonian order seemed to require as much effort as spinless calculations at higher order, and spin calculations were not pursued any further with this approach. (An additional difficulty is the lack of higher post-Newtonian order spin corrections to the equations of motion, which are difficult to obtain for fluid balls.)

The more recent black-hole perturbation approach obtains high-order (in some cases exact) expressions for the influence of radiation reaction on the orbital phase which are valid in the limit of extreme mass ratio. The basis of this approach is the perturbation of known, exact solutions of the Einstein equations (the Schwarzschild

---

*Like non-spin effects, spin effects appear in the secular phase evolution of the wave forms at a certain order, and at every order in v/c (0.5PN order) beyond it except for the first. Thus, dissipative spin-orbit effects appear at 1.5PN, 2.5PN, 3PN... orders and spin-spin effects appear at 2PN, 3PN, 3.5PN... orders.

and Kerr spacetimes) with a test body using the Teukolsky equation [14] or an equivalent. During the last several years, analytical techniques for post-Newtonian expansion in the context of the black-hole perturbation approach have been developed to very high orders in v/c (for recent reviews, see [15]). However, most black-hole perturbation papers treat the test body as a nonspinning point particle with a δ-function energy-momentum tensor, and thus do not give results for the case of two spinning bodies.

Recently, the black-hole perturbation approach has been extended to the case of two spinning bodies [16,17]. In [16], Mino, Shibata, and Tanaka calculated the gravitational wave forms and radiation reaction of a spinning particle falling into a Kerr black hole. In [17], Tanaka *et al.* obtained an expression for the non-precessional 2.5PN spin-orbit contribution to the secular phase evolution of a binary composed of a spinning test particle in quasicircular orbit around a Kerr black hole. These results were obtained using an energy-momentum tensor for the test body which mimics the effects of an extended, spinning object but can be expressed in terms of a δ-function for ease of calculation. This "spinning-particle" δ-function energy-momentum tensor is based on the work of Dixon [18]. We call it the MST tensor after Mino, Shibata, and Tanaka [16], who distilled it into the compact form we will use.

In this paper, we use the MST energy-momentum tensor for the first time in the curved-space, post-Newtonian approach to derive new gravitational-wave generation results. (Cho [19], in work parallel to our own, has recently used a similar approach to re-derive the wave forms of Kidder, Will, and Wiseman [13] in a slightly different form.) We reproduce (with a shorter calculation) the 1PN and 1.5PN spin-orbit corrections to the radiative multipoles derived in [12]. We also derive all of the (previously unknown) 2PN non-precessional spin-orbit corrections to the wave forms, by calculating 2PN spin-orbit corrections to the radiative multipoles and combining them with the well-known 1.5PN equations of motion (in which there is no 2PN spin-

orbit term). Because of the harmonics of the orbital frequency involved, there is no 2PN spin-orbit contribution to the radiation reaction-induced secular phase evolution of the wave forms (the most accurately measurable effect).

In the future, we plan to use the methods of this paper to calculate all the non-precessional 2.5PN spin-orbit effects, including the nonvanishing radiation reaction and resulting secular evolution of the frequency and phase of the wave forms. That secular evolution is likely to be quite important for data analysis. Investigations by Tagoshi *et al.* [20], comparing post-Newtonian expansions to exact numerical results in the test-mass limit, indicate that spin effects are important for extraction of information from observed waves at least up through 3PN order. To obtain the 2.5PN secular evolution requires the calculation not only of additional radiative multipoles, but also of the 2.5PN spin-orbit corrections to the equations of motion. The latter problem is qualitatively different (and more difficult); thus we will address it in a future paper.

This paper is organized as follows. In Sec. II we present the MST energy-momentum tensor [16] and review its properties. In Sec. III we review the post-Newtonian expansions of basic variables used in our calculations. Then in Sec. IV we calculate the STF radiative multipoles needed to obtain the 2PN spin-orbit terms in the wave forms. In Sec. V we evaluate all the 2PN (non-precessional) spin-orbit terms in the wave forms of a binary in quasicircular orbit with spins parallel or antiparallel to the orbital angular momentum, and in Sec. VI we briefly discuss their significance. In an Appendix we use our methods to derive the 1PN and 1.5PN STF radiative multipoles, and compare with the results of Refs. [13,12].

Throughout this paper, we use units such that Newton's gravitational constant and the speed of light equal unity. We also use the tensor notation conventions of [8,9]: curved brackets () on tensor indices to indicate symmetrization, square brackets [] to indicate antisymmetrization, and angled brackets $\langle\rangle$ or the superscript STF to

indicate the symmetric trace-free part. A capitalized superscript L indicates a multi-index $i_1 \cdots i_\ell$; e.g., I^L represents I^{ijk} in the case $\ell = 3$. We also write outer products of vectors in shorthand; e.g., $x^{ijk} = x^i x^j x^k$ and $x^L = x^{i_1} \cdots x^{i\ell}$. Greek indices run from 0 to 3, and Latin indices from 1 to 3.

II. SPINNING PARTICLE ENERGY-MOMENTUM TENSOR

Our starting point is the spinning particle energy-momentum tensor given in terms of the Dirac δ-function [16],

$$T^{\alpha\beta}(x) = \int d\tau \left\{ p^{(\alpha}(x,\tau)\, u^{\beta)}(x,\tau) \frac{\delta^{(4)}(x - z(\tau))}{\sqrt{-g}} - \nabla_\gamma \left[S^{\gamma(\alpha}(x,\tau) u^{\beta)}(x,\tau) \frac{\delta^{(4)}(x - z(\tau))}{\sqrt{-g}} \right] \right\}. \tag{4.2.1}$$

Here $z^\mu(\tau)$ is the worldline of the particle, $u^\mu(\tau) = dz^\mu/d\tau$, $p^\mu(\tau)$ is the particle's linear momentum, and $S^{\mu\nu}(\tau)$ is an antisymmetric tensor representing the particle's spin angular momentum. We focus only on spin-orbit interactions, i.e. discard all terms higher than first order in spin. In this case τ becomes the particle's proper time and u^μ becomes its four-velocity [see Eq. (2.4) of Ref. [16]].

The bitensors $p^\alpha(x,\tau)$, $u^\alpha(x,\tau)$, and $S^{\alpha\beta}(x,\tau)$ are spacetime extensions of p^μ, u^μ, and $S^{\mu\nu}$ away from the particle's worldline,[†] defined by

$$p^\alpha(x,\tau) = \bar{g}^\alpha{}_\mu(x, z(\tau)) p^\mu(\tau), \tag{4.2.2a}$$

$$u^\alpha(x,\tau) = \bar{g}^\alpha{}_\mu(x, z(\tau)) u^\mu(\tau), \tag{4.2.2b}$$

$$S^{\alpha\beta}(x,\tau) = \bar{g}^\alpha{}_\mu(x, z(\tau)) \bar{g}^\beta{}_\nu(x, z(\tau)) S^{\mu\nu}(\tau). \tag{4.2.2c}$$

Here $\bar{g}^\alpha{}_\mu(x,z)$ is a bitensor of parallel displacement with the properties

---

[†]We use indices α, β, ... to denote quantities associated with the field point x, and μ, ν, ... to denote those associated with the worldline $z(\tau)$.

$$\lim_{x\to z} \bar{g}^{\alpha}{}_{\mu}(x, z(\tau)) = \delta^{\alpha}_{\mu}, \tag{4.2.3a}$$

$$\lim_{x\to z} \nabla_{\beta}\, \bar{g}^{\alpha}{}_{\mu}(x, z(\tau)) = 0. \tag{4.2.3b}$$

The definition of $S^{\mu\nu}$ is arbitrary up to the choice of a spin supplementary condition (the analog of a gauge condition). We use

$$S^{\mu\nu} u_{\mu} = 0. \tag{4.2.4}$$

Note that in post-Newtonian theory at least three spin supplementary conditions are in common use. We choose (4.2.4) because it makes our radiative multipoles consistent with the standard post-Newtonian equations of motion, thus simplifying the calculations (cf. Ref. [12], Appendix A). We introduce a spin vector S^{μ} which is related to the spin tensor by

$$S^{\mu\nu} = \epsilon^{\mu\nu\rho\sigma} u_{\rho} S_{\sigma}, \tag{4.2.5a}$$

$$S^{\mu} u_{\mu} = 0, \tag{4.2.5b}$$

where $\epsilon^{\mu\nu\rho\sigma}$ is the Levi-Civita tensor.[‡] The spin supplementary condition is identically satisfied by (4.2.5a). On the other hand, we need to impose the condition (4.2.5b) on S^{μ} to fix the one remaining degree of freedom S^{0}.

For later convenience, we separate the MST energy-momentum tensor (4.2.1) into the usual point-particle piece (the first term) plus a spin-orbit piece,

$$T^{\alpha\beta}_{(\mathrm{SO})}(x) = -\int d\tau\, \nabla_{\gamma} \left[S^{\gamma(\alpha} u^{\beta)} \frac{\delta^{(4)}(x - z(\tau))}{\sqrt{-g}} \right]. \tag{4.2.6}$$

When evaluating the radiative multipoles of a system of masses, we encounter integrals of the form

$$\int d^3x\, F^{L}(x) T^{\alpha\beta}(x). \tag{4.2.7}$$

[‡]We use the convention defined in Eq. (8.10) of Ref. [21].

The spin-orbit contribution to this expression can be evaluated by substituting (4.2.6), using Leibniz' rule to rewrite the integral, and discarding the spatial integral of a three-divergence. The result for a many-body system is

$$\int d^3x\, F^L(x) T^{\alpha\beta}_{(\mathrm{SO})}(x) = \sum_A \Bigg[S_A^{\gamma(\alpha} v_A^{\beta)} \frac{\partial_\gamma F^L}{\sqrt{-g}} - \partial_0 \left(S_A^{0(\alpha} v_A^{\beta)} \frac{F^L}{\sqrt{-g}} \right) - \left(\Gamma^\gamma{}_{\gamma\delta} S_A^{\delta(\alpha} v_A^{\beta)} + S_A^{\gamma(\alpha} \Gamma^{\beta)}{}_{\gamma\delta} v_A^\delta \right) \frac{F^L}{\sqrt{-g}} \Bigg], \tag{4.2.8}$$

where A labels the bodies, $v^\alpha = u^\alpha/u^0$, and ∂_γ is shorthand for $\partial/\partial x^\gamma$ evaluated at $x = x_A$.

III. POST-NEWTONIAN EXPANSIONS OF BASIC VARIABLES

We now switch from fully covariant expressions to post-Newtonian expansions in harmonic coordinates. Spatial indices on the right hand sides of the equations in this section can be raised and lowered freely with the Kronecker δ. We use the expansion parameter ϵ which is related to the orbital variables by $\epsilon \sim M/r \sim v^2$, where M is the total mass of the system, r is the orbital separation, and v the orbital velocity. We assume the bodies are compact, i.e. each body's spin has magnitude $|\boldsymbol{S}_A| \sim \chi m_A^2$, where χ is of order unity (see [12] for further discussion).

When evaluating the post-Newtonian expansions of basic variables in this section and the radiative multipoles in Sec. IV, we encounter divergent expressions—in our case, self-interaction terms. Such divergences are inevitable when using any δ-function source, and we follow previous authors in discarding them (see the discussion at the end of Ref. [8], Sec. II). We do not claim any rigorous justification for doing so; however, since it is asserted in the non-spinning case [8] that this procedure can be justified to $O(\epsilon^2)$, and since we consider corrections only up to $O(\epsilon)$ beyond lowest order spin effects, we expect that the formal use of the δ-function is justified to the same degree as in the non-spinning case. Informally, we note that the usual post-

Newtonian equations of motion for spinning bodies can be obtained by taking the divergence of the MST energy-momentum tensor (4.2.1) and discarding self-interaction divergences [16].

The metric components in harmonic coordinates are well known [9] as

$$g_{00} = -[1 - 2U + O(\epsilon^2)], \tag{4.3.1a}$$

$$g_{i0} = O(\epsilon^{3/2}), \tag{4.3.1b}$$

$$g_{ij} = \delta_{ij}[1 + 2U + O(\epsilon^2)], \tag{4.3.1c}$$

$$\sqrt{-g} = 1 + 2U + O(\epsilon^{3/2}), \tag{4.3.1d}$$

where only the lowest-order expression for the potential U is needed,

$$U(\boldsymbol{x}) = \sum_A \frac{m_A}{|\boldsymbol{x} - \boldsymbol{x}_A|} + O(\epsilon^2). \tag{4.3.2}$$

By differentiating (III), we find the dominant Christoffel symbols

$$\Gamma^0_{i0} = \Gamma^i{}_{00} = -a^i, \tag{4.3.3a}$$

$$\Gamma^i{}_{jk} = \delta^{ij}a^k + \delta^{ik}a^j - \delta^{jk}a^i, \tag{4.3.3b}$$

where $a^i = \partial_i U$. All others are of higher post-Newtonian order, and can be neglected for the purposes of this paper. The metric components (III), together with the condition $u^\mu u_\mu = -1$, give us the expansion of the four-velocity

$$u^0 = 1 + \left(\frac{v^2}{2} + U\right) + O(\epsilon^2), \tag{4.3.4a}$$

$$u^i = v^i \left[1 + \left(\frac{v^2}{2} + U\right) + O(\epsilon^2)\right]. \tag{4.3.4b}$$

We express the components of the spin tensor in terms of the spatial components of the spin vector by combining (4.2.5a), (4.2.5b), (III), and (III) to obtain

$$S^{i0} = (\boldsymbol{v} \times \boldsymbol{S})^i + O(\epsilon^{3/2}), \tag{4.3.5a}$$

$$S^{ij} = \epsilon^{ijk}\left[(1 + \frac{1}{2}v^2 - U)S^k - (\boldsymbol{v} \cdot \boldsymbol{S})v^k\right] + O(\epsilon^2), \tag{4.3.5b}$$

where ϵ^{ijk} is from here on used to indicate the antisymmetric symbol $[ijk]$. Substituting (III) back into (4.2.6), we find that the post-Newtonian orders of the components of $T^{\alpha\beta}_{(\mathrm{SO})}$ are

$$T^{00}_{(\mathrm{SO})} \sim T^{ij}_{(\mathrm{SO})} \sim m\frac{mv}{r} \sim m \times O(\epsilon^{3/2}), \tag{4.3.6a}$$

$$T^{i0}_{(\mathrm{SO})} \sim m\frac{m}{r} \sim m \times O(\epsilon), \tag{4.3.6b}$$

where m is the mass of either body. This contrasts with the point-mass order counting,

$$T^{00}_{(\mathrm{PM})} \sim m, \tag{4.3.7a}$$

$$T^{i0}_{(\mathrm{PM})} \sim m \times O(\epsilon^{1/2}), \tag{4.3.7b}$$

$$T^{ij}_{(\mathrm{PM})} \sim m \times O(\epsilon). \tag{4.3.7c}$$

We also note that the second and third terms on the right hand side of (4.2.8) are $O(\epsilon)$ with respect to the first if F^L is an outer product of position vectors (as is the case when computing multipoles).

IV. STF RADIATIVE MULTIPOLES

In this section we calculate the symmetric, trace-free (STF) radiative multipoles necessary to obtain the 2PN spin-orbit contributions to the wave form. In Sec. IV C we specialize to the case of non-precessing orbits.

The STF radiative multipoles are given to $O(\epsilon^{5/2})$ by Blanchet [Eq. (4.3) of Ref. [10]]. However, we only need the $O(\epsilon)$ expressions

$$\begin{aligned} I^L(t) = {} & \int d^3x\, \hat{x}^L \left(T^{00} + T^{ii}\right) - \frac{4(2\ell+1)}{(\ell+1)(2\ell+3)}\frac{d}{dt}\int d^3x\, \hat{x}^{La} T^{0a} \\ & + \frac{1}{2(2\ell+3)}\frac{d^2}{dt^2}\int d^3x\, \hat{x}_L |\boldsymbol{x}|^2 \left(T^{00} + T^{ii}\right) + O(\epsilon^2), \end{aligned} \tag{4.4.1}$$

$$\begin{aligned} J^L(t) = {} & \epsilon^{ab\langle i}\left[\int d^3x\, \hat{x}^{L-1\rangle a}(1+4U)T^{0b} - \frac{2\ell+1}{(\ell+2)(2\ell+3)}\frac{d}{dt}\int d^3x\, \hat{x}^{L-1\rangle ac} T^{bc}\right. \\ & \left. + \frac{1}{2(2\ell+3)}\frac{d^2}{dt^2}\int d^3x\, \hat{x}^{L-1\rangle a}|\boldsymbol{x}|^2 T^{0b}\right] + O(\epsilon^2), \end{aligned} \tag{4.4.2}$$

where $\hat{x}^L$ denotes the symmetric trace-free part of x^L. We also define $I^L_{(\mathrm{SO})}$ and $J^L_{(\mathrm{SO})}$ by substituting $T^{\mu\nu}_{(\mathrm{SO})}$ for $T^{\mu\nu}$ in (4.4.1) and (4.4.2). In (4.4.1) and (4.4.2) we have discarded self-interaction terms, which are always divergent when using a δ-function source. We have also discarded terms involving only gravitational potentials (referred to as "non-compact" terms in [8]), whose spin-orbit contributions do not appear until higher post-Newtonian orders than considered in this paper.

Spin-orbit corrections to the multipoles and wave form follow an order-counting scheme different from the usual point-mass terms. Substituting (III) into (4.4.1) and (4.4.2), we find that the lowest order spin-orbit correction to a multipole appears in the current quadrupole $J^{ij}_{(\mathrm{SO})}$ [12]. This term contributes to the wave-form amplitude at 1PN order, but because it is a subharmonic of the dominant (mass quadrupole) radiation, it does not contribute to the radiation reaction until 1.5PN order. The next-order effects appear in the current octupole $J^{ijk}_{(\mathrm{SO})}$ and the mass quadrupole $I^{ij}_{(\mathrm{SO})}$, and contribute to the wave forms and radiation reaction at 1.5PN order. (These are the terms given in [13]; we evaluate them with our methods in the appendix.) Following this progression, the 2PN wave forms require evaluation of $J^{ijk\ell}_{(\mathrm{SO})}$ and $I^{ijk}_{(\mathrm{SO})}$ to lowest order, and of $J^{ij}_{(\mathrm{SO})}$ to $O(\epsilon)$ beyond lowest order.

A. N-body case

We first evaluate the spin-orbit contributions to the multipole integrals (4.4.1) and (4.4.2) as sums over N bodies.

The expression for the current hexadecapole is the easiest to evaluate. It is needed only to lowest order and thus involves only the first term in (4.4.2),

$$J^{ijk\ell}_{(\mathrm{SO})} = \epsilon^{ab\langle i} \int d^3x\, \hat{x}^{jk\ell\rangle a} T^{0b}_{(\mathrm{SO})}, \tag{4.4.3}$$

which is straightforwardly obtained from the first term of (4.2.8) as

$$J^{ijk\ell}_{(\mathrm{SO})} = \frac{5}{2} \sum_A \left(S^i_A x^{jk\ell}_A \right)^{\mathrm{STF}}. \tag{4.4.4}$$

The mass octupole is also needed only to lowest order,

$$I^{ijk}_{(\mathrm{SO})} = \int d^3x\, \hat{x}^{ijk} \left(T^{00}_{(\mathrm{SO})} + T^{aa}_{(\mathrm{SO})} \right) - \frac{7}{9}\frac{d}{dt} \int d^3x\, \hat{x}^{ijka} T^{0a}_{(\mathrm{SO})}. \tag{4.4.5}$$

Again, using the first term of (4.2.8) it is straightforward to evaluate the integrals. When evaluating the time derivative in the second term we neglect time derivatives of the spins (i.e., precession). We could do this even if considering spin precession, because those derivatives appear $O(\epsilon)$ beyond the spins themselves [cf. Eqs. (F18,F19) of Ref. [9], where due to a typographical error a factor of $(M/r)^3$ was omitted from in front of the last term in each equation].[§] We are left with

$$I^{ijk}_{(\mathrm{SO})} = \sum_A \left[\frac{9}{2} (\boldsymbol{v}_A \times \boldsymbol{S}_A)^i x_A^{jk} - 3 (\boldsymbol{x}_A \times \boldsymbol{S}_A)^i x_A^j v_A^k \right]^{\mathrm{STF}} \tag{4.4.6}$$

Because the two-index current moment is needed to $O(\epsilon)$ we must keep all three terms in (4.4.2),

$$J^{ij}_{(\mathrm{SO})} = \epsilon^{ab\langle i} \left[\int d^3x\, \hat{x}^{j\rangle a} (1 + 4U) T^{0b}_{(\mathrm{SO})} - \frac{5}{28}\frac{d}{dt} \int d^3x\, \hat{x}^{j\rangle ac} T^{bc}_{(\mathrm{SO})} + \frac{1}{14}\frac{d^2}{dt^2} \int d^3x\, \hat{x}^{j\rangle a} T^{0b}_{(\mathrm{SO})} \right]. \tag{4.4.7}$$

Again, time derivatives of the spins appear only in higher-order terms and may be discarded at this order. Carefully evaluating the integrals according to (4.2.8), we obtain

$$\begin{aligned} J^{ij}_{(\mathrm{SO})} = \sum_A \Big[& \frac{3}{2} x_A^i S_A^j + \frac{1}{14} \boldsymbol{v}_A \cdot \boldsymbol{x}_A v_A^i S_A^j + \frac{2}{7} \boldsymbol{S}_A \cdot \boldsymbol{x}_A v_A^{ij} + \frac{11}{28} |\boldsymbol{x}_A|^2 a_A^i S_A^j - \\ & \frac{17}{7} \boldsymbol{S}_A \cdot \boldsymbol{v}_A x_A^i v_A^j + \frac{1}{7} \boldsymbol{a}_A \cdot \boldsymbol{S}_A x_A^{ij} - \frac{17}{14} \boldsymbol{S}_A \cdot \boldsymbol{x}_A x_A^i a_A^j + (\frac{3}{2} U_A + \frac{43}{28} |\boldsymbol{v}_A|^2 + \\ & \frac{11}{14} \boldsymbol{a}_A \cdot \boldsymbol{x}_A) x_A^i S_A^j \Big]^{\mathrm{STF}} \end{aligned} \tag{4.4.8}$$

[§]Although we do not consider spin precession in this paper, the N-body and two-body multipoles we present are (instantaneously) valid even in the precessing case. One simply has to put in the spin vectors as (slowly varying) functions of time—which is easier said than done.

In addition to the spin-orbit multipoles, we need the lowest order contributions to I^{ijk} and J^{ij} from the usual point-mass energy-momentum tensor. These multipoles are given by

$$I^{ijk}_{(\mathrm{PM})} = \sum_A m_A x_A^{\langle ijk\rangle}, \tag{4.4.9}$$

$$J^{ij}_{(\mathrm{PM})} = \sum_A m_A (\boldsymbol{x}_A \times \boldsymbol{v}_A)^{\langle i} x_A^{j\rangle} \tag{4.4.10}$$

and contribute to the wave forms at 0.5PN order.

B. Two-body case

We now specialize to the case of two bodies of mass m_1 and m_2 in an arbitrary (possibly precessing) orbit, and express the multipoles in terms of the relative coordinate $\boldsymbol{x}$ (whose origin is at body 2).

It is convenient to use the mass parameters

$$M = m_1 + m_2, \tag{4.4.11a}$$

$$\eta = m_1 m_2 / M^2, \tag{4.4.11b}$$

$$\Delta = (m_1 - m_2)/M. \tag{4.4.11c}$$

It is also convenient to use the dimensionless, symmetrized spin parameters introduced by Will and Wiseman [9],

$$\boldsymbol{\chi}_a = \frac{1}{2}\left(\frac{\boldsymbol{S}_1}{m_1^2} - \frac{\boldsymbol{S}_2}{m_2^2}\right), \tag{4.4.12a}$$

$$\boldsymbol{\chi}_s = \frac{1}{2}\left(\frac{\boldsymbol{S}_1}{m_1^2} + \frac{\boldsymbol{S}_2}{m_2^2}\right), \tag{4.4.12b}$$

We eliminate the potentials and accelerations in (4.4.8) with the well-known Newtonian expressions

$$U_A = U(\boldsymbol{x}_A) = \frac{m_B}{r}, \tag{4.4.13}$$

$$\boldsymbol{a}_A = \frac{-M}{r^3}\boldsymbol{x}_A, \tag{4.4.14}$$

where $B \neq A$ and $r = |\boldsymbol{x}|$.

The spins of the bodies introduce a correction to the relation between $\boldsymbol{x}_1$, $\boldsymbol{x}_2$, and the relative coordinate $\boldsymbol{x}$,

$$\begin{aligned}\boldsymbol{x}_1 &= \boldsymbol{x}\left[\frac{m_2}{M} + \frac{1}{2}\eta\Delta\Big(v^2 - \frac{M}{r}\Big)\right] - M\eta\boldsymbol{v}\times(\boldsymbol{\chi}_a + \Delta\boldsymbol{\chi}_s),\\ \boldsymbol{x}_2 &= \boldsymbol{x}\left[-\frac{m_1}{M} + \frac{1}{2}\eta\Delta\Big(v^2 - \frac{M}{r}\Big)\right] - M\eta\boldsymbol{v}\times(\boldsymbol{\chi}_a + \Delta\boldsymbol{\chi}_s).\end{aligned} \tag{4.4.15}$$

(Compare Eq. (3.13) of Ref. [12] and Eq. (F11) of Ref. [9], where the missing factor of η in the latter is a typographical error.) This correction is 1.5PN order; therefore it enters our 2PN calculation through contributions from the 0.5PN (point-mass) multipoles (4.4.9).

Applying the transformation (4.4.15) and including the contributions from the point-mass multipoles, we find the two-body forms of (4.4.4), (4.4.6), and (4.4.8) to be

$$J^{ijk\ell} = \frac{5}{2}M^2\eta^2(\chi_a - \Delta\chi_s)^{\langle i}x^{jk\ell\rangle}, \tag{4.4.16}$$

$$I^{ijk} = -M\eta\Delta x^{\langle ijk\rangle} + M^2\eta^2\left\{\frac{3}{2}[\boldsymbol{v}\times(\boldsymbol{\chi}_a - 5\Delta\boldsymbol{\chi}_s)]^i x^{jk} - 3[\boldsymbol{x}\times(\boldsymbol{\chi}_a - \Delta\boldsymbol{\chi}_s)]^i x^{jk}\right\}^{\rm STF}, \tag{4.4.17}$$

$$\begin{aligned}J^{ij} = {}& -\mu\Delta(\boldsymbol{x}\times\boldsymbol{v})^{\langle i}x^{j\rangle} + \frac{3}{2}M^2\eta(\chi_a + \Delta\chi_s)^{\langle i}x^{j\rangle} + \frac{3}{4}M^2\eta\Delta\left(v^2 - \frac{M}{r}\right)\\ &\times(\Delta\chi_a + \chi_s)^{\langle i}x^{j\rangle} + \frac{1}{28}M^2\eta^2\left\{\left[\left(23\frac{M}{r} - 13v^2\right)\chi_a + \Delta\left(47\frac{M}{r} - 141v^2\right)\chi_s\right]^i x^j\right.\\ &+2(\boldsymbol{x}\cdot\boldsymbol{v})(15\chi_a + 13\Delta\chi_s)^i v^j + 2\frac{M}{r^3}[\boldsymbol{x}\cdot(29\boldsymbol{\chi}_a - \Delta\boldsymbol{\chi}_s)]x^{ij}\\ &\left.-4[\boldsymbol{x}\cdot(5\boldsymbol{\chi}_a + 9\Delta\boldsymbol{\chi}_s)]v^{ij} - 4[\boldsymbol{v}\cdot(3\boldsymbol{\chi}_a - 31\Delta\boldsymbol{\chi}_s)]x^i v^j\right\}^{\rm STF}.\end{aligned} \tag{4.4.18}$$

The first terms in (4.4.17) and (4.4.18) are the lowest order non-spin terms. The second term in (4.4.18) is easily verified as identical to the lowest order (1PN) spin-orbit contribution obtained by Kidder [Eq. (3.20a) of Ref. [12]].

C. Quasicircular orbits

We now specialize to the case where the two bodies orbit each other in a circular trajectory, which adiabatically shrinks (inspirals) under radiation reaction. For spinning bodies, this is only possible when both spin vectors are parallel or antiparallel to the orbital angular momentum, eliminating spin-orbit precession.

We express our results in terms of the orthonormal vectors $\boldsymbol{n} = \boldsymbol{x}/r$, $\boldsymbol{\lambda} = \boldsymbol{v}/v$, and $\boldsymbol{z} = \boldsymbol{n} \times \boldsymbol{\lambda}$ (parallel to all angular momenta). The majority of the terms in (4.4.16-4.4.18) vanish, and we are left with the greatly simplified expressions

$$J^{ijk\ell} = \frac{5}{2} M^2 \eta^2 r^3 (\chi_a - \Delta\chi_s) n^{\langle ijk} z^{\ell\rangle}, \tag{4.4.19}$$

$$\begin{aligned} I^{ijk} = &-M\eta\Delta r^3 n^{\langle ijk\rangle} + \frac{3}{2} M^2 \eta^2 v r^2 \Big[(\chi_a - 5\Delta\chi_s) n^{ijk} \\ &+2(\chi_a - \Delta\chi_s) n^i \lambda^{jk}\Big]^{\rm STF}, \end{aligned} \tag{4.4.20}$$

$$\begin{aligned} J^{ij} = &-M\eta\Delta r^2 v n^{\langle i} z^{j\rangle} + \frac{3}{2} M^2 \eta r (\chi_a + \Delta\chi_s) n^{\langle i} z^{j\rangle} \\ &+\frac{1}{14} M^3 \eta^2 (5\chi_a - 47\Delta\chi_s) n^{\langle i} z^{j\rangle}. \end{aligned} \tag{4.4.21}$$

V. WAVE FORM

Having evaluated the necessary radiative multipoles, we obtain the gravitational wave form

$$h^{ij} = \frac{1}{R} \sum_{\ell=2}^{\infty} \Big[\frac{4}{\ell!} \overset{(\ell)}{I}{}^{ijL-2} N^{L-2} + \frac{8\ell}{(\ell+1)!} \epsilon^{pq(i} \overset{(\ell)}{J}{}^{j)pL-2} N^{qL-2} \Big]^{\rm TT}, \tag{4.5.1}$$

where TT denotes the transverse traceless projection, (ℓ) denotes the ℓth time derivative, and $\boldsymbol{N}$ is the unit vector pointing toward the observer [cf. Eq. (E5a) of Ref. [9]].

We evaluate the time derivatives using the equation of motion for circular orbits, $\boldsymbol{a} = -\omega^2 \boldsymbol{x}$, where the standard form of the post-Newtonian expansion is given by

$$\omega^2 = \frac{M}{r^3} \Big\{ 1 - (3-\eta)\frac{M}{r} - 2[\Delta\chi_a + (1+\eta)\chi_s]\frac{Mv}{r} + O(\epsilon^2) \Big\} \tag{4.5.2}$$

[cf. Eqs. (7.1) and (F20) of Ref. [9]]. The 1.5PN spin-orbit term in the equation of motion [the third term in (4.5.2)] contributes to the 2PN spin-orbit term in h^{ij} through time derivatives of the 0.5PN point-mass multipoles [cf. the first terms in (4.4.20) and (4.4.21)]. If we were to consider spin-orbit precession, time derivatives of spin expressions appearing in the multipoles (4.4.16)-(4.4.18) would also factor into (4.5.1).

Evaluating the time derivatives in (4.5.1), using (4.5.2) and the identity $v = \omega r$ to write v and M/r in terms of $M\omega$, and collecting all terms of order $(M\omega)^2$, we obtain

$$\begin{aligned}
h^{ij} = {}& \frac{2M\eta}{R}(M\omega)^2\Big[(\Delta^2\chi_a + \Delta\chi_s)\Big(\Big(-\frac{14}{3}n^{ij} + 4\lambda^{ij}\Big)(\boldsymbol{\lambda}\cdot\boldsymbol{N}) - \frac{28}{3}n^{(i}\lambda^{j)}(\boldsymbol{n}\cdot\boldsymbol{N})\Big) \\
&+\Big(2\chi_a - \frac{8}{3}\Delta^2\chi_a - \frac{2}{3}\Delta\chi_s\Big)(\boldsymbol{n}\times\boldsymbol{N})^{(i}z^{j)}\Big]^{\rm TT} \\
&+\frac{2M\eta^2}{R}(M\omega)^2\Big[\Big(19\chi_a + 37\Delta\chi_s\Big)\Big(\frac{1}{6}(\boldsymbol{N}\cdot\boldsymbol{\lambda})n^{ij} + \frac{1}{3}(\boldsymbol{N}\cdot\boldsymbol{n})n^{(i}\lambda^{j)}\Big) \\
&-4(\chi_a + \Delta\chi_s)(\boldsymbol{N}\cdot\boldsymbol{\lambda})\lambda^{ij} + (\chi_a - \Delta\chi_s)\Big\{(\boldsymbol{n}\times\boldsymbol{N})^{(i}z^{j)}\Big(-\frac{7}{6} - \frac{10}{3}(\boldsymbol{N}\cdot\boldsymbol{\lambda})^2 \\
&+\frac{7}{2}(\boldsymbol{N}\cdot\boldsymbol{n})^2\Big) - \frac{20}{3}(\boldsymbol{N}\cdot\boldsymbol{\lambda})(\boldsymbol{N}\cdot\boldsymbol{z})(\boldsymbol{n}\times\boldsymbol{N})^{(i}\lambda^{j)} + \frac{7}{3}(\boldsymbol{N}\cdot\boldsymbol{n})(\boldsymbol{N}\cdot\boldsymbol{z})(\boldsymbol{n}\times\boldsymbol{N})^{(i}n^{j)} \\
&-\frac{10}{3}(\boldsymbol{N}\cdot\boldsymbol{n})(\boldsymbol{N}\cdot\boldsymbol{z})(\boldsymbol{\lambda}\times\boldsymbol{N})^{(i}\lambda^{j)} - \frac{20}{3}(\boldsymbol{N}\cdot\boldsymbol{n})(\boldsymbol{N}\cdot\boldsymbol{\lambda})(\boldsymbol{z}\times\boldsymbol{N})^{(i}\lambda^{j)}\Big\}\Big]^{\rm TT}. \qquad (4.5.3)
\end{aligned}$$

Finally, we project out the amplitudes of the h_+ and $h_\times$ polarizations. This is done by taking

$$h_+ = \frac{1}{2}(p_i p_j - q_i q_j)h^{ij}, \qquad (4.5.4a)$$

$$h_\times = \frac{1}{2}(p_i q_j + q_i p_j)h^{ij}. \qquad (4.5.4b)$$

Note that the TT projection in (4.5.1) is subsumed in this operation (cf. Sec. VIIA of [9]). The standard convention [9] is to use the unit triad composed of $\boldsymbol{N}$ (the direction to the observer), $\boldsymbol{p}$ (pointing from the descending node of the orbit to the ascending node), and $\boldsymbol{q} = \boldsymbol{N}\times\boldsymbol{p}$. The orbital phase ψ is measured from the ascending node, and the orbital inclination angle i is given by $\cos i = \boldsymbol{z}\cdot\boldsymbol{N}$. Thus we have

$$\boldsymbol{n} = \boldsymbol{p}\cos\psi + (\boldsymbol{q}\cos i + \boldsymbol{N}\sin i)\sin\psi, \qquad (4.5.5a)$$

$$\boldsymbol{\lambda} = -\boldsymbol{p}\sin\psi + (\boldsymbol{q}\cos i + \boldsymbol{N}\sin i)\cos\psi, \tag{4.5.5b}$$

$$\boldsymbol{z} = -\boldsymbol{q}\sin i + \boldsymbol{N}\cos i. \tag{4.5.5c}$$

Following [22], we organize the amplitude contributions of the wave-form polarizations according to post-Newtonian order and physical origin as

$$\begin{aligned} h_{+,\times} = \frac{2M\eta}{R}x\Big[&H^{(0)}_{+,\times} + \cdots + x^{3/2}H^{(3/2)}_{+,\times} + x^{3/2}H^{(3/2,\mathrm{SO})}_{+,\times} \\ &+x^2H^{(2)}_{+,\times} + x^2H^{(2,\mathrm{SO})}_{+,\times} + x^2H^{(2,\mathrm{SS})}_{+,\times} + \cdots\Big], \end{aligned} \tag{4.5.6}$$

where $x = (M\omega)^{2/3}$. The 2PN spin-orbit contributions to the wave-form polarizations are given by

$$\begin{aligned} H^{(2,\mathrm{SO})}_{+} = \sin i\Bigg(&\left\{\frac{-1}{24}\Big[\left(109+15c^2\right)\chi_a + 7\left(1+3c^2\right)\Delta\chi_s\Big]\eta + \frac{1}{4}(1+c^2)(\chi_a+\Delta\chi_s)\right\} \\ &\times\cos\psi + \left\{\frac{9}{8}\Big[\left(11+5c^2\right)\chi_a + \left(1+7c^2\right)\Delta\chi_s\Big]\eta - \frac{9}{4}(1+c^2)(\chi_a+\Delta\chi_s)\right\} \\ &\times\cos 3\psi\Bigg) \end{aligned} \tag{4.5.7a}$$

$$\begin{aligned} H^{(2,\mathrm{SO})}_{\times} = c\sin i\Bigg(&\left\{\frac{-1}{24}\Big[\left(127-3c^2\right)\chi_a + \left(25+3c^2\right)\Delta\chi_s\Big]\eta + \frac{1}{2}(\chi_a+\Delta\chi_s)\right\}\sin\psi \\ &+\left\{\frac{9}{8}\Big[\left(19-3c^2\right)\chi_a + \left(5+3c^2\right)\Delta\chi_s\Big]\eta - \frac{9}{2}(\chi_a+\Delta\chi_s)\right\}\sin 3\psi\Bigg), \end{aligned} \tag{4.5.7b}$$

where $c \equiv \cos i$.

It is clear that these 2PN contributions to the wave-form amplitudes do not contribute to the radiation reaction at 2PN order because the harmonics (ω and 3ω) average to zero when beat against the "Newtonian" terms $H^{(0)}_{+,\times}$ at frequency 2ω [cf. Eqs. (3,4) of Ref. [22]].

VI. SUMMARY

We have calculated all the non-precessional 2PN spin-orbit effects on the gravitational wave forms of compact bodies in quasicircular orbit, and have shown that there

is no spin-orbit radiation reaction effect at 2PN order. Our calculation was greatly simplified over previous spinning-body post-Newtonian efforts [13,12] by the use of a δ-function energy-momentum tensor for spinning particles. We have presented the wave-form polarizations in "ready-to-use" form (cf. [22]).

Note that terms of $O(\eta)$ contribute significantly to (V). These are the terms that could not have been obtained by the black-hole perturbation approach. Their presence leads us to expect that the 2.5PN radiation reaction will also contain significant terms of $O(\eta)$ which are not found in [17,23,20].

In this paper, we treated the bodies only to linear order in their spins (i.e., considered only spin-orbit effects). Spin-spin effects can be treated by a more complicated calculation using the MST energy-momentum tensor. However, because spin-spin effects appear at 2PN order, consistency would require that one also include the effects of the bodies' quadrupole moments [24].

ACKNOWLEDGMENTS

We thank Kip Thorne for helpful comments on the manuscript. BJO thanks Alan Wiseman for many stimulating discussions. BJO was supported in part by NSF Grants AST-9417371 and INT-9417348, NASA Grants NAGW-4268 and NAG5-4351, and by an NSF Graduate Fellowship. HT was supported by the Japanese Society for the Promotion of Science. AO was supported in part by Monbusho Grant-in-Aid for Scientific Research No. 09440106.

APPENDIX

In this appendix, we derive the 1.5PN spin-orbit multipoles $I^{ij}_{(\mathrm{SO})}$ and $J^{ijk}_{(\mathrm{SO})}$ obtained in [12].

The general expressions are quite simple, requiring (4.4.1) and (4.4.2) only to lowest order,

$$I^{ij}_{(\mathrm{SO})} = \int d^3x\, \hat{x}^{ij} \left(T^{00}_{(\mathrm{SO})} + T^{aa}_{(\mathrm{SO})} \right) - \frac{4}{3}\frac{d}{dt} \int d^3x\, \hat{x}^{ija} T^{0a}_{(\mathrm{SO})}, \tag{4.A1}$$

$$J^{ijk}_{(\mathrm{SO})} = \epsilon^{ab\langle i} \int d^3x\, \hat{x}^{jk\rangle a} T^{0b}_{(\mathrm{SO})}. \tag{4.A2}$$

Using (4.2.8) and (III) only to lowest order, it is straightforward to evaluate these expressions in the N-body case as

$$I^{ij}_{(\mathrm{SO})} = \sum [4x^i_A (\boldsymbol{v}_A \times \boldsymbol{S}_A)^j - \frac{4}{3}\frac{d}{dt} \left\{ x^i_A (\boldsymbol{x}_A \times \boldsymbol{S}_A)^j \right\}]^{\mathrm{STF}}, \tag{4.A3}$$

$$J^{ijk}_{(\mathrm{SO})} = \sum 2[x^{ij}_A S^k_A]^{\mathrm{STF}}. \tag{4.A4}$$

Using the transformation (4.4.15) to the relative coordinate, we find the two-body forms of the multipoles to be

$$I^{ij}_{(\mathrm{SO})} = \frac{8}{3} M^2 \eta^2 [2x^i (\boldsymbol{v} \times \boldsymbol{\chi}_s)^j - v^i (\boldsymbol{x} \times \boldsymbol{\chi}_s)^j]^{\mathrm{STF}}, \tag{4.A5}$$

$$J^{ijk}_{(\mathrm{SO})} = 4M^2 \eta^2 [x^{ij} \chi^k_s]^{\mathrm{STF}}. \tag{4.A6}$$

These results agree with those obtained using the fluid body energy-momentum tensor [12,9].

---

[1] K. S. Thorne, in *Black Holes and Relativistic Stars*, ed. R. M. Wald (University of Chicago Press, Chicago, in press; gr-qc/9706079). See also references therein.

[2] B. Barish *et al.*, LIGO Advanced Research and Development Program Proposal, Caltech/MIT (unpublished, 1996).

[3] R. Narayan, T. Piran, and A. Shemi, Astrophys. J. **379**, L17 (1991).

[4] E. S. Phinney, Astrophys. J. **380**, L17 (1991).

[5] A. V. Tutukov and L. R. Yungelson, Mon. Not. Roy. Astron. Soc. **260**, 675 (1993).

[6] V. M. Lipunov, K. A. Postnov, and M. E. Prokhorov, Mon. Not. Roy. Astron. Soc. **288**, 245 (1997).

[7] B. S. Sathyaprakash, in *Relativistic Gravitation and Gravitational Radiation*, ed. J.-P. LaSota and J.-A. Marck (Cambridge University Press, Cambridge, 1997), p. 361. See also references therein.

[8] L. Blanchet, T. Damour, and B. R. Iyer, Phys. Rev. D **51**, 5360 (1995).

[9] C. M. Will and A. G. Wiseman, Phys. Rev. D **54** 4813 (1996).

[10] L. Blanchet, Phys. Rev. D **54**, 1417 (1996).

[11] T. A. Apostolatos, C. Cutler, G. J. Sussman, and K. S. Thorne, Phys. Rev. D **49**, 6274 (1994).

[12] L. E. Kidder, Phys. Rev. D **52**, 821 (1995).

[13] L. E. Kidder, C. M. Will, and A. G. Wiseman, Phys. Rev. D **47**, R4183 (1993).

[14] S. A. Teukolsky, Astrophys. J. **185**, 635 (1973).

[15] Y. Mino, M. Sasaki, M. Shibata, H. Tagoshi, and T. Tanaka, Prog. Theor. Phys. Suppl. **128**, 1 (1997).

[16] Y. Mino, M. Shibata, and T. Tanaka, Phys. Rev. D **53**, 622 (1996).

[17] T. Tanaka, Y. Mino, M. Sasaki, and M. Shibata, Phys. Rev. D **54**, 3762 (1996).

[18] W. G. Dixon, in *Isolated Gravitating Systems in General Relativity*, ed. J. Ehlers (North-Holland, Amsterdam, 1979), p. 156. See also references therein.

[19] H. T. Cho, "Post-Newtonian approximation for spinning particles," gr-qc/9703071.

[20] H. Tagoshi, M. Shibata, T. Tanaka, and M. Sasaki, Phys. Rev. D **54**, 1439 (1996).

[21] C. W. Misner, K. S. Thorne, and J. A. Wheeler, *Gravitation* (Freeman, San Francisco,

1973).

[22] L. Blanchet, B. R. Iyer, C. M. Will, and A. G. Wiseman, Class. Quantum Grav. **13**, 575 (1996).

[23] M. Shibata, M. Sasaki, H. Tagoshi, and T. Tanaka, Phys. Rev. D **51**, 1646 (1995).

[24] E. Poisson, Phys. Rev. D **57** (in press), gr-qc/9709032.

Chapter 5 Gravitational radiation instability in hot young neutron stars

Written with Lee Lindblom and Sharon M. Morsink

To appear in Phys. Rev. Lett. **80** (1998)

We show that gravitational radiation drives an instability in hot young rapidly rotating neutron stars. This instability occurs primarily in the $l = 2$ r-mode and will carry away most of the angular momentum of a rapidly rotating star by gravitational radiation. On the timescale needed to cool a young neutron star to about $T = 10^9$K (about one year) this instability can reduce the rotation rate of a rapidly rotating star to about $0.076\Omega_K$, where Ω_K is the Keplerian angular velocity where mass shedding occurs. In older colder neutron stars this instability is suppressed by viscous effects, allowing older stars to be spun up by accretion to larger angular velocities.

Recently Andersson [1] discovered (and Friedman and Morsink [2] confirmed more generally) that gravitational radiation tends to drive the r-modes of all rotating stars unstable. In this paper we examine the timescales associated with this instability in some detail. We show that gravitational radiation couples to these modes primarily through the current multipoles, rather than the usual mass multipoles. We also evaluate the effects of internal fluid dissipation which tends to suppress this instability. We find that gravitational radiation is stronger than viscosity in these modes and so this instability severely limits the rotation rates of hot young neutron stars. We show that such stars can spin down by the emission of gravitational radiation to about 7.6% of their maximum rotation rates on the timescale (about one year) needed to cool these stars to 10^9K.

The r-modes of rotating barotropic Newtonian stars are solutions of the perturbed fluid equations having (Eulerian) velocity perturbations

$$\delta\vec{v} = \alpha R\Omega \left(\frac{r}{R}\right)^l \vec{Y}^B_{ll} e^{i\omega t}, \tag{5.1}$$

where R and Ω are the radius and angular velocity of the unperturbed star, α is an

arbitrary constant, and $\vec{Y}^B_{lm}$ is the magnetic type vector spherical harmonic defined by

$$\vec{Y}^B_{lm} = [l(l+1)]^{-1/2} r\vec{\nabla} \times (r\vec{\nabla} Y_{lm}). \tag{5.2}$$

Papaloizou and Pringle [3] first showed that the Euler equation for $r-$modes determines the frequencies as

$$\omega = -\frac{(l-1)(l+2)}{l+1}\Omega. \tag{5.3}$$

Further use of the Euler equation (as first noted by Provost, Berthomieu and Rocca [4]) in the barotropic case (a good approximation for neutron stars) determines that only the $l = m$ r-modes exist, and that $\delta\vec{v}$ must have the radial dependence given in Eq. (5.1). These expressions for the velocity perturbation and frequency are only the lowest order terms in expansions for these quantities in powers of Ω. The exact expressions contain additional terms of order Ω^3.

The lowest order expressions for the (Eulerian) density perturbation $\delta\rho$ can also be deduced from the perturbed fluid equations (Ipser and Lindblom [5]):

$$\frac{\delta\rho}{\rho} = \alpha R^2\Omega^2 \frac{d\rho}{dp}\left[\frac{2l}{2l+1}\sqrt{\frac{l}{l+1}}\left(\frac{r}{R}\right)^{l+1} + \delta\Psi(r)\right] Y_{l+1\,l}\, e^{i\omega t}, \tag{5.4}$$

where $\delta\Psi(r)$ is proportional to the gravitational potential $\delta\Phi$ and satisfies

$$\frac{d^2\delta\Psi}{dr^2} + \frac{2}{r}\frac{d\delta\Psi}{dr} + \left[4\pi G\rho\frac{d\rho}{dp} - \frac{(l+1)(l+2)}{r^2}\right]\delta\Psi = -\frac{8\pi G l}{2l+1}\sqrt{\frac{l}{l+1}}\rho\frac{d\rho}{dp}\left(\frac{r}{R}\right)^{l+1}. \tag{5.5}$$

Eq. (5.4) is the complete expression for $\delta\rho$ to order Ω^2. The next order terms are proportional to Ω^4.

Our interest here is to study the evolution of these modes due to the dissipative influences of viscosity and gravitational radiation. For this purpose it is useful to consider the effects of radiation on the evolution of the energy of the mode (as measured in the co-rotating frame of the equilibrium star) $\tilde{E}$:

$$\tilde{E} = \frac{1}{2}\int \left[\rho\,\delta\vec{v}\cdot\delta\vec{v}^{\,*} + \left(\frac{\delta p}{\rho} - \delta\Phi\right)\delta\rho^{*}\right] d^3x. \tag{5.6}$$

This energy evolves on the secular timescale of the dissipative processes. The general expression for the time derivative of $\tilde{E}$ for a mode with time dependence $e^{i\omega t}$ and azimuthal angular dependence $e^{im\varphi}$ is

$$\frac{d\tilde{E}}{dt} = -\int \left(2\eta\delta\sigma^{ab}\delta\sigma^{*}_{ab} + \zeta\delta\sigma\delta\sigma^{*}\right) d^3x - \omega(\omega + m\Omega)\sum_{l\geq 2} N_l\omega^{2l}\left(|\delta D_{lm}|^2 + |\delta J_{lm}|^2\right). \tag{5.7}$$

The thermodynamic functions η and ζ that appear in Eq. (5.7) are the shear and bulk viscosities of the fluid. The viscous forces are driven by the shear $\delta\sigma_{ab}$ and expansion $\delta\sigma$ of the perturbation, defined by the usual expressions

$$\delta\sigma_{ab} = \tfrac{1}{2}(\nabla_a\delta v_b + \nabla_b\delta v_a - \tfrac{2}{3}\delta_{ab}\nabla_c\delta v^c), \tag{5.8}$$

$$\delta\sigma = \nabla_a\delta v^a. \tag{5.9}$$

Gravitational radiation couples to the evolution of the mode through the mass δD_{lm} and current δJ_{lm} multipole moments of the perturbed fluid,

$$\delta D_{lm} = \int \delta\rho\, r^l Y^{*}_{lm} d^3x, \tag{5.10}$$

$$\delta J_{lm} = \frac{2}{c}\sqrt{\frac{l}{l+1}}\int r^l(\rho\,\delta\vec{v} + \delta\rho\,\vec{v})\cdot\vec{Y}^{B*}_{lm} d^3x, \tag{5.11}$$

with coupling constant

$$N_l = \frac{4\pi G}{c^{2l+1}}\frac{(l+1)(l+2)}{l(l-1)[(2l+1)!!]^2}. \tag{5.12}$$

The terms in the expression for $d\tilde{E}/dt$ due to viscosity and the gravitational radiation generated by the mass multipoles are well known [6]. The terms involving the current multipole moments have been deduced from the general expressions given by Thorne [7].

We can now use Eq. (5.7) to evaluate the stability of the r-modes. Viscosity always tends to decrease the energy $\tilde{E}$, while gravitational radiation may either increase or

decrease it. The sum that appears in Eq. (5.7) is positive definite; thus the effect of gravitational radiation is determined by the sign of $\omega(\omega + m\Omega)$. For r-modes this quantity is negative definite:

$$\omega(\omega + l\Omega) = -\frac{2(l-1)(l+2)}{(l+1)^2}\Omega^2 < 0. \tag{5.13}$$

Therefore gravitational radiation tends to increase the energy of these modes. For small angular velocities the energy $\tilde{E}$ is positive definite: the positive term $|\delta\vec{v}|^2$ in Eq. (5.6) (proportional to Ω^2) dominates the indefinite term $(\delta p/\rho - \delta\Phi)\delta\rho^*$ (proportional to Ω^4). Thus, gravitational radiation tends to make *every* r-mode unstable in slowly rotating stars. This confirms the discovery of Andersson [1] and the more general arguments of Friedman and Morsink [2]. To determine whether these modes are actually stable or unstable in rotating neutron stars, therefore, we must evaluate the magnitudes of all the dissipative terms in Eq. (5.7) and determine which dominates.

Here we estimate the relative importance of these dissipative effects in the small angular velocity limit using the lowest order expressions for the $r-$mode $\delta\vec{v}$ and $\delta\rho$ given in Eqs. (5.1) and (5.4). The lowest order expression for the energy of the mode $\tilde{E}$ is

$$\tilde{E} = \tfrac{1}{2}\alpha^2\Omega^2 R^{-2l+2}\int_0^R \rho\, r^{2l+2} dr. \tag{5.14}$$

The lowest order contribution to the gravitational radiation terms in the energy dissipation comes entirely from the current multipole moment δJ_{ll}. This term can be evaluated to lowest order in Ω using Eqs. (5.1) and (5.11):

$$\delta J_{ll} = \frac{2\alpha\Omega}{cR^{l-1}}\sqrt{\frac{l}{l+1}}\int_0^R \rho\, r^{2l+2} dr. \tag{5.15}$$

The other contributions from gravitational radiation to the dissipation rate are all higher order in Ω. The mass multipole moment contributions are higher order because *a*) the density perturbation $\delta\rho$ from Eq. (5.4) is proportional to Ω^2 while the velocity

perturbation $\delta\vec{v}$ is proportional to Ω; and b) the density perturbation $\delta\rho$ generates gravitational radiation at order $2l+4$ in ω while $\delta\vec{v}$ generates radiation at order $2l+2$.

The contribution of gravitational radiation to the imaginary part of the frequency of the mode $1/\tau_{GR}$ can be computed as follows,

$$\frac{1}{\tau_{GR}} = -\frac{1}{2\tilde{E}}\left(\frac{d\tilde{E}}{dt}\right)_{GR}. \tag{5.16}$$

Using Eqs. (5.14)–(5.16) we obtain an explicit expression for the gravitational radiation timescale associated with the r-modes:

$$\frac{1}{\tau_{GR}} = -\frac{32\pi G\Omega^{2l+2}}{c^{2l+3}}\frac{(l-1)^{2l}}{[(2l+1)!!]^2}\left(\frac{l+2}{l+1}\right)^{2l+2}\int_0^R \rho\, r^{2l+2} dr. \tag{5.17}$$

The time derivative of the energy due to viscous dissipation is driven by the shear $\delta\sigma_{ab}$ and the expansion $\delta\sigma$ of the velocity perturbation. The shear can be evaluated using Eqs. (5.1) and (5.8) and its integral over the constant r two-spheres performed in a straightforward calculation. Using the formulae for the viscous dissipation rate Eq. (5.7) and the energy Eq. (5.14), we obtain the contribution of shear viscosity to the imaginary part of the frequency of the mode,

$$\frac{1}{\tau_V} = (l-1)(2l+1)\int_0^R \eta r^{2l} dr \left(\int_0^R \rho\, r^{2l+2} dr\right)^{-1}. \tag{5.18}$$

The expansion $\delta\sigma$, which drives the bulk viscosity dissipation in the fluid, can be re-expressed in terms of the density perturbation. The perturbed mass conservation law gives the relationship $\delta\sigma = -i(\omega + m\Omega)\Delta\rho/\rho$, where $\Delta\rho$ is the Lagrangian perturbation in the density. The perturbation analysis used here is not of sufficiently high order (in Ω) to evaluate the lowest order contribution to $\Delta\rho$. However, we are able to evaluate the Eulerian perturbation $\delta\rho$ as given in Eq. (5.4). We expect that the integral of $|\delta\rho/\rho|^2$ over the interior of the star will be similar to (i.e., within about a factor of two of) the integral of $|\Delta\rho/\rho|^2$. Thus, we estimate the magnitude of the bulk viscosity contribution to the dissipation by

$$\frac{1}{\tau_B} \approx \frac{(\omega + m\Omega)^2}{2\tilde{E}} \int \zeta \frac{\delta\rho\, \delta\rho^*}{\rho^2} d^3x. \tag{5.19}$$

Using Eqs. (5.4) and (5.14) for $\delta\rho/\rho$ and $\tilde{E}$, Eq. (5.19) becomes an explicit formula for the contribution to the imaginary part of the frequency due to bulk viscosity.

To evaluate the dissipative timescales associated with the r-modes using the formulae in Eqs. (5.17)–(5.19), we need models for the structures of neutron stars as well as expressions for the viscosities of neutron star matter. We have evaluated these timescales for $1.4M_\odot$ neutron star models based on several realistic equations of state [8]. We use the standard formulae for the shear and bulk viscosities of hot neutron star matter [9]

$$\eta = 347\rho^{9/4}T^{-2}, \tag{5.20}$$

$$\zeta = 6.0 \times 10^{-59}\rho^2(\omega + m\Omega)^{-2}T^6, \tag{5.21}$$

where all quantities are given in cgs units. The timescales for the more realistic equations of state are comparable to those based on a simple polytropic model $p = \kappa\rho^2$ with κ chosen so that the radius of a $1.4M_\odot$ star is 12.53 km. The dissipation timescales for this polytropic model (which can be evaluated analytically) are $\tilde{\tau}_{GR} = -3.26\text{s}$, $\tilde{\tau}_V = 2.52 \times 10^8\text{s}$ and $\tilde{\tau}_B = 6.99 \times 10^8\text{s}$ for the fiducial values of the angular velocity $\Omega = \sqrt{\pi G\bar{\rho}}$ and temperature $T = 10^9\text{K}$ in the $l = 2$ r-mode. The gravitational radiation timescales increase by about one order of magnitude for each incremental increase in l, while the viscous timescales decrease by about 20%.

The evolution of an r-mode due to the dissipative effects of viscosity and gravitational radiation reaction is determined by the imaginary part of the frequency of the mode,

$$\frac{1}{\tau(\Omega)} = \frac{1}{\tilde{\tau}_{GR}} \left(\frac{\Omega^2}{\pi G\bar{\rho}}\right)^{l+1} + \frac{1}{\tilde{\tau}_V} \left(\frac{10^9\text{K}}{T}\right)^2 + \frac{1}{\tilde{\tau}_B} \left(\frac{T}{10^9\text{K}}\right)^6 \left(\frac{\Omega^2}{\pi G\bar{\rho}}\right). \tag{5.22}$$

Eq. (5.22) is displayed in a form that makes explicit the angular velocity and temperature dependences of the various terms. Dissipative effects cause the mode to decay

exponentially as $e^{-t/\tau}$ (i.e., the mode is stable) as long as $\tau > 0$. From Eqs. (5.17)–(5.19) we see that $\tilde{\tau}_V > 0$ and $\tilde{\tau}_B > 0$ while $\tilde{\tau}_{GR} < 0$. Thus gravitational radiation drives these modes towards instability while viscosity tries to stabilize them. For small Ω the gravitational radiation contribution to the imaginary part of the frequency is very small since it is proportional to Ω^{2l+2}. Thus for sufficiently small angular velocities, viscosity dominates and the mode is stable. For sufficiently large Ω, however, gravitational radiation will dominate and drive the mode unstable. It is convenient to define a critical angular velocity Ω_c where the sign of the imaginary part of the frequency changes from positive to negative: $1/\tau(\Omega_c) = 0$. If the angular velocity of the star exceeds Ω_c then gravitational radiation reaction dominates viscosity and the mode is unstable.

For a given temperature and mode l the equation for the critical angular velocity, $0 = 1/\tau(\Omega_c)$, is a polynomial of order $l + 1$ in Ω_c^2, and thus each mode has its own critical angular velocity. However, only the smallest of these (always the $l = 2$ r-mode here) represents the critical angular velocity of the star. Fig. 5.1 depicts the critical angular velocity for a range of temperatures relevant for neutron stars. The solid curve in Fig. 5.1 represents the critical angular velocity for the polytropic model discussed above. Fig. 5.2 depicts the critical angular velocities for $1.4M_\odot$ neutron star models computed from a variety of realistic equations of state [8]. Fig. 5.2 illustrates that the minimum critical angular velocity (in units of $\sqrt{\pi G\bar{\rho}}$) is extremely insensitive to the equation of state. The minima of these curves occur at $T \approx 2 \times 10^9$K, with $\Omega_c \approx 0.043\sqrt{\pi G\bar{\rho}}$. The maximum angular velocity for any star occurs when the material at the surface effectively orbits the star. This 'Keplerian' angular velocity Ω_K is very nearly $\frac{2}{3}\sqrt{\pi G\bar{\rho}}$ for any equation of state. Thus the minimum critical angular velocity due to instability of the r-modes is about $0.065\Omega_K$ for any equation of state [10].

To determine how rapidly a young neutron star is allowed to spin after cooling,

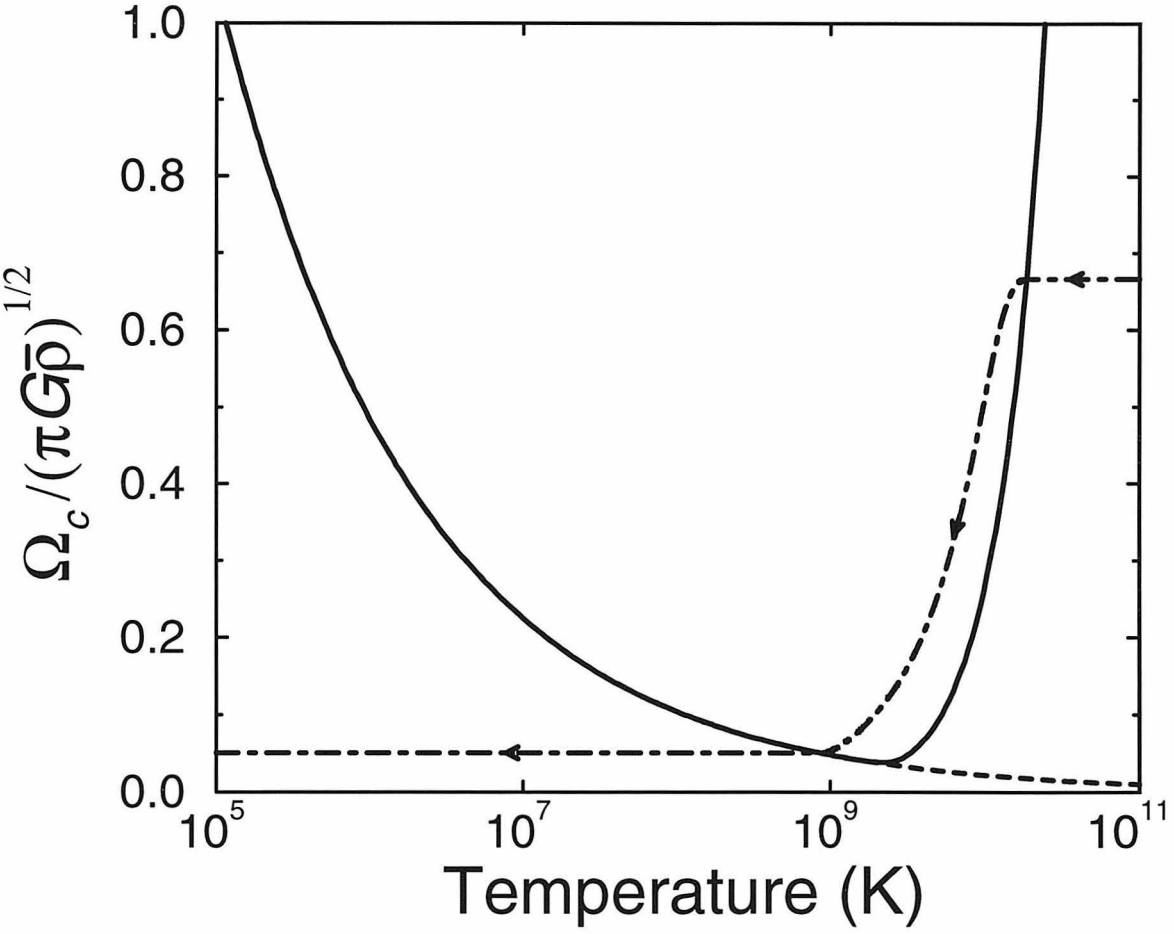

FIG. 5.1. Critical angular velocities for a $1.4M_\odot$ polytropic neutron star with (solid) and without (dashed) bulk viscosity. Also the evolution of a rapidly rotating neutron star (dash-dot) as the star cools and emits gravitational radiation.

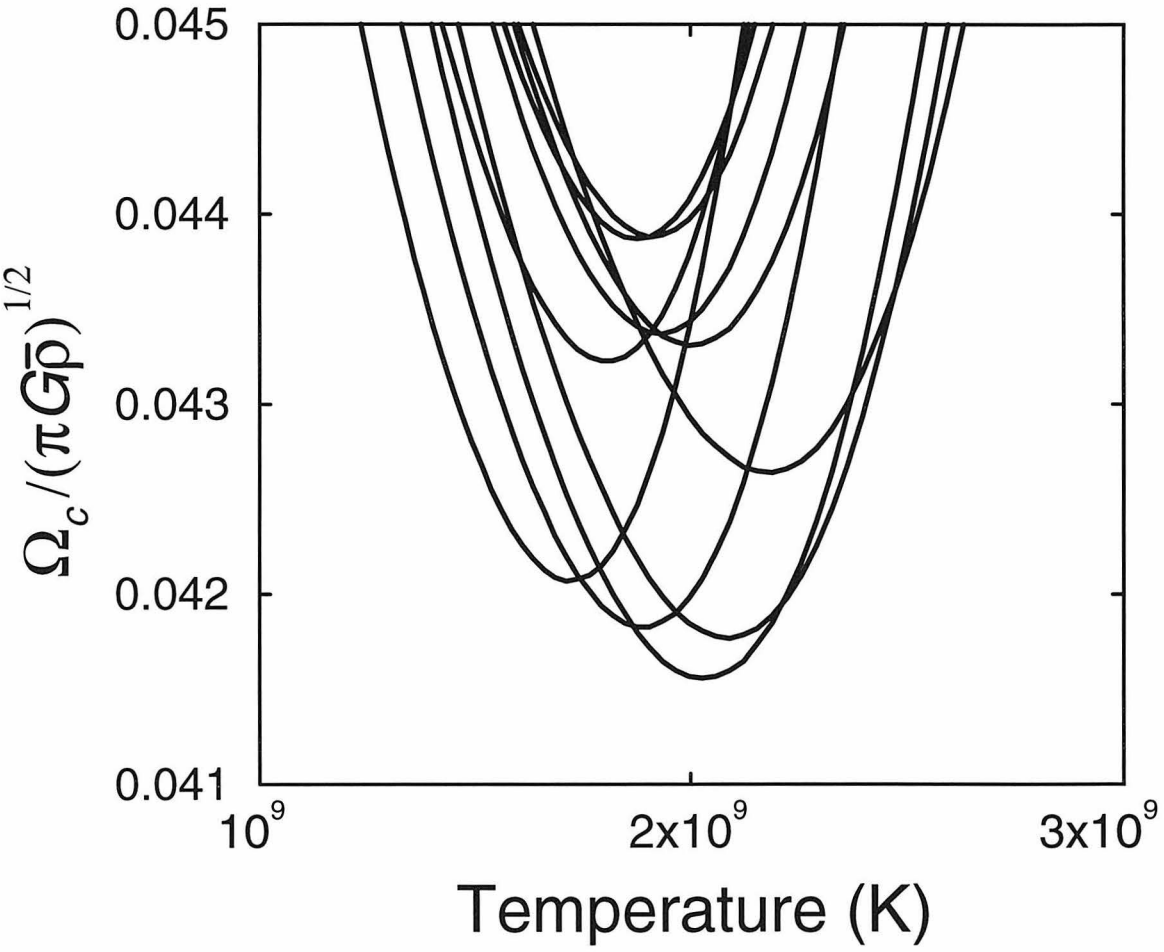

FIG. 5.2. Critical angular velocities of realistic $1.4M_\odot$ neutron star models.

we must compare the rate it cools with the rate it loses angular momentum by gravitational radiation. We approximate the cooling with a simple model based on the emission of neutrinos through the modified URCA process [11]. We compute the time evolution of the angular velocity of the star by setting $dJ/dt = J/\tau$, where J is the angular momentum of the star and τ is the timescale given in Eq. (5.22). The result is a simple first order differential equation for $\Omega(t)$ which we solve for initial angular velocity $\Omega = \Omega_K$ and initial temperature 10^{11}K. The solution is shown as the dash-dot line in Fig. 5.1. The gravitational radiation timescale is so short that the star radiates away its angular momentum almost as quickly as it cools. The angular velocity of the star decreases from Ω_K to $0.076\Omega_K$ in a period of about one year [12]. Thus, we conclude that young neutron stars will be spun down by the emission of gravitational radiation within their first year to a rotation period of about $13P_{\rm min}$, where $P_{\rm min} = 2\pi/\Omega_K$. The Crab pulsar with present rotation period 33ms and initial period 19ms (based on the measured braking index) rotates more slowly than this limit if $P_{\rm min} < 1.5$ms.

Our analysis here is based on the assumption that a young hot neutron star may be modeled as a simple ordinary fluid. Once the star cools below the superfluid transition temperature (about 10^9K) the analysis presented here must be modified [13]. We expect the r-mode instability to be completely suppressed (with $\Omega_c = \Omega_K$) when the star becomes a superfluid [14]. This makes it possible for old recycled pulsars to be spun up to large angular velocities by accretion if they are not re-heated much above 10^9K in the process. If non-perfect fluid effects enter above 10^9K, however, the spin down process may be terminated at a higher angular velocity than the $0.076\Omega_K$ figure computed here. The detection of a young fast pulsar [15] would provide evidence for such effects at temperatures higher than 10^9K. Magnetic fields could also damp these modes; however preliminary estimates based on standard magnetosphere-mode coupling models [16] suggest that such damping is too weak to suppress the relatively

low frequency r-mode instability.

ACKNOWLEDGMENTS

We thank N. Andersson, J. Friedman, J. Ipser, S. Phinney, B. Schutz, and K. Thorne for helpful discussions. This research was supported by NSF grants AST-9417371, PHY-9507740, PHY-9796079, NASA grant NAG5-4093, an NSF graduate fellowship, and NSERC of Canada.

---

[1] N. Andersson, to appear in Astrophys. J. (gr-qc/9706075).

[2] J. L. Friedman and S. M. Morsink, to appear in Astrophys. J. (9706073).

[3] J. Papaloizou and J. E. Pringle, Mon. Not. R. Astr. Soc. **182**, 423 (1978).

[4] J. Provost, G. Berthomieu, and A. Rocca, Astron. Astrophys. **94**, 126, (1981).

[5] J. Ipser and L. Lindblom, in preparation (1998).

[6] J. Ipser and L. Lindblom, Astrophys. J. **373**, 213 (1991).

[7] K. S. Thorne, Rev. Mod. Phys. **52**, 299 (1980).

[8] See references in S. Bonazzola, J. Frieben and E. Gourgoulhon, Astrophys. J. **460**, 379 (1996).

[9] C. Cutler and L. Lindblom, Astrophys. J. **314**, 234 (1987); R. F. Sawyer, Phys. Rev. D **39**, 3804 (1989).

[10] Note that the minimum Ω_c is rather small, and thus the small Ω expansions used here are expected to be quite good. Also, the approximation used to evaluate τ_B in Eq. (5.19) is not expected have a large effect on this minimum value: e.g., if $\tilde{\tau}_B$ were off by a factor

of ten, then the high T portion of the curve in Fig. 5.1 would be moved along the T axis by a factor of about $1.5 \approx (10)^{1/6}$. Since the shear viscosity influence on the curve (the dashed line in Fig. 5.1) is so flat in this temperature range, the minimum value of Ω_c would not be significantly changed.

[11] S. L. Shapiro and S. Teukolsky, Black Holes, White Dwarfs, and Neutron Stars (Wiley 1983). Viscosity also converts rotational energy into heat. However in the high temperature range this energy is converted primarily by bulk viscosity into neutrinos which are quickly radiated away. We do not expect this rotational re-heating to significantly impede the cooling process.

[12] Our assumption that the spindown timescale is τ of Eq. (5.22) is based on the fact that the $r-$mode will grow (within a few minutes) to a point where the mode contains a substantial fraction of the total angular momentum of the star before being saturated by non-linear effects. Eq. (5.22) is a low Ω expansion so the early time values of τ are also somewhat uncertain. Fortunately the final angular velocity state of the star is quite insensitive to the details of the cooling and spindown.

[13] The formation of a solid crust below $\rho \approx 2 \times 10^{14}\mathrm{g/cm}^3$ also affects these modes; however this density appears to be too low to affect the $r-$mode instability.

[14] L. Lindblom and G. Mendell, Astrophys. J. **444**, 805 (1995).

[15] F. E. Marshall *et al.*, astro-ph/9803214.

[16] O. Blaes *et al.*, Astrophys. J. **343**, 839 (1989).

Chapter 6 Gravitational waves from hot young rapidly rotating neutron stars

Written with Lee Lindblom, Curt Cutler, Bernard F. Schutz, Alberto Vecchio, and Nils Andersson

To appear in Phys. Rev. D **58** (1998)

Gravitational radiation drives an instability in the r-modes of young rapidly rotating neutron stars. This instability is expected to carry away most of the angular momentum of the star by gravitational radiation emission, leaving a star rotating at about 100 Hz. In this paper we model in a simple way the development of the instability and evolution of the neutron star during the year-long spindown phase. This allows us to predict the general features of the resulting gravitational waveform. We show that a neutron star formed in the Virgo cluster could be detected by the LIGO and VIRGO gravitational wave detectors when they reach their "enhanced" level of sensitivity, with an amplitude signal-to-noise ratio that could be as large as about 8 if near-optimal data analysis techniques are developed. We also analyze the stochastic background of gravitational waves produced by the r-mode radiation from neutron-star formation throughout the universe. Assuming a substantial fraction of neutron stars are born with spin frequencies near their maximum values, this stochastic background is shown to have an energy density of about 10^{-9} of the cosmological closure density, in the range 20 Hz to 1 kHz. This radiation should be detectable by "advanced" LIGO as well.

I. INTRODUCTION

Recently Andersson [1] discovered that gravitational radiation tends to destabilize the r-modes of rotating stars. Friedman and Morsink [2] then showed that this instability is generic, in the sense that gravitational radiation tends to make *all* r-modes in *all* rotating stars unstable. Lindblom, Owen, and Morsink [3] have recently evaluated the timescales associated with the growth of this instability. Gravitational

radiation couples to these modes through the current multipoles rather than the more typical mass multipole moments. This coupling is stronger than anyone anticipated for these modes, and is so strong in fact that the viscous forces present in hot young neutron stars are not sufficient to suppress the gravitational radiation driven instability. Gravitational radiation is expected therefore to carry away most of the angular momentum of hot young neutron stars. These results have now been verified by Andersson, Kokkotas, and Schutz [4].

In this paper we study the gravitational waveforms that are produced as the r-mode instability grows and radiates away the bulk of the angular momentum of a hot young rapidly rotating neutron star. The properties of the r-modes and the instability associated with them are reviewed in Sec. II. The equations that describe (approximately) the evolution of the r-modes as they grow and spin down a rapidly rotating neutron star are derived in Sec. III. These equations are solved numerically and the results are also presented in Sec. III. The gravitational waveforms associated with the r-mode instability are evaluated in Sec. IV. General analytical and detailed numerical expressions for these waveforms are presented. In Sec. V we evaluate the detectability of this type of gravitational wave signal by the laser interferometer gravitational wave detectors such as LIGO [5], VIRGO [6], and GEO [7]. We consider the detectability of signals produced by single nearby sources, and also the detectability of a stochastic background of sources from throughout the universe. Finally, in Sec. VI we discuss the prospects for gravitational-wave astronomy opened up by the r-modes.

II. THE R-MODE INSTABILITY

The r-modes of rotating Newtonian stars are generally defined to be solutions of the perturbed fluid equations having (Eulerian) velocity perturbations of the form

$$\delta\vec{v} = R\Omega f(r/R)\vec{Y}^B_{lm}e^{i\omega t}, \tag{6.2.1}$$

where R and Ω are the radius and angular velocity of the unperturbed star, $f(r/R)$ is an arbitrary dimensionless function, and $\vec{Y}^B_{lm}$ is the magnetic type vector spherical harmonic defined by

$$\vec{Y}^B_{lm} = [l(l+1)]^{-1/2} r\vec{\nabla} \times (r\vec{\nabla}Y_{lm}). \tag{6.2.2}$$

For barotropic stellar models, of primary concern to us here, the Euler equation determines the form of these modes: The radial dependence $f(r/R)$ is determined to be $f(r/R) = \alpha(r/R)^l$, where α is an arbitrary constant [8]. These modes exist with velocity perturbations as given by Eq. (6.2.1) if and only if $l = m$ [8]. Also, the frequencies of these modes are given by [9]

$$\omega = -\frac{(l-1)(l+2)}{l+1}\Omega. \tag{6.2.3}$$

These modes represent large scale oscillating currents that move (approximately) along the equipotential surfaces of the rotating star. The restoring force for these oscillations is the Coriolis force; hence the frequencies of these modes are low compared to the usual f and $p-$modes in slowly rotating stars. These expressions for $\delta\vec{v}$ and ω are the lowest order terms in an expansion in terms of the angular velocity Ω. The exact expressions contain additional terms of order Ω^3. There may exist other modes of rotating barotropic stellar models with properties similar to these classical r-modes; however, our discussion here is limited to the properties of these classical r-modes.

The density perturbation associated with the r-modes can be deduced by evaluating the inner product of $\vec{v}$ (the unperturbed fluid velocity) with the perturbed Euler equation, and the equation for the perturbed gravitational potential [10]:

$$\delta\rho = \alpha R^2\Omega^2\rho\frac{d\rho}{dp}\left[\frac{2l}{2l+1}\sqrt{\frac{l}{l+1}}\left(\frac{r}{R}\right)^{l+1} + \delta\Psi(r)\right] \times Y_{l+1\,l}\,e^{i\omega t}. \tag{6.2.4}$$

The quantity $\delta\Psi$ is proportional to the perturbed gravitational potential $\delta\Phi$, and is the solution to the ordinary differential equation

$$\frac{d^2\delta\Psi(r)}{dr^2}+\frac{2}{r}\frac{d\delta\Psi(r)}{dr}+\left[4\pi G\rho\frac{d\rho}{dp}-\frac{(l+1)(l+2)}{r^2}\right]\delta\Psi(r) = -\frac{8\pi Gl}{2l+1}\sqrt{\frac{l}{l+1}}\rho\frac{d\rho}{dp}\left(\frac{r}{R}\right)^{l+1}, \tag{6.2.5}$$

which satisfies appropriate asymptotic boundary conditions. We note that $\delta\rho$ is proportional to Ω^2 and hence is small (i.e., higher order in Ω) compared to $\delta\vec{v}$ in slowly rotating stars. We also note that $\delta\rho$ is proportional to $Y_{l+1\,l}$—having spherical harmonic index one order in l higher than that of the velocity perturbation. Equation (6.2.4) is the complete expression for the density perturbation to order Ω^2. The exact expression for $\delta\rho$ includes additional terms of order Ω^4.

The r-modes evolve with time dependence $e^{i\omega t-t/\tau}$ as a consequence of ordinary hydrodynamics and the influence of the various dissipative processes. The real part of the frequency of these modes, ω, is given in Eq. (6.2.3), while the imaginary part $1/\tau$ is determined by the effects of gravitational radiation, viscosity, etc. The simplest way to evaluate $1/\tau$ is to compute the time derivative of the energy $\tilde{E}$ of the mode (as measured in the rotating frame). $\tilde{E}$ can be expressed as a real quadratic functional of the fluid perturbations:

$$\tilde{E}=\frac{1}{2}\int\left[\rho\delta\vec{v}\cdot\delta\vec{v}^*+\left(\frac{\delta p}{\rho}-\delta\Phi\right)\delta\rho^*\right]d^3x. \tag{6.2.6}$$

Thus the time derivative of $\tilde{E}$ is related to the imaginary part of the frequency $1/\tau$ by

$$\frac{d\tilde{E}}{dt}=-\frac{2\tilde{E}}{\tau}. \tag{6.2.7}$$

Since the specific expressions for the time derivative of $\tilde{E}$ due to the influences of gravitational radiation [11] and viscosity [12] are well known, Eq. (6.2.7) may be used to evaluate the imaginary part of the frequency.

It is convenient to decompose $1/\tau$:

$$\frac{1}{\tau(\Omega)} = \frac{1}{\tau_{GR}(\Omega)} + \frac{1}{\tau_S(\Omega)} + \frac{1}{\tau_B(\Omega)}, \tag{6.2.8}$$

where $1/\tau_{GR}$, $1/\tau_S$, and $1/\tau_B$ are the contributions due to gravitational radiation emission, shear viscosity and bulk viscosity respectively. Expressions for these individual contributions for the $r-$modes are given by [3]:

$$\frac{1}{\tau_{GR}} = -\frac{32\pi G\Omega^{2l+2}}{c^{2l+3}} \frac{(l-1)^{2l}}{[(2l+1)!!]^2} \left(\frac{l+2}{l+1}\right)^{2l+2} \times \int_0^R \rho\, r^{2l+2} dr, \tag{6.2.9}$$

$$\frac{1}{\tau_S} = (l-1)(2l+1) \int_0^R \eta r^{2l} dr \left(\int_0^R \rho\, r^{2l+2} dr\right)^{-1}. \tag{6.2.10}$$

and

$$\frac{1}{\tau_B} \approx \frac{4R^{2l-2}}{(l+1)^2} \int \zeta \left|\frac{\delta\rho}{\rho}\right|^2 d^3x \left(\int_0^R \rho\, r^{2l+2} dr\right)^{-1}, \tag{6.2.11}$$

where $\delta\rho$ is given in Eq. (6.2.4). We note that the expression for $1/\tau_B$ in Eq. (6.2.11) is only approximate. The exact expression should contain the Lagrangian density perturbation $\Delta\rho$ in place of the Eulerian perturbation $\delta\rho$. The bulk viscosity (see Eq. 6.2.13) is a very strong function of the temperature, being proportional to T^6. Thus, the result of any error that might occur in our approximation for $1/\tau_B$ is simply to shift slightly the temperature needed to achieve a given viscosity timescale. Numerical estimates show that changing this quantity by even a factor of one hundred (as suggested by Ref. [4]), does not substantially affect the important physical quantities computed here (i.e. the spindown rate or the final angular velocity of the star).

We have evaluated these expressions for the imaginary parts of the frequency for a "typical" neutron star model with a polytropic equation of state: $p = k\rho^2$, with k chosen so that a $1.4M_\odot$ model has the radius 12.53km. We use the usual expressions for the viscosity of hot neutron star matter [13]:

$$\eta = 347\rho^{9/4}T^{-2}, \tag{6.2.12}$$

$$\zeta = 6.0 \times 10^{-59}\left(\frac{l+1}{2\Omega}\right)^2 \rho^2 T^6, \tag{6.2.13}$$

where all quantities are expressed in cgs units. We have evaluated the expressions, Eqs. (6.2.9)–(6.2.11), for the dissipative timescales with fiducial values of the angular velocity $\Omega = \sqrt{\pi G\bar{\rho}}$ and temperature $T = 10^9$K. These fiducial timescales $\tilde{\tau}_{GR}$, $\tilde{\tau}_V$, and $\tilde{\tau}_B$ are given in Table 6.1 for the r-modes with $2 \leq l \leq 6$. It will be useful in the following to define a timescale associated with the viscous dissipation $1/\tau_V = 1/\tau_S + 1/\tau_B$. The viscous timescale τ_V and the gravitational timescale τ_{GR} can be expressed then in terms of the fiducial timescales in a way that makes their temperature and angular velocity dependences explicit:

$$\frac{1}{\tau_V} = \frac{1}{\tilde{\tau}_S}\left(\frac{10^9\text{K}}{T}\right)^2 + \frac{1}{\tilde{\tau}_B}\left(\frac{T}{10^9\text{K}}\right)^6\left(\frac{\Omega^2}{\pi G\bar{\rho}}\right), \tag{6.2.14}$$

$$\frac{1}{\tau_{GR}} = \frac{1}{\tilde{\tau}_{GR}}\left(\frac{\Omega^2}{\pi G\bar{\rho}}\right)^{l+1}. \tag{6.2.15}$$

III. EVOLUTION OF THE R-MODES

To determine the gravitational waveform that will result from the instability in the r-modes, we must estimate how the neutron star evolves as the instability grows and radiates the angular momentum of the star away to infinity. Initially the mode will be a small perturbation that is described adequately by the linear analysis that we have described above. However, as the mode grows, non-linear hydrodynamic effects become important and eventually dominate the dynamics. At the present time we do not have available the tools to follow exactly this non-linear phase of the evolution. Instead, we propose a simple approximation that includes (we believe) the basic features of the exact evolution.

TABLE 6.1. Gravitational radiation and viscous timescales (in seconds) are presented for $T = 10^9$ K and $\Omega = \sqrt{\pi G \bar{\rho}}$.

l	$\tilde{\tau}_{GR}$	$\tilde{\tau}_S$	$\tilde{\tau}_B$
2	-3.26×10^0	2.52×10^8	6.99×10^8
3	-3.11×10^1	1.44×10^8	5.13×10^8
4	-2.85×10^2	1.07×10^8	4.01×10^8
5	-2.37×10^3	8.79×10^7	3.26×10^8
6	-1.82×10^4	7.58×10^7	2.74×10^8

We treat the star as a simple system having only two degrees of freedom: the uniformly rotating equilibrium state parameterized by its angular velocity Ω, and the r-mode parameterized by its amplitude α. The total angular momentum J of this simple model of the star is given by,

$$J = I\Omega + J_c, \tag{6.3.1}$$

where I is the moment of inertia of the equilibrium state of the star, and J_c is the canonical angular momentum of the r-mode.

In this simple model of the star the angular momentum J is a function of the two parameters that characterize the state of the system: $J = J(\Omega, \alpha)$. We can determine this functional relationship approximately as follows. The canonical angular momentum of an r-mode can be expressed in terms of the velocity perturbation $\delta\vec{v}$ by [14],

$$J_c = -\frac{l}{2(\omega + l\Omega)} \int \rho\, \delta\vec{v} \cdot \delta\vec{v}^* d^3x. \tag{6.3.2}$$

For the $l = 2$ r-mode of primary interest to us here this expression reduces (at lowest order in Ω) to

$$J_c = -\tfrac{3}{2}\Omega\alpha^2 \tilde{J} M R^2, \tag{6.3.3}$$

where $\tilde{J}$ is defined by

$$\tilde{J} = \frac{1}{MR^4} \int_0^R \rho r^6 dr. \tag{6.3.4}$$

For the polytropic models studied in detail here the dimensionless constant $\tilde{J} = 1.635 \times 10^{-2}$. The moment of inertia I can also be conveniently expressed as

$$I = \tilde{I} M R^2, \tag{6.3.5}$$

where $\tilde{I}$ is given by

$$\tilde{I} = \frac{8\pi}{3MR^2} \int_0^R \rho r^4 dr. \tag{6.3.6}$$

For the polytropic models considered here $\tilde{I} = 0.261$. Thus, our simple model of the angular momentum of the perturbed star is

$$J(\Omega, \alpha) = (\tilde{I} - \tfrac{3}{2}\tilde{J}\alpha^2)\Omega M R^2. \tag{6.3.7}$$

The perturbed star loses angular momentum primarily through the emission of gravitational radiation. Thus, we compute the evolution of $J(\Omega, \alpha)$ by using the standard multipole expression for angular momentum loss. The $l = 2$ r-mode is the primary source of gravitational radiation in our simple model of this system, and this mode loses angular momentum primarily through the $l = m = 2$ current multipole. Thus the angular momentum of the star evolves as

$$\frac{dJ}{dt} = -\frac{c^3}{16\pi G} \left(\frac{4\Omega}{3}\right)^5 (S_{22})^2. \tag{6.3.8}$$

The $l = m = 2$ current multipole moment S_{22} for this system is given by

$$S_{22} = \sqrt{2} \frac{32\pi}{15} \frac{GM}{c^5} \alpha \Omega R^3 \tilde{J}. \tag{6.3.9}$$

Combining Eq. (6.3.8) for the angular momentum evolution of the star with Eqs. (6.2.9), and (6.3.7), we obtain one equation for the evolution of the parameters Ω and α that determine the state of the star:

$$(\tilde{I} - \tfrac{3}{2}\alpha^2\tilde{J})\frac{d\Omega}{dt} - 3\alpha\Omega\tilde{J}\frac{d\alpha}{dt} = \frac{3\alpha^2\Omega\tilde{J}}{\tau_{GR}}. \tag{6.3.10}$$

During the early part of the evolution of the star, the perturbation analysis of the r-modes described earlier applies. In addition to radiating angular momentum from the star via gravitational radiation, the mode will also lose energy via gravitational radiation and neutrino emission (from the bulk viscosity) and also deposit energy into the thermal state of the star due to shear viscosity. It is most convenient to obtain the equation for the energy balance during this part of the evolution in terms of the energy $\tilde{E}$ of the mode as defined in Eq. (6.2.6). For the $l = 2$ r-mode $\tilde{E}$ is given by

$$\tilde{E} = \tfrac{1}{2}\alpha^2\Omega^2 MR^2\tilde{J}. \tag{6.3.11}$$

The time derivative of $\tilde{E}$ is precisely the quantity that was used to determine the imaginary part of the frequency of the mode in Eq. (6.2.7):

$$\frac{d\tilde{E}}{dt} = -2\tilde{E}\left(\frac{1}{\tau_{GR}} + \frac{1}{\tau_V}\right). \tag{6.3.12}$$

Equation (6.3.12) together with (6.3.11) therefore provides a second equation for determining the evolution of the parameters Ω and α that specify the state of the star:

$$\Omega\frac{d\alpha}{dt} + \alpha\frac{d\Omega}{dt} = -\alpha\Omega\left(\frac{1}{\tau_{GR}} + \frac{1}{\tau_V}\right). \tag{6.3.13}$$

Equations (6.3.10) and (6.3.13) can be combined then to determine the evolution of Ω and α during the portion of the evolution in which the perturbation remains small:

$$\frac{d\Omega}{dt} = -\frac{2\Omega}{\tau_V}\frac{\alpha^2 Q}{1+\alpha^2 Q}, \tag{6.3.14}$$

$$\frac{d\alpha}{dt} = -\frac{\alpha}{\tau_{GR}} - \frac{\alpha}{\tau_V}\frac{1-\alpha^2 Q}{1+\alpha^2 Q}. \tag{6.3.15}$$

The equation of state dependent parameter Q that appears in Eqs. (6.3.14) and (6.3.15) is defined by $Q = 3\tilde{J}/2\tilde{I}$. For the polytropic model considered in detail

here $Q = 9.40 \times 10^{-2}$. We note that during the initial linear evolution phase the angular velocity of the star Ω is nearly constant, evolving according to Eq. (6.3.14) on the viscous dissipation timescale. During this phase the amplitude of the mode α grows exponentially on a timescale that is comparable to the gravitational radiation timescale.

After a short time (about 500 s in our numerical solutions) the amplitude becomes so large that non-linear effects can no longer be ignored. We have not yet developed the tools needed to follow the evolution exactly during this non-linear phase. However, we do have some intuition about the non-linear hydrodynamical evolution of gravitationally driven instabilities in rotating stars. This intuition comes from the studies of the effects of gravitational radiation reaction on the evolution of the ellipsoidal models [15,16]. In that case the unstable mode grows exponentially until its amplitude is of order unity. At that point a kind of non-linear saturation occurs, and the growth of the mode stops. The excess angular momentum of the star is radiated away and the star evolves toward a new lower angular momentum equilibrium state. We expect a similar situation to pertain in the evolution of the r-modes. Thus, we expect non-linear effects will saturate and halt the further growth of the mode when the amplitude of the mode becomes of order unity. Thus, when the amplitude α grows to the value

$$\alpha^2 = \kappa, \tag{6.3.16}$$

(where κ is a constant of order unity) we stop evolving the star using Eqs. (6.3.14) and (6.3.15). Instead we set $d\alpha/dt = 0$ during the saturated non-linear phase of the evolution, while continuing to evolve the angular velocity Ω by Eq. (6.3.10) as angular momentum is radiated away to infinity by gravitational radiation. During this phase, then the angular velocity evolves by

$$\frac{d\Omega}{dt} = \frac{2\Omega}{\tau_{GR}} \frac{\kappa Q}{1 - \kappa Q}. \tag{6.3.17}$$

The r-mode will evolve during the saturated non-linear phase of its evolution approximately according to Eqs. (6.3.16) and (6.3.17). During this phase the star will lose most of its angular momentum, and spin down to a state having an angular velocity that is much smaller than $\Omega_K \approx \frac{2}{3}\sqrt{\pi G\bar{\rho}}$. The star will eventually (in about 1 year in our numerical solutions) evolve to a point where the angular velocity and temperature become sufficiently low that the r-mode is no longer unstable. The end of the evolution is characterized by a phase in which the viscous forces and gravitational radiation damp out the energy remaining in the mode and move the star slowly to its final equilibrium configuration. During this final phase, the mode is again of small amplitude and so the linear approximation is adequate to describe the evolution. We monitor the quantity on the right side of Eq. (6.3.15) throughout the non-linear evolution phase. When it becomes negative we change the evolution equations again, from Eqs. (6.3.16) and (6.3.17) back to the linear equations Eqs. (6.3.14) and (6.3.15).

In summary then, we model the evolution of the r-mode as having three distinct phases: (i) The hot young neutron star is born rapidly rotating with a small initial excitation in the $l = 2$ r-mode. This mode initially grows exponentially according to Eqs. (6.3.14) and (6.3.15). (ii) The amplitude of the mode saturates due to non-linear hydrodynamic effects at a value of order unity. The bulk of the angular momentum of the star is radiated away by gravitational radiation during this phase according to Eqs. (6.3.16) and (6.3.17). (iii) The final phase of the evolution begins when the right side of Eq. (6.3.15) becomes negative so that the mode begins to be damped out. During the final phase the star evolves again according to Eqs. (6.3.14) and (6.3.15).

In order to complete our model for the evolution of the r-modes we must specify how the temperature of the star evolves with time. We do this by adopting one of the standard descriptions of the cooling of hot young neutron stars. These stars are expected to cool primarily due to the emission of neutrinos via a modified URCA process. The temperature during this phase falls quickly by a simple power law

cooling formula [17]:

$$\frac{T(t)}{10^9 K} = \left[\frac{t}{\tau_c} + \left(\frac{10^9 K}{T_i} \right)^6 \right]^{-1/6} , \tag{6.3.18}$$

where T_i is the initial temperature of the neutron star, and τ_c is a parameter that characterizes the cooling rate. For the modified URCA process $\tau_c \approx 1$y. A typical value for the initial temperature is $T_i \approx 10^{11}$K. Equation (6.3.18) can now be inserted into Eqs. (6.3.14)–(6.3.17) to provide explicit differential equations for the time evolution of the angular velocity of the star and the amplitude of the mode. These equations can be solved numerically in a straightforward manner.

Figs. 6.1 and 6.2 illustrate the solutions to these equations. The dashed curves in Figs. 6.1 and 6.2 show the critical angular velocity Ω_c, defined by $1/\tau(\Omega_c) = 0$, above which the r-modes are unstable. Figure 6.1 shows the evolution (Ω plotted versus T) of the angular velocity of the star for $\kappa = 1.0$ and a range of values of the initial value of the parameter α. In these simulations we have assumed that the initial angular velocity of the star is $\Omega = \Omega_K$. This figure illustrates that the final non-linear part of the evolution is remarkably insensitive to the initial size of the perturbation.

Figure 6.2 illustrates the dependence of the evolution on the parameter κ by showing several evolutions with initial values of $\alpha = 10^{-6}$. The parameter κ measures the degree of saturation that occurs in the non-linear spindown phase of the star. In our numerical studies we examine the limited range $0.25 \leq \kappa \leq 2$. If κ is taken to be too small, the mode simply does not grow to the point that non-linear effects can stop its growth. Conversely if κ is taken too large, then our simple evolution equations based in part on the linear perturbation theory become singular, e.g. Eq. (6.3.17). The equations break down because the (negative) canonical angular momentum of the mode equals the (positive) angular momentum of the equilibrium configuration, and therefore Eq. (6.3.1) yields the unphysical result that the star has no net angular momentum.

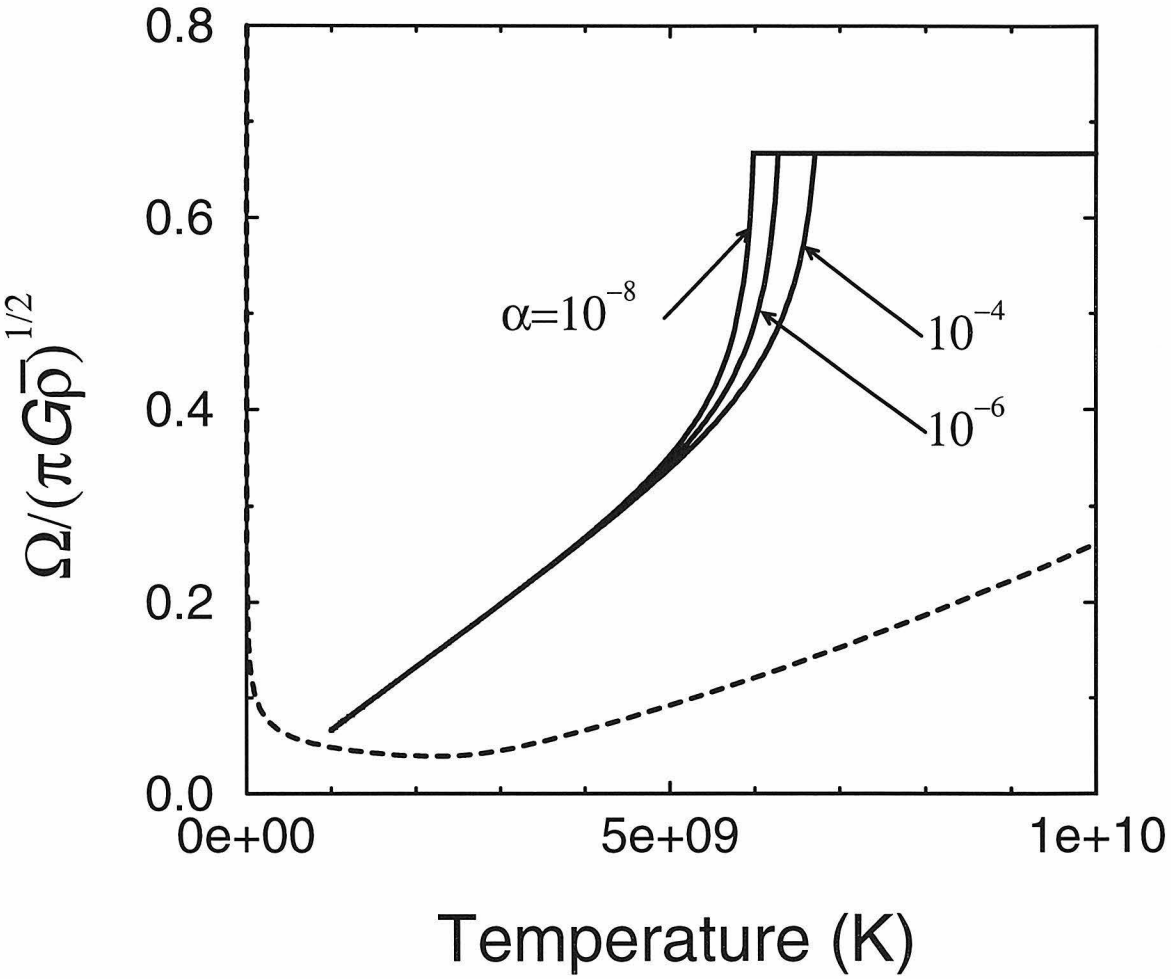

FIG. 6.1. Angular velocity evolution as gravitational radiation spins down a hot rapidly rotating neutron star. α measures the amplitude of the initial perturbation. The dashed curve shows the critical angular velocity Ω_c above which the r-modes are unstable.

We artificially stop all of our evolution curves when the temperature of the star falls to 10^9 K. Below this temperature we expect superfluidity and perhaps other non-perfect fluid effects to make our simple simulation highly inaccurate [18]. Figure 6.2 illustrates that the gravitational radiation instability in the r-modes is nevertheless effective in radiating away most of the angular momentum of the star before the star cools to the point that superfluidity or other effects are expected to become important. Figure 6.2 shows that the amount of angular momentum lost in this process is remarkably insensitive to the value of κ. Thus, the final upper limit on the angular velocity of the star is (fortunately) fairly insensitive to our assumption about the exact nature of the non-linear portion of the star's evolution.

In this simple model of the evolution of the unstable star, we have ignored the effect that viscous heating might have on the cooling rate of the star. If there were too much viscous heating, then the cooling formula given in Eq. (6.3.18) would not be correct. We have evaluated the importance of this re-heating effect by comparing the rate at which thermal energy is being radiated away from the star by neutrinos according to Eq. (6.3.18) with the rate that viscous dissipation deposits thermal energy into the star. Neutrino cooling removes energy from the thermal state of the star at the rate [17]

$$\frac{dU}{dt} = 7.4 \times 10^{39} \left(\frac{T}{10^9 \mathrm{K}} \right)^8 \mathrm{ergs/s}. \tag{6.3.19}$$

Thermal energy is generated by shear viscosity as the star evolves, but not by bulk viscosity. Bulk viscosity radiates away its excess energy directly by neutrinos without significantly interacting with the thermal energy contained in the star. Thus, energy is transfered from the canonical energy of the r-mode to the thermal energy of the star by the formula

$$\frac{dE_c}{dt} = \frac{2\alpha^2 \Omega^2 M R^2 \tilde{J}}{\tau_S}. \tag{6.3.20}$$

Figure 6.3 compares the values of dU/dt and dE_c/dt for our numerical evolution

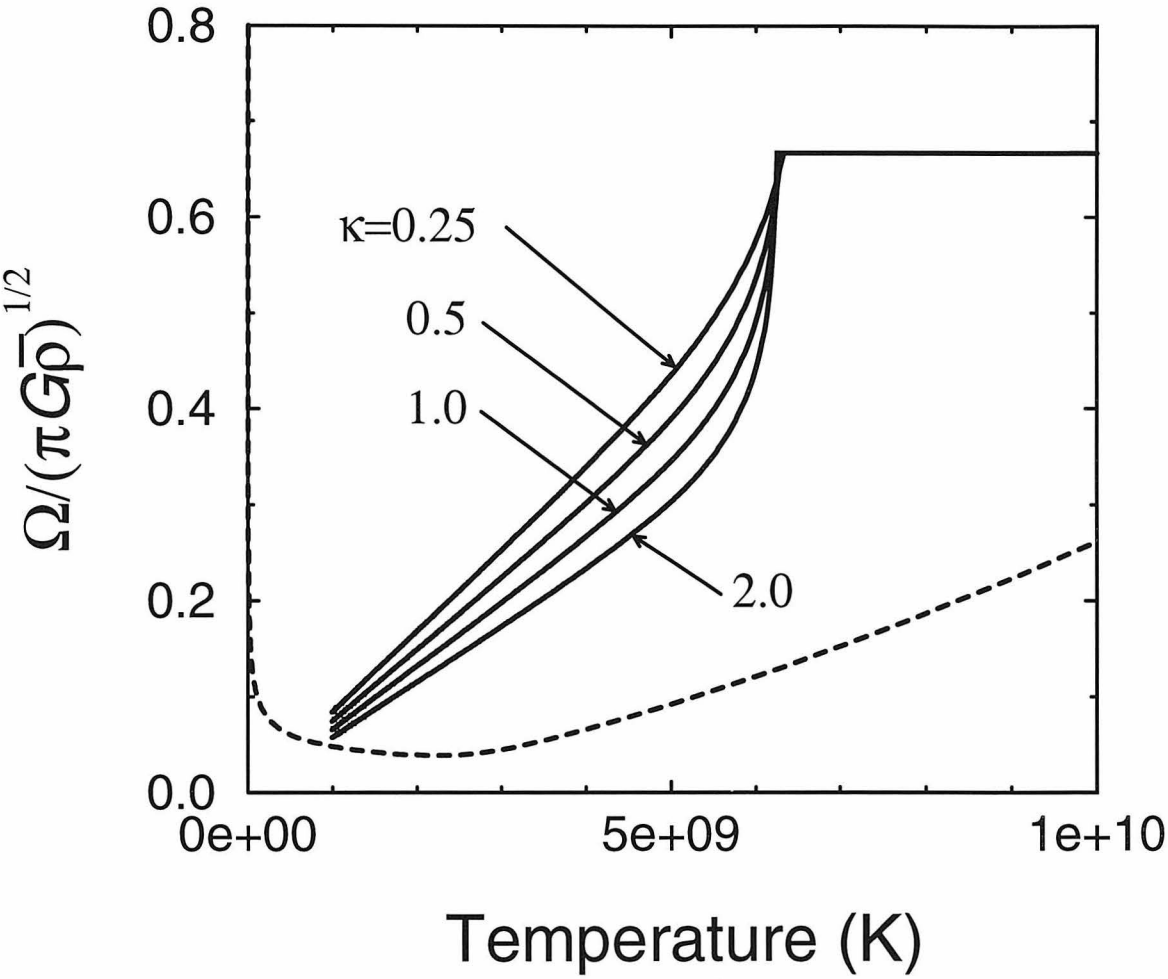

FIG. 6.2. Evolution of the angular velocity of the star depends on the parameter κ in the non-linear saturated phase, but the final angular velocity of the star is insensitive to this. The dashed curve is the same as in Fig. 1.

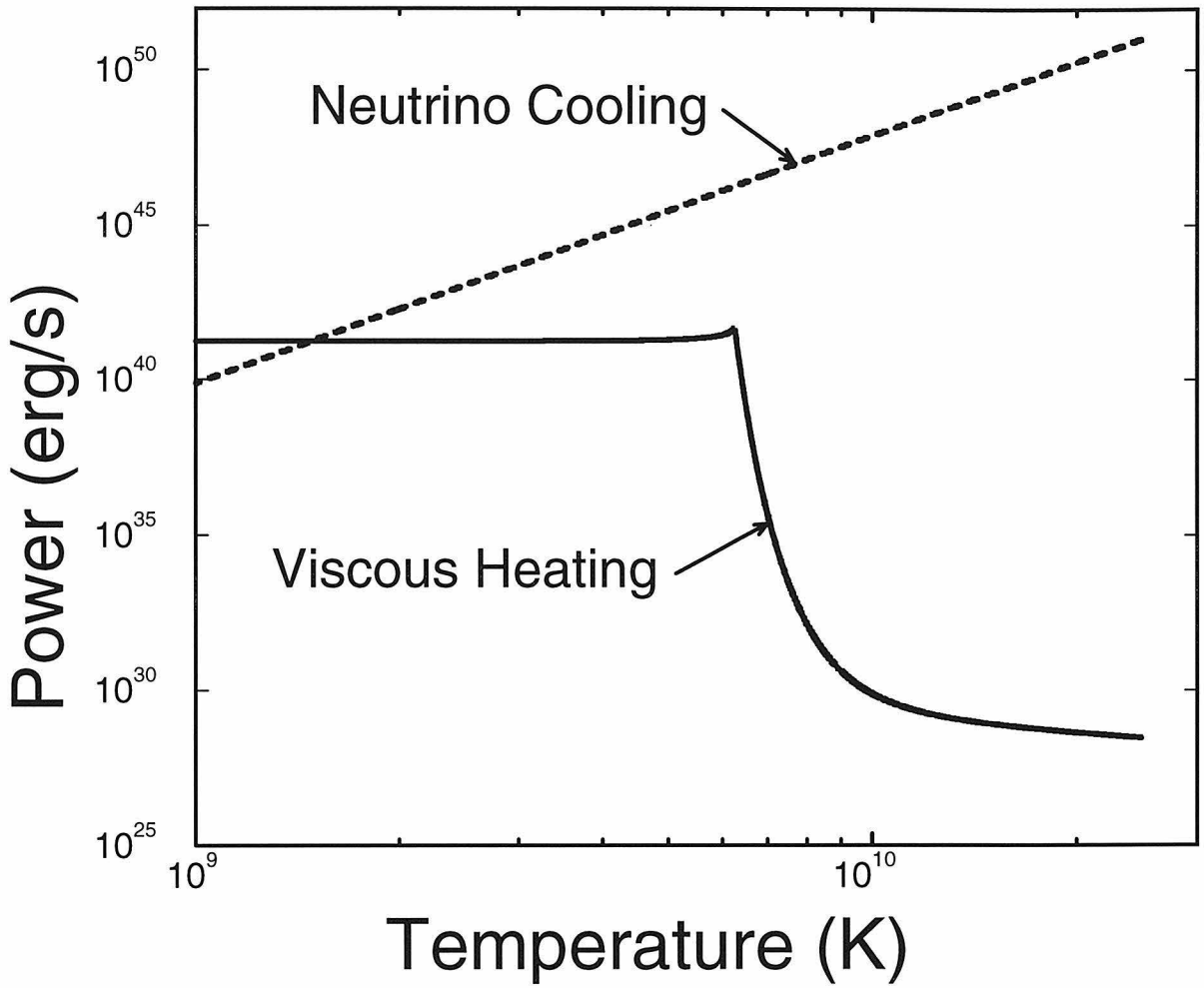

FIG. 6.3. Cooling rate due to neutrino emission is compared to the viscous heating rate in our numerical evolution of the unstable r-modes.

with $\kappa = 1.0$ and initial $\alpha = 10^{-6}$. We find that viscosity does not deposit energy into the thermal state of the star at a significant rate until the temperature of the system falls to about 10^9 K. At this point the star has already lost most of its angular momentum to gravitational radiation, and other dissipative effects (such as those associated with superfluidity) which are not modeled here will start to play a significant role [18]. Thus, we are justified in ignoring the effects of viscous re-heating on the thermal evolution of the star during the early part of its evolution modeled here.

The modified URCA process that determines the thermal evolution used in our evolutions is the standard mechanism by which neutron stars are expected to cool

down to about 10^9 K. Other less standard mechanisms have also been proposed which could significantly speed up the cooling [17]. These mechanisms include neutrino emission processes that require the presence of exotic species (such as quarks or pions) as free particles in the cores of these stars. We have ignored these possibilities in the evolutions described above. If these particles do exist in the cores of neutron stars, we expect that they will only be present in a small volume of material at the centers of these stars. The cores of these stars may well cool rapidly, but the outer layers where the r-mode is large will continue to cool at the rate given in Eq. (6.3.18) until thermal conduction can move energy from the outer layers back into the core.

To estimate what effect a somewhat more rapid cooling might have on the evolution of the r-modes, we have artificially varied the value of the parameter τ_c that determines the cooling rate in Eq. (6.3.18). Figure 6.4 shows the results of the evolution of an r-mode with initial $\alpha = 10^{-6}$ and $\kappa = 1.0$ for several values of τ_c. We see that while the details of the evolution are somewhat effected, the total amount of angular momentum radiated away by gravitational radiation, and the final angular velocity of the star are fairly insensitive to the rate at which the star cools to 10^9 K.

IV. GRAVITATIONAL WAVEFORMS

As the r-mode grows and evolves it emits gravitational radiation. In this section we calculate the waveforms for the gravitational wave strain $h(t)$ and its Fourier transform $\tilde{h}(f)$ that are produced by this r-mode instability. These are the quantities that can be measured by the gravitational wave detectors now under construction (LIGO, VIRGO, GEO, etc.). During the non-linear saturation phase of the r-mode evolution, gravitational radiation controls the dynamics. In this case $\tilde{h}(f)$ turns out to be independent of the details of the evolution, and thus can be determined quite generally. An evolutionary model *is* needed, however, to determine df/dt, the time dependence of the various quantities, and the initial and final frequencies of the

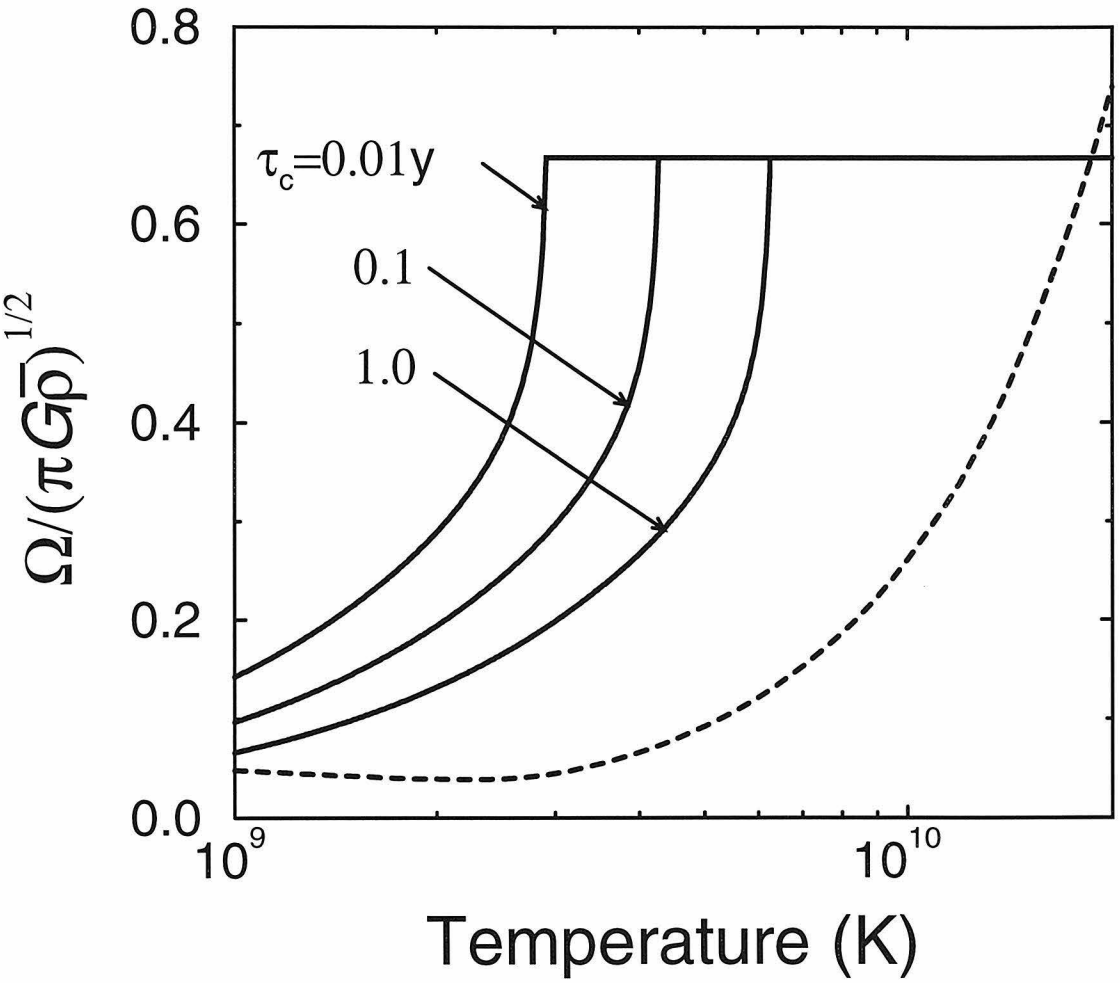

FIG. 6.4. Angular velocity evolution due to gravitational radiation emission using several values for the timescale τ_c on which the star cools.

saturation phase. In this section we present the general model independent derivation of $\tilde{h}(f)$ for the non-linear saturated phase of the evolution. We also give expressions for the gravitational wave strain that apply to the early phases of the evolution using the simple model discussed in Sec. III.

The frequency-domain gravitational waveform

$$\tilde{h}(f) \equiv \int_{-\infty}^{\infty} e^{2\pi i f t} h(t)\, dt \tag{6.4.1}$$

is determined completely by the assumption that the angular momentum radiated as gravitational waves comes directly from the angular momentum of the star. This assumption is expected to be satisfied during the non-linear saturated phase of the evolution, but not during the early evolution when the mode is growing exponentially. This derivation is based on Blandford's analysis (as discussed in [19]) of white dwarf collapse to a neutron star which is halted by centrifugal forces (see also [20,21]). Such a star can only collapse to a neutron star by shedding its excess angular momentum through gravitational waves. In that situation as in the non-linear saturation phase of the r-mode evolution, gravitational radiation determines the rate at which angular momentum leaves the system, and this in turn determines the rate at which the frequency of the radiation evolves with time.

In the stationary phase approximation (which is always valid for a secular instability) the gravitational wave strain $h(t)$ is related to its Fourier transform $\tilde{h}(f)$ by

$$|h(t)|^2 = |\tilde{h}(f)|^2 \left|\frac{df}{dt}\right|. \tag{6.4.2}$$

Throughout this discussion we treat $h(t)$ as a complex quantity with purely positive frequency. For the $l = 2$ mode of primary importance here, the mode frequency is $\omega = \frac{4}{3}\Omega$, or $f = \frac{2}{3\pi}\Omega$, where f is the frequency of the emitted gravitational waves measured in Hz. Assuming the star is uniformly rotating, its angular momentum is $J = I\Omega$, where I is the star's moment of inertia. The moment of inertia is fairly

independent of angular velocity (especially at small angular velocities where most of the detectable signal from these sources is likely to originate) and is also fairly independent of the amplitude of the excited r-mode (see Eq. 6.3.7). Thus, I is reasonably well approximated by its non-rotating value. Thus

$$\frac{dJ}{df} = \frac{3\pi}{2} I. \tag{6.4.3}$$

The rate at which angular momentum is radiated away by a source is related to the gravitational wave amplitude by the expression [11]

$$\frac{dJ}{dt} = 4\pi D^2 \frac{m}{\omega} \frac{1}{16\pi} \omega^2 \langle h_+^2 + h_\times^2 \rangle \tag{6.4.4}$$

where h_+ and $h_\times$ are the amplitudes of the two polarizations of gravitational waves, D is the distance to the source, and $\langle \ldots \rangle$ denotes an average over the orientation of the source and its location on the observers sky. Using $dt/df = dJ/df\,(dJ/dt)^{-1}$ and combining Eqs. (6.4.2)–(6.4.4) we obtain

$$\langle |\tilde{h}_+(f)|^2 + |\tilde{h}_\times(f)|^2 \rangle = \frac{3I}{4D^2 f}. \tag{6.4.5}$$

The measured value of $|\tilde{h}(f)|^2$ depends on the orientation of the source and its location on the detector's sky. Averaged over these angles, its value is given by

$$\langle |\tilde{h}(f)|^2 \rangle = \tfrac{1}{5} \langle |\tilde{h}_+(f)|^2 + |\tilde{h}_\times(f)|^2 \rangle. \tag{6.4.6}$$

We are actually interested in the average over source locations in three-dimensional space, not just the two angles on the sky. The spatial average weights more strongly those orientations that yield stronger signals, effectively increasing $\langle |\tilde{h}(f)|^2 \rangle$ by about $\frac{3}{2}$. Combining these results then, the average value of $\tilde{h}$ produced by our fiducial r-mode source (with $M = 1.4 M_\odot$, $D = 20$Mpc, $R = 12.5$km) is

$$\tilde{h}(f) = 5.7 \times 10^{-25} \sqrt{\frac{1\ \text{kHz}}{f}}\ \text{Hz}^{-1}. \tag{6.4.7}$$

Note that this expression does not depend (in the frequency domain) on the details of the evolutionary model apart from the upper and lower frequency cutoffs. This

expression, Eq. (6.4.7), only depends on the assumption that the frequency of the mode evolves as angular momentum is radiated by the star according to Eq. (6.4.3). We expect this to be satisfied during the non-linear saturated phase of the r-mode evolution, but probably not during the early linear growth phase of the mode.

To obtain the complete waveforms for a particular evolutionary model, we start with the usual expression for the gravitational field in terms of its multipoles [11]. We average this expression over angles in the manner described above to obtain

$$h(t) = \sqrt{\frac{3}{80\pi}}\frac{\omega^2 S_{22}}{D}. \tag{6.4.8}$$

For the simple two-parameter evolution of the r-mode instability described in Sec. III, this expression can be simplified using Eq. (6.3.9) to

$$h(t) = 4.4 \times 10^{-24}\alpha \left(\frac{\Omega}{\sqrt{\pi G\bar{\rho}}}\right)^3 \left(\frac{20\,\mathrm{Mpc}}{D}\right). \tag{6.4.9}$$

This simple evolutionary model also gives a simple formula for the frequency evolution. During the non-linear saturation phase of the evolution Eq. (6.3.17) can be written as

$$\frac{df}{dt} \approx -1.8\kappa \left(\frac{f}{1\ \mathrm{kHz}}\right)^7 \mathrm{Hz/s}, \tag{6.4.10}$$

where we have assumed that $\kappa Q \ll 1$. The time for the gravitational wave frequency to evolve to its minimum value f_{min} is obtained by integrating Eq. (6.4.10):

$$t \approx \frac{1.0}{\kappa}\left(\frac{120\mathrm{Hz}}{f_{\mathrm{min}}}\right)^6 \mathrm{y}. \tag{6.4.11}$$

Analogous model dependent expressions can also be derived for the early linear phase of the evolution. During this period the amplitude α grows exponentially on the gravitational timescale according to Eq. (6.3.14), while the frequency of the mode changes extremely slowly according to Eq. (6.3.15). Solving these equations approximately gives

$$\frac{df}{dt} \approx -\frac{2.7\alpha^2}{t}\left(\frac{f}{1\text{ kHz}}\right)^3, \tag{6.4.12}$$

Using Eq. (6.4.9) this implies that $\tilde{h}$ during the linear growth phase is given approximately by

$$\tilde{h}(f) \approx 4.7 \times 10^{-25}\sqrt{t}\left(\frac{f}{1\text{ kHz}}\right)^{3/2} \text{Hz}^{-1}. \tag{6.4.13}$$

where $t \equiv t(f)$ is obtained from Eq. (6.4.12). The factor $f^{3/2}$ that appears in Eq. (6.4.13) is essentially constant, being given by the initial mode frequency as determined by the initial angular velocity of the star. Since this factor is essentially constant during the linear evolution phase, this implies that $\tilde{h}(f)$ grows as $\sqrt{t}$. The duration of the initial linear growth phase can be estimated from the solution for the amplitude α:

$$\Delta t = 1.5 \times 10^3 \left(\frac{1\text{ kHz}}{f}\right)^6 \frac{\ln\left(\sqrt{\kappa}/\alpha_o\right)}{\ln\left(10^6\right)}\,\text{s}, \tag{6.4.14}$$

where α_o is the initial size of the perturbation. During this interval, the mode frequency decreases by an amount of order $0.1\kappa\,\text{Hz}$. This is the width of the initial spikes shown in Figs. 7 and 8. The maximum amplitude achieved by $\tilde{h}$ can also be determined from Eqs. (6.4.13) and (6.4.14):

$$\max(\tilde{h}) \approx 1.8 \times 10^{-23}\left(\frac{1\text{ kHz}}{f}\right)^{9/2} \times \left[\frac{\log\left(\sqrt{\kappa}/\alpha_o\right)}{\log\left(10^6\right)}\right]^{1/2} \text{Hz}^{-1}. \tag{6.4.15}$$

This expression for $\max(\tilde{h})$ is fairly insensitive to the duration of the growth phase, and as well to the exact point at which the transition to the non-linear saturation phase occurs. The value of $\max(\tilde{h})$ *is* rather sensitive to our expression for df/dt however. If df/dt were to differ during the linear growth phase from the expression used here by any small effect (such as non-linear modifications of the frequency of the mode) then the the resulting change on $\max(\tilde{h})$ could be large. The analytical

expressions given here, Eqs. (6.4.13)–(6.4.15), do however accurately represent (to within a few percent) the exact numerical solutions to the equations for our simple model in this region.

Figure 6.5 illustrates our full numerical solutions for the time dependence of the gravitational wave amplitude $h(t)$ for several values of the parameters α with $\kappa = 1$. Figure 6.6 illustrates the time dependence of $h(t)$ for various values of κ with $\alpha = 10^{-6}$. All of these curves represent the gravitational radiation emitted by a neutron star initially spinning with angular velocity $\Omega = \Omega_K = \frac{2}{3}\sqrt{\pi G\bar{\rho}}$. In this section and the next we terminate the evolution once the star has cooled to 10^9K. Below this temperature the evolution will be significantly affected by mechanisms not dealt with in this paper, such as the superfluid transition, the re-heating of the star by viscous dissipation in the mode, and dissipation mechanisms (e.g. plate tectonics) associated with the rapidly forming crust.

Figs. 6.7 and 6.8 illustrate the frequency dependence of $\tilde{h}(f)$ for a $1.4M_\odot$ neutron star located at 20 Mpc using the same values of α and κ used in Figs. 6.5 and 6.6. Figure 6.7 illustrates that $\tilde{h}(f)$ is remarkably insensitive to the initial size of the perturbation α. The sharp vertical spikes appearing at the high-frequency ends of these curves are due to the extremely monochromatic gravitational waves emitted during the linear growth phase. The structure of this spike in our model is accurately described by Eqs. (6.4.13)–(6.4.15), but it is not clear that this spike is a robust feature of our model. During the phase of the evolution that produces the spike, the amplitude of the mode is quite small except for a period of about one minute. Thus the total amount of radiated energy and angular momentum contained in this spike is quite small. The spike is not likely to play an important role in the detection of these sources even if it is a real feature of the r-mode instability.

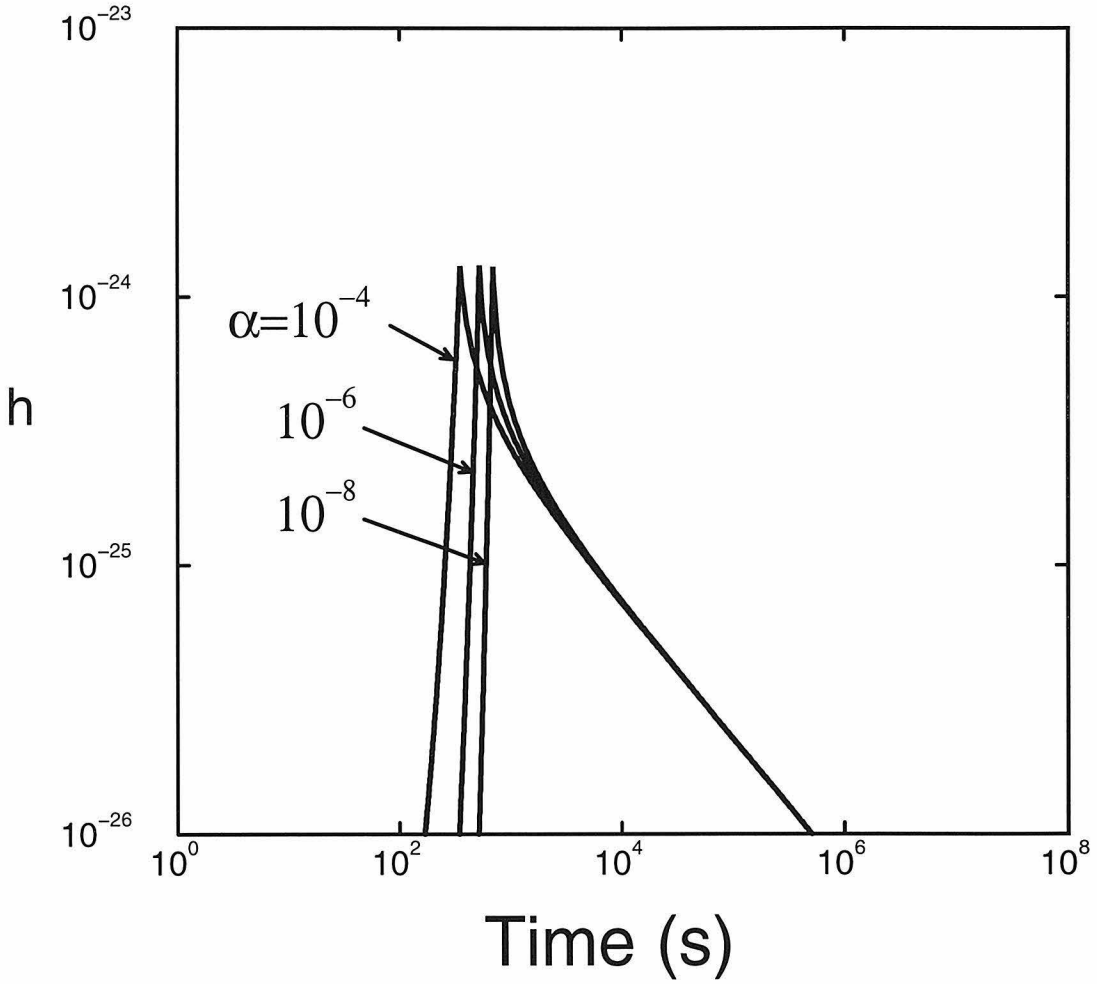

FIG. 6.5. Time dependence of the gravitational wave amplitude $h(t)$ for a detector located at $D = 20\,\mathrm{Mpc}$. The peak amplitude is very insensitive to the initial size of the perturbation α.

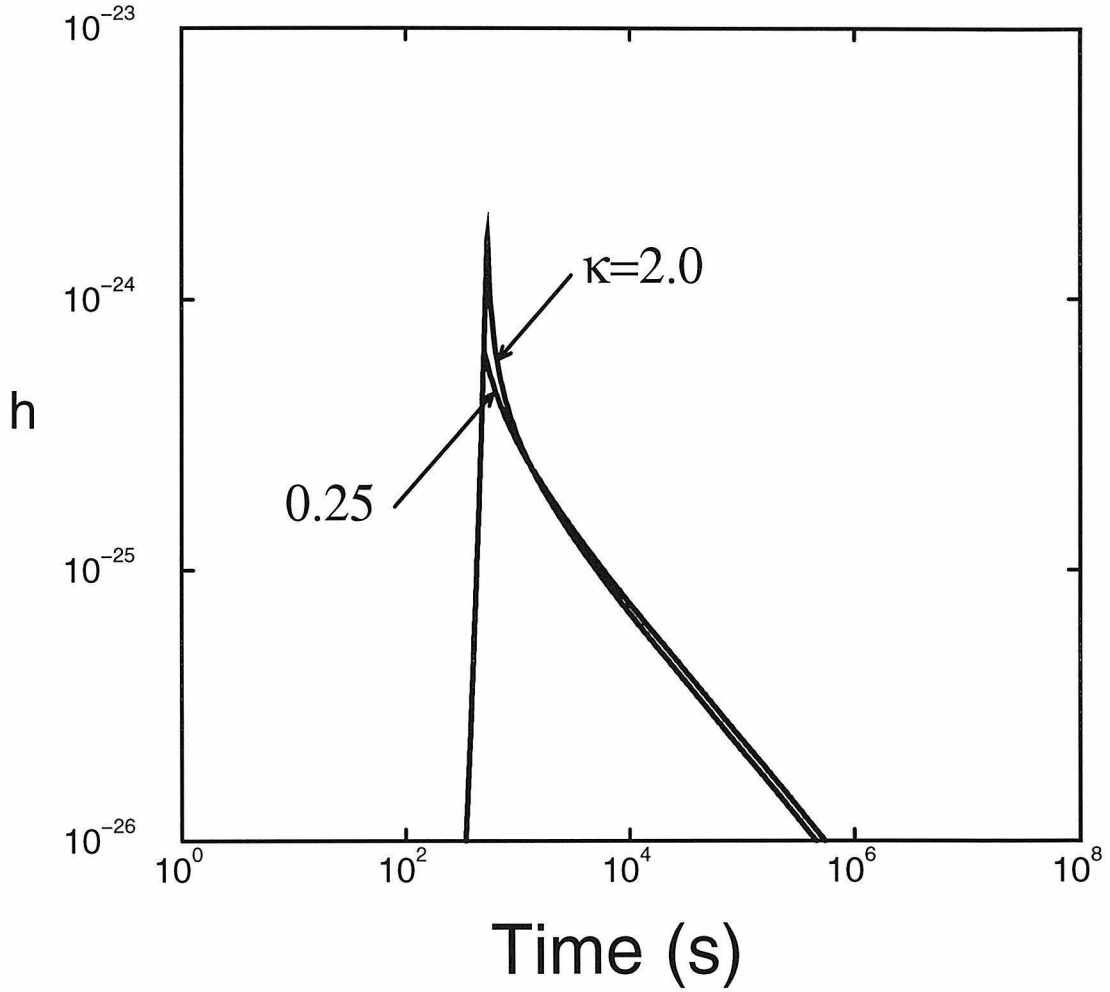

FIG. 6.6. Time dependence of the gravitational wave amplitude $h(t)$. The late time amplitude is rather insensitive to the non-linearity parameter κ.

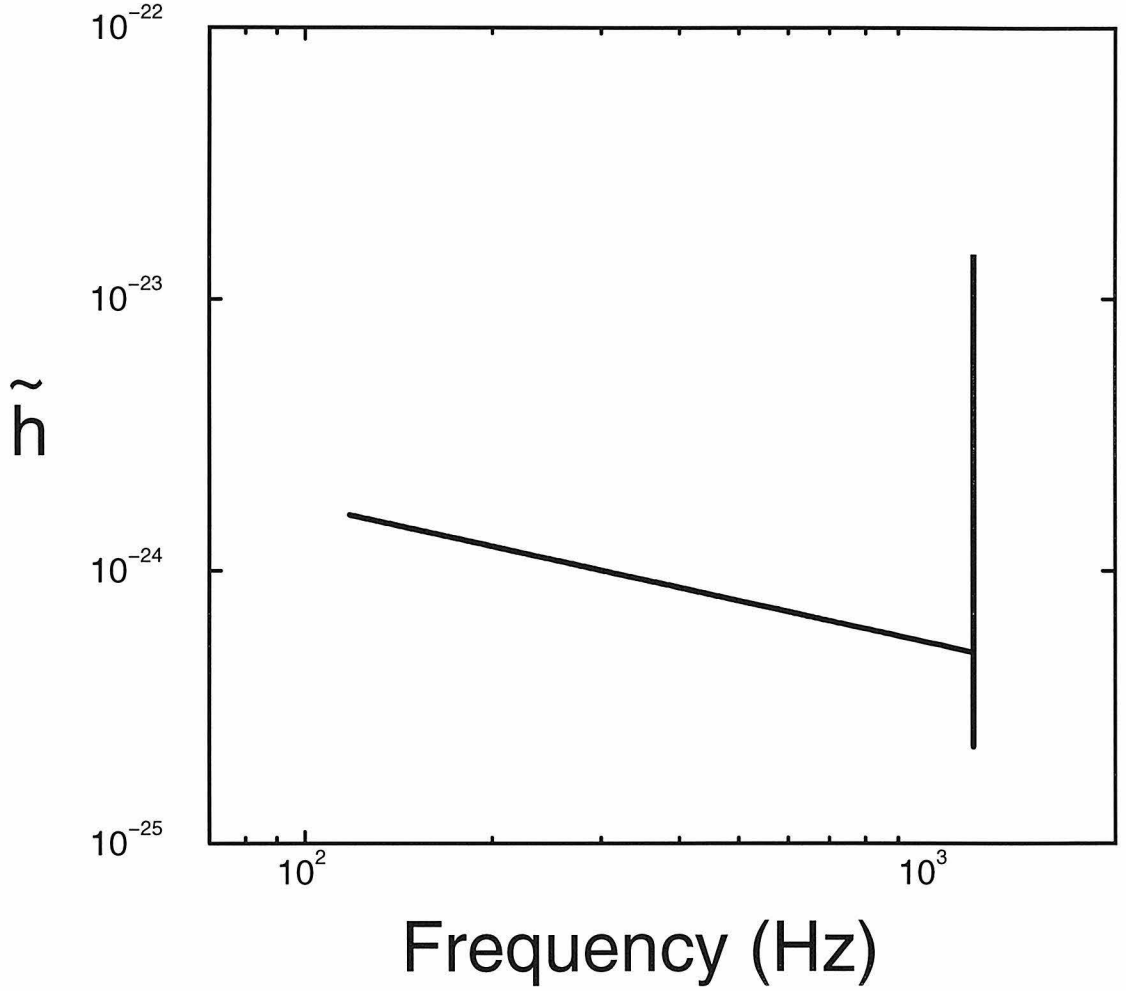

FIG. 6.7. Frequency dependence of the gravitational wave amplitude $\tilde{h}$ for a source located at 20 Mpc.

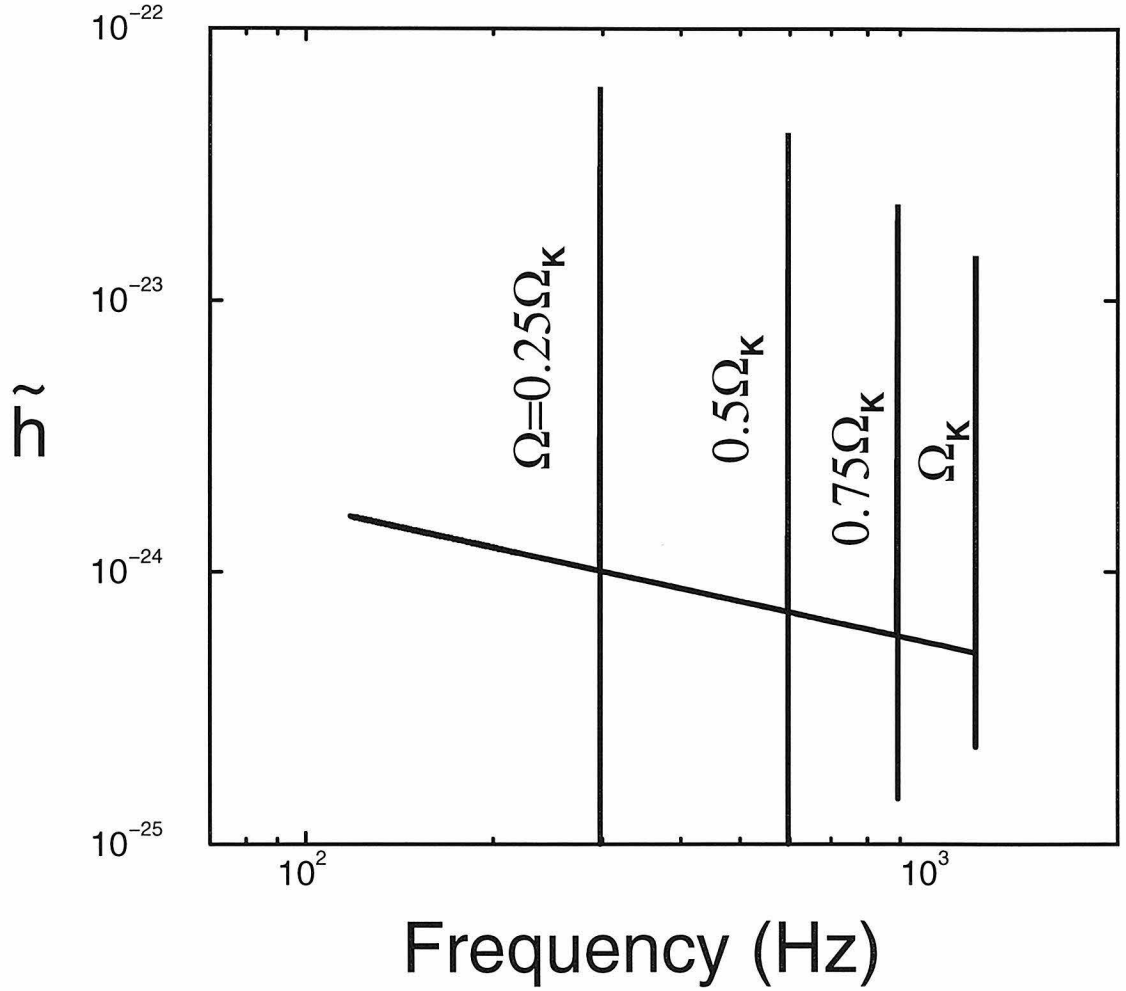

FIG. 6.8. Frequency dependence of the gravitational wave amplitude $\tilde{h}$ for various values of the initial angular velocity of the star.

V. DETECTABILITY

In this section we discuss the detectability of the gravitational radiation emitted by young neutron stars spinning down due to the r-mode instability. This radiation might be detected as strong sources from single spindown events or as a stochastic background made up of many weaker sources.

A. Single Sources

First we estimate the signal-to-noise ratio S/N for a single source located at a distance D, chosen to be large enough so that there is likely to be a reasonable event rate (say a few events per year). This distance D must be large enough then to include several thousand galaxies (assuming that the observed supernova rate is comparable to the neutron star formation rate). Thus we take this fiducial distance to have the value $D = 20\,\mathrm{Mpc}$ [22], the approximate distance to the Virgo cluster of galaxies. We estimate the optimal value of S/N that could be obtained by matched filtering. Because matched filtering is probably not feasible for these sources, this estimate provides only an upper limit of what might be achieved. We briefly discuss two more realistic search strategies based on barycentered Fourier transforms of the data [23].

Using matched filtering, the power signal-to-noise ratio $(S/N)^2$ of the detection is given by

$$\left(\frac{S}{N}\right)^2 = 2\int_0^\infty \frac{|\tilde{h}(f)|^2}{S_h(f)}\,df \tag{6.5.1}$$

where $S_h(f)$ is the power spectral density of the detector strain noise. The constant in front of the integral in Eq. (6.4.5) is 2 (instead of 4 as in Ref. [24]) because our h is complex (with purely positive frequency). Equation (6.5.1) can also be written

$$\left(\frac{S}{N}\right)^2 = 2\int \frac{df}{f}\left(\frac{h_c}{h_{\mathrm{rms}}}\right)^2. \tag{6.5.2}$$

Here the rms strain noise $h_{\rm rms}$ in the detector is given by

$$h_{\rm rms} \equiv \sqrt{f\, S_h(f)}, \tag{6.5.3}$$

where $S_h(f)$ is the power spectral density of the noise, and the characteristic amplitude h_c of the signal is defined by [19]

$$h_c \equiv h\sqrt{f^2 \left|\frac{dt}{df}\right|}. \tag{6.5.4}$$

The quantity multiplying h on the right side of Eq. (6.5.4) is generally interpreted as the number of cycles radiated while the frequency changes by an amount of order f. This interpretation is correct as long as the frequency evolution is very smooth.

However, our evolutionary model of the frequency evolution contains a discontinuity as the mode stops linearly evolving and saturates. Consequently the actual number of cycles spent near the initial frequency is far fewer than indicated by Eq. (6.5.4). The quantity h_c is a useful estimator of the effective filtered amplitude of a signal because the *integral* of $(h_c/h_{\rm rms})^2$ always gives the optimal $(S/N)^2$. Therefore a spike in h_c must be interpreted with some caution—the peak value of the spike is useless unless one also knows the bandwidth of the spike.

In Figure 6.9 we plot h_c versus frequency, superimposed on $h_{\rm rms}$ for three LIGO interferometer configurations. In the saturation phase (i.e., not including the spike) h_c is well approximated by

$$h_c \approx 5.7 \times 10^{-22} \left(\frac{f}{1\ \text{kHz}}\right)^{1/2}. \tag{6.5.5}$$

We plot $h_{\rm rms}$ for the LIGO "first interferometers" [5] (which we abbreviate LIGO I), the "enhanced interferometers" [25] (LIGO II), and the "advanced interferometers" [5] (LIGO III). The noise power spectral density for LIGO I is well approximated by the analytical fit [26]

$$S_h(f) = \frac{S_o}{3}\left[\left(\frac{f_o}{f}\right)^4 + 2\left(\frac{f}{f_o}\right)^2\right] \tag{6.5.6}$$

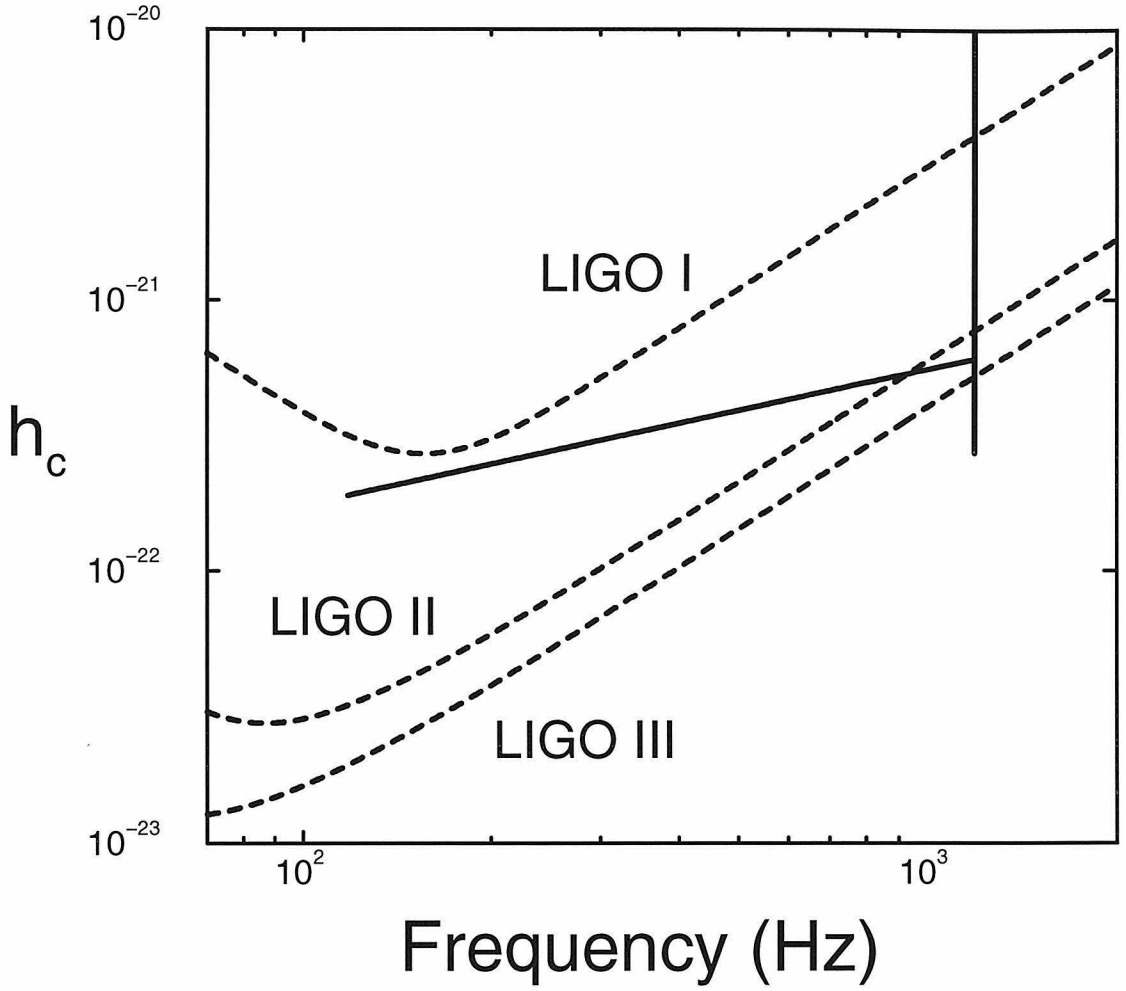

FIG. 6.9. Characteristic gravitational wave amplitude h_c (solid curve) compared to the noise amplitude $h_{\rm rms}$ (dashed curves) for LIGO.

where $S_o = 4.4 \times 10^{-46}$ Hz^{-1} and $f_o = 175$ Hz. For LIGO II we construct the approximation

$$S_h(f) = \frac{S_o}{11}\left\{2\left(\frac{f_0}{f}\right)^{9/2} + \frac{9}{2}\left[1 + \left(\frac{f}{f_0}\right)^2\right]\right\} \tag{6.5.7}$$

where $S_o = 8.0 \times 10^{-48}$ Hz^{-1} and $f_o = 112$Hz. For LIGO III the noise spectral density is well approximated by [27]

$$S_h(f) = \frac{S_o}{5}\left\{\left(\frac{f_0}{f}\right)^4 + 2\left[1 + \left(\frac{f}{f_0}\right)^2\right]\right\} \tag{6.5.8}$$

where $S_o = 2.3 \times 10^{-48}$ Hz^{-1} and $f_o = 76$ Hz.

Most of the contribution to S/N in Eq. (6.5.2) comes from the saturation phase of the evolution which is largely model independent as discussed earlier. Given a detector noise curve, S/N is thus independent of most details of the waveform except the final frequency of the neutron star. We therefore have

$$\left(\frac{S}{N}\right)^2 = \frac{9I}{10D^2}\int_{f_{\rm min}}^{f_{\rm max}} \frac{df}{f\,S_h(f)}. \tag{6.5.9}$$

The minimum frequency $f_{\rm min}$ reached by the r-mode evolution is about 120 Hz. At frequencies slightly larger than $f_{\rm min}$, the LIGO II noise is dominated by photon shot noise. If we ignore the other noise components, $S_h(f)$ becomes

$$S_h(f) = 2.6 \times 10^{-52} f^2. \tag{6.5.10}$$

For $f_{\rm max} \gg f_{\rm min}$ the integral is dominated by the lower cutoff. Thus, the LIGO II S/N is given approximately by

$$\frac{S}{N} \approx 8.8 \left(\frac{I}{10^{45}{\rm cgs}}\right)^{1/2} \left(\frac{D}{20\,{\rm Mpc}}\right)^{-1} \left(\frac{f_{\rm min}}{120\,{\rm Hz}}\right)^{-1}. \tag{6.5.11}$$

Including the other components of the noise decreases S/N somewhat. For the numerical evolutions of our simple model with $\kappa = 1.0$ which terminate at 10^9 K, we find we find $S/N = 1.2$, 7.6, and 10.6 for LIGO I, II, and III respectively at $D = 20$ Mpc. These last three results scale with I and D just as in Eq. (6.5.11), but the dependence on $f_{\rm min}$ is now more complicated. The contribution to S/N from the high frequency spike in our model is 0.6 for LIGO II, and about 0.1 for LIGO I. While the height of the spike in h_c may not be a robust feature of our simple model, the contribution that this spike makes to the overall S/N probably is. These numbers indicate that the gravitational radiation from the r-mode instability is a probable source for LIGO II if some near-optimal data analysis strategy can be developed. It appears unlikely that the radiation from the high frequency spike will be detectable.

Given the recent discovery of the ultrafast young pulsar PSR J0537–6910 in the Large Magellanic Cloud [28], it is interesting to examine the effect on detectability of a

relatively high superfluid transition temperature. If the initial period of PSR J0537–6910 was about 7 ms (as extrapolated from the braking indices of typical young pulsars), that could indicate a superfluid transition temperature of about 2×10^9 K and final gravitational-wave frequency of about 200 Hz. Cutting off our simulations at this point in the evolution, we obtain for LIGO II the S/N of about 5.

It is clear from Fig. 6.9 that the first-generation LIGO and VIRGO detectors will not see r-mode events from the Virgo cluster. Their sensitivity is a factor of about 8 worse than the enhanced detectors. We have also considered the possibility that GEO [7] might detect these sources by using narrow-banding, where it can improve its sensitivity in a restricted frequency range at the expense of worse sensitivity elsewhere. However, for the kind of broad-spectrum signal produced by the r-mode instability, narrow-banding is in fact neutral: the gain of signal-to-noise ratio in the selected band is just compensated by the loss over the rest of the spectrum. So GEO is not likely to see these signals either. Nor will advanced resonant detectors: at their frequencies and in their relatively narrow bandwidths, there is just not enough power in these signals if the sources are in the Virgo cluster. For example, the proposed GRAIL detector [29] operating at its quantum-limited sensitivity ($S_h = 1.6 \times 10^{-48}$ Hz^{-1}) between 500 and 700 Hz would have $S/N \approx 1$ for a source at the distance of the Virgo cluster.

Matched filtering using the year-long waveform templates that would be needed to describe these sources completely could yield the signal-to-noise ratios quoted above. However, this is not a practical strategy for this type of signal due to the prohibitively large number of templates that would be needed to parameterize our ignorance of these sources and the resulting high computational cost of filtering the data with these templates. Other strategies equivalent to combining the results of shorter template searches might well be computationally feasible, although they would obtain less than the optimal S/N.

The barycentered fast Fourier transform (FFT) technique that has been designed to search for nearly periodic signals [23] might well provide one such method. Figure 6.10 shows the spindown age

$$\tau_{\rm sd} = -f\,\frac{dt}{df} \tag{6.5.12}$$

for a neutron star spinning down due to the r-mode instability. This quantity provides a reasonably good estimate of the time spent by the evolving star in the saturated non-linear phase, but it is not a good estimate of the amount of time spent during the linear growth phase (for the reasons outlined above). During the saturated phase $\tau_{\rm sd}$ is given approximately by

$$\tau_{\rm sd} \approx \frac{580}{\kappa}\left(\frac{1\ {\rm kHz}}{f}\right)^6\ {\rm s} \approx \frac{6t}{\kappa}. \tag{6.5.13}$$

The signal becomes quite monochromatic after about one day, in the sense that the spindown timescale is long compared to the inevitable daily modulation of the signal due to the motion of the Earth. Thus the search techniques for periodic sources should work well. In many cases the supernova will be observed, yielding the location of the source and allowing a search over spindown parameters only, a *directed spindown search.*

The most straightforward way to conduct a directed spindown search is to search over generic spindown parameters as discussed by Brady and Creighton [30]. This involves re-sampling the data so as to render sinusoidal a signal with arbitrary (smooth) frequency evolution, then Fourier transforming it. The signal frequency evolution (which determines the re-sampling) is modeled as

$$f(t) = f_0 \sum_{n=0}^{N} \frac{1}{n!}\left(\frac{t}{\tau_n}\right)^n, \tag{6.5.14}$$

where f_0 is the frequency at the beginning of the FFT, t is the time measured from the beginning of the FFT, and τ_n are expansion parameters with $\tau_1 = \tau_{\rm sd}$. The number N of spindown parameters needed is set by the requirement that the frequency drift

due to the next term in the series (6.5.14) be less than one frequency bin of the FFT (which is in turn determined by the integration time $\tau_{\rm int}$). This implies (assuming $\tau_n \approx \tau_{\rm sd}$) that

$$\tau_{\rm int}^{N+1} \approx \frac{N!}{f_0} \tau_{\rm sd}^N. \tag{6.5.15}$$

One must choose a set of points in the spindown parameter space for which to perform the re-sampling and FFT. Too few points and one misses signals by re-sampling at the wrong rate; too many and the computational cost of performing all the FFTs becomes prohibitive if data analysis is to be performed "on-line," i.e. keep up with data acquisition. The points in parameter space are chosen using a metric which relates distance in parameter space to loss of S/N [23]. The integration time, which is set so as to optimize the sensitivity of an on-line search for the (fixed) computational power available, is far shorter than a year even for a teraflop computer. Therefore such a search would achieve at best a fraction of the optimal S/N [30]. It is possible that a hierarchical version of this strategy could be developed, in which the best candidates from a year of shorter FFTs are somehow combined to give an improved confidence level. Developing such a strategy would require extensive further investigation.

One way to increase the sensitivity of a directed spindown search would be to constrain the spindown parameter space by taking advantage of whatever information we have about the source from physical models. In practice we do not have and probably will never have completely reliable models for this type of system. The phenomenological model presented here has many physical assumptions that may prove to be inadequate. For instance, in the saturation phase it is highly unlikely that the star can be represented simply as a uniformly rotating equilibrium configuration plus a linear perturbation. When the mode reaches saturation, the mean velocity perturbation is comparable to the rotation rate of the star. Thus in the saturation phase, the velocity field may develop complicated nonlinear structures (such as the

cyclones on Jupiter) that produce gravitational radiation involving many different multipoles. Long-lived non-axisymmetric structures requiring higher-order modes are seen in the density perturbations of simulations of star formation when there is enough angular momentum [31]. Although the physics is very different in such simulations, a priori we see no reason to believe that the velocity analogues of these structures are not formed by the r-mode instability.

However, not all of the physics affects the waveforms. Some kind of phenomenological model of the signal (as opposed to the star) could be enough to substantially reduce the volume of spindown parameter space to be searched. For a reasonable model of the neutron star, all of the terms in the expansion for df/dt might be determined from a relatively small number of phenomenological parameters. Although quite crude, the model of r-mode instability gravitational waveforms provided here has several features which should be fairly robust: the form of $\tilde{h}(f)$ during the spindown phase, the approximate frequency range of the expected radiation, the approximate timescale for the spindown to occur, etc. Presumably these robust features can be used to reduce considerably the volume of general spindown parameter space which need be searched.

B. Stochastic Background

We now consider the gravitational-wave stochastic background generated by spindown radiation from neutron star formation throughout the universe. A stochastic background is detected by looking for correlations in the response of two or more detectors. The sensitivity of the network to the background drops rapidly for gravitational wave frequencies much higher than the inverse light-travel time between detectors. For the present application, the important networks are therefore the VIRGO-GEO pair (high frequency cut-off $f_{\rm cut} \approx 400$ Hz) and the Washington-Louisiana pair of LIGO detectors ($f_{\rm cut} \approx 100$ Hz). The gravitational radiation generated by the

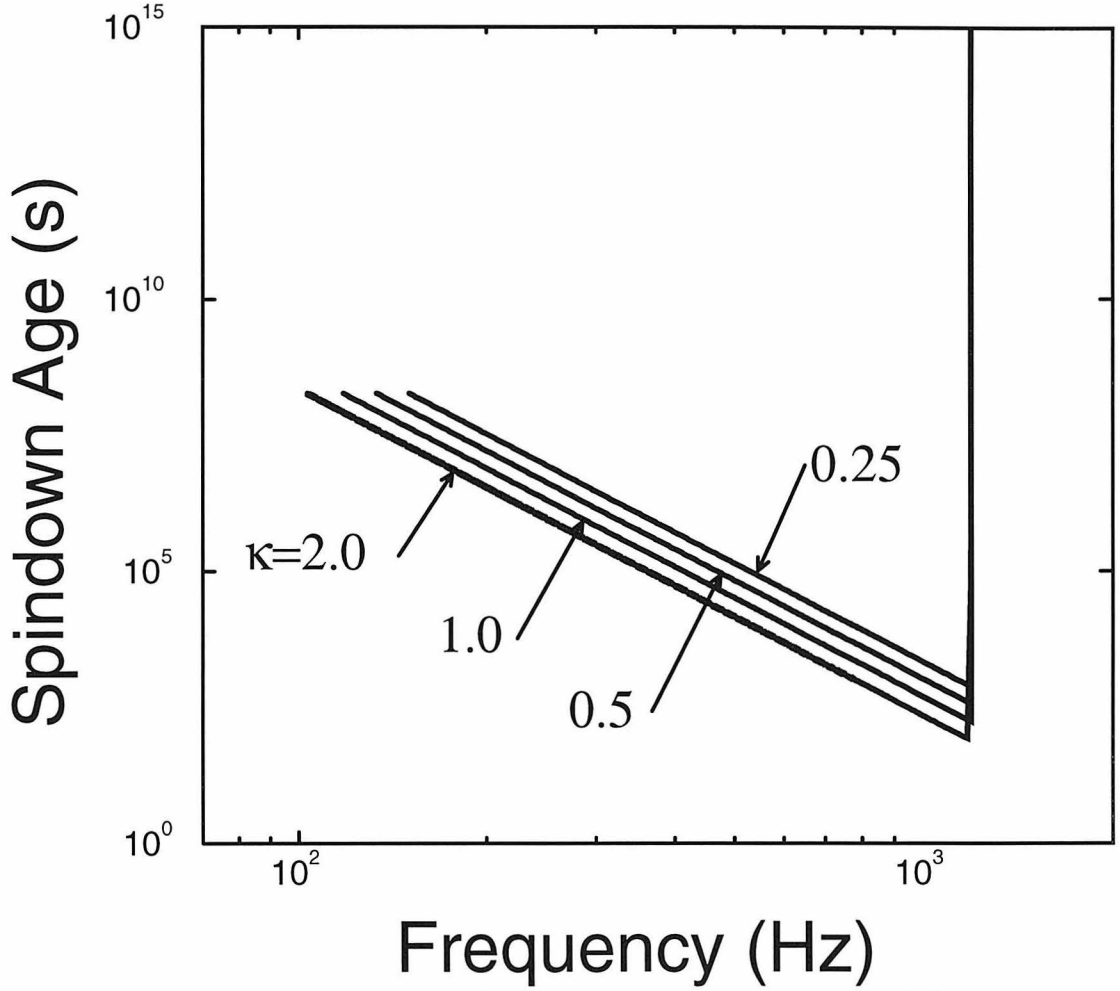

FIG. 6.10. Spindown age for an r-mode-driven young neutron star for different values of the nonlinearity parameter κ.

r-mode spin-down process has significant power at these relatively low-frequencies, $f \approx 100 - 400$ Hz. In addition the cosmological redshift (with $z \approx 1 - 4$) of these sources has the beneficial effect of shifting much of the radiation into the detectable band.

Neutron stars have presumably been formed since the beginning of star formation. If each neutron star formation event converts a reasonable fraction of a solar mass into gravitational radiation via the r-mode instability, then the sum of this radiation constitutes a random background that may be detectable by LIGO III. We now make a rough estimate of the spectrum and detectability of this background radiation. A more detailed analysis is being carried out by Vecchio and Cutler [32].

The spectrum of the gravitational wave background is typically represented by the following dimensionless quantity:

$$\mathbf{\Omega}_{\rm gw}(f) \equiv \frac{1}{\rho_c}\frac{d\,\rho_{\rm gw}}{d\,\log f}, \tag{6.5.16}$$

where $\rho_{\rm gw}$ is the energy density in gravitational waves, and $\rho_c = 3c^2H_0^2/3\pi G \approx 1.6 \times 10^{-8} h_{100}^2$ erg/cm^3 is the critical energy density just needed to close the universe. (H_0 is the Hubble constant and h_{100} is H_0 divided by 100 km/s/Mpc.) The signal-to-noise with which this background can be detected in a correlation experiment between two detectors (here assumed to have uncorrelated noise) is given by [33,34]

$$\left(\frac{S}{N}\right)^2 = \frac{9H_0^4T}{50\pi^4}\int_0^\infty df \frac{\gamma^2(f)\Omega_{\rm gw}^2(f)}{f^6\,{}^1S_h(f)\,{}^2S_h(f)}. \tag{6.5.17}$$

where T is the integration time, ${}^1S_h(f)$ and ${}^2S_h(f)$ are the noise spectral densities of the two detectors, and $\gamma(f)$ is the (dimensionless) overlap reduction function, which accounts for the fact that the detectors will typically have different locations and orientations.

We can get a rough estimate of $\mathbf{\Omega}_{\rm gw}(f)$ due to the stochastic background of gravitational radiation from the r-mode instability as follows. A $1.4M_\odot$ neutron star rotating with Keplerian angular velocity $\Omega_K \approx \frac{2}{3}\sqrt{\pi G\bar{\rho}}$ has rotational kinetic energy

$E_{\rm K} \approx 0.025 M_\odot c^2$, two-thirds of which is radiated as gravitational waves. For now, assume that all neutron stars are born with angular velocity Ω_K. For a single supernova occurring at $z = 0$, the spin-down radiation has spectrum $dE_{\rm gw}/df \approx \frac{4}{3} E_{\rm K}\, f/f_{\rm max}^2$, where $f_{\rm max} \approx 2\Omega_K/3\pi \approx 1400$ Hz.

We are chiefly interested in $\mathbf{\Omega}_{\rm gw}(f)$ for $f < f_{\rm min} \approx 120$ Hz, since that is the range where the pair of LIGO II detectors will have their best sensitivity. Let $n(z)\, dV\, dz$ be the number of supernovae occurring within co-moving volume dV and redshift interval dz. In the frequency range of interest then the spectrum of gravitational radiation in the universe today is given by

$$\frac{d\,\rho_{\rm gw}(f)}{df}\Delta f = \frac{4E_{\rm K}}{3f_{\rm max}^2}\int_{z_{\rm min}(f)}^{z_{\rm max}(f)} n(z)\frac{f'\Delta f' dz}{1+z}, \tag{6.5.18}$$

where $f'\Delta f' = (1+z)^2 f \Delta f$ are the values of the frequencies as emitted by the source, $z_{\rm min}(f) \equiv \max\{0, f_{\rm min}/f - 1\}$, $z_{\rm max}(f) \equiv \min\{z_*, f_{\rm max}/f - 1\}$, and z_* corresponds to the maximum redshift where there was significant star formation. The factor $1+z$ in the denominator in Eq. (6.5.18) accounts for the redshift in energy of the gravitational radiation.

To evaluate the integral in Eq. (6.5.18), we must make some assumption about the rate of Types Ib, Ic, and II supernovae (which are the ones that leave behind neutron stars). The combined rate in our galaxy at present is roughly one per 100 years. If this rate had been constant, the Galaxy would today contain about 10^8 neutron stars. However at earlier times, for z between 1 and 4, the rate (with respect to proper time) was significantly higher. A reasonable estimate is that our Galaxy contains 3×10^8 neutron stars today. Let $n(z)\Delta z$ be the density of neutron star births (per unit comoving volume) between redshifts z and $z + \Delta z$. As a rough, first-cut at this problem, we model $n(z)$ as constant $n(z) \equiv n_o$ for $0 < z < z_*$, where $z_* \approx 4$, and take $n(z) = 0$ for $z > z_*$. In this case the integral in Eq. (6.5.18) can be performed to obtain:

$$\frac{\mathbf{\Omega}_{gw}(f)}{Af^2} = \begin{cases} 0, & 0 < f < f_1, \\ (z_* + 1)^2 - (f_{\min}/f)^2, & f_1 < f < f_{\min}, \\ z_*(z_* + 2), & f_{\min} < f < f_2, \\ (f_{\max}/f)^2 - 1, & f_2 < f < f_{\max}, \\ 0, & f > f_{\max}, \end{cases} \tag{6.5.19}$$

where $A \equiv 2n_o E_{\rm K}/(3\rho_c f_{\max}^2)$, $f_1 \equiv f_{\min}/(1+z_*)$ and $f_2 \equiv f_{\max}/(1+z_*)$.

We can estimate the value of the constant n_o as follows. We assume that the number of neutron stars in a given location is roughly proportional to the luminosity of the visible matter at that location. The total luminosity of our Galaxy is $1.4\times10^{10}L_\odot$ [35], while the number of neutron stars in the Galaxy is about 3×10^8. Thus the neutron star mass to total luminosity of matter ratio is about $0.03M_\odot/L_\odot$. The mean luminosity of the universe is $1.0\times10^8 h_{100}L_\odot/{\rm Mpc}^3$ [36]. Thus, the mean mass density of neutron stars is about $\rho_{\rm ns} \approx 3\times10^6 h_{100}M_\odot/{\rm Mpc}^3 \approx 1.1\times10^{-5}h_{100}^{-1}\,\rho_{\rm c}$. The current density of neutron stars is related to the constant n_o by $\rho_{\rm ns} \approx 1.4M_\odot z_* n_o \approx 5.6M_\odot n_o$. Thus $\frac{2}{3}n_o E_{\rm K}/\rho_{\rm c} \approx 3.3\times10^{-8}h_{100}^{-1}$. For LIGO, the most important range in Eq. (6.5.19) is $f_1 < f < f_{\min}$; we can re-write the result for this portion in the more useful form

$$\mathbf{\Omega}_{\rm gw}(f) \approx 2.4\times10^{-10}h_{100}^{-1}\left[\left(\frac{f}{24\,{\rm Hz}}\right)^2 - 1\right]. \tag{6.5.20}$$

Evaluating at $f = 50$ Hz, with $h_{100} = 0.7$ we find $\mathbf{\Omega}_{\rm gw}(f = 50\,{\rm Hz}) \approx 1.1\times10^{-9}$.

Using the above spectrum Eq. (6.5.19), we evaluate the S/N using Eq. (6.5.17). For an integration time of $T = 10^7$s we find $S/N = 0.0022$, 0.34, and 2.6 for LIGO I, II, and III respectively. Since there has been some discussion of building a second kilometer-size interferometer in Europe, we also consider the sensitivity to the r-mode background of this detector paired with VIRGO. We assume that the detectors will be located less than about 300 km apart and have the same orientation. (To model this, we simply set $\gamma(f) = 1$ in the integral Eq. 6.5.17). We find $S/N = 5.6$ assuming both these detectors have LIGO II sensitivity, $S/N = 0.9$ assuming one detector

has LIGO I sensitivity while the other has LIGO III sensitivity, and $S/N = 23$ assuming both have LIGO III sensitivity. Thus we see that detection of the r-mode background will have to wait either for development of "advanced" interferometers or for the construction of two nearby detectors with "enhanced" sensitivity. Two nearby "advanced" interferometers could see quite a strong signal. All the above results on correlation measurements of the stochastic background assume that magnets will be eliminated from the LIGO design. With the current design long-range correlated magnetic fields from Schuman resonances and lightning strikes will mimic a stochastic background with $\mathbf{\Omega}_{\rm gw}$ approximately 10^{-7} to 10^{-9} [37].

These calculations assumed that all neutron stars are born with spins near their maximal value Ω_K. It should be clear, however, that these results for the S/N achievable by the LIGO pair depend only on the stars being born with spins greater than about 300 Hz. Of course, it could well be that some fraction F of neutron stars are born with rapid spins, while $(1-F)$ are born slowly spinning. The values of S/N in this case could be estimated from those given above by multiplying by F. (See Spruit & Phinney [38] for a recent argument that most neutron stars should be born with very slow rotation rates.)

It has previously been suggested that there could be a detectable gravitational wave background produced by supernova events [39,40]. The stochastic background due gravitational radiation from the r-modes differs from that previously envisioned in two important respects. Previously it was assumed that the radiation would be emitted in short bursts, forming a random but not continuous background. For the r-mode background, the long duration of the emission guarantees that it will be a continuous hum rather than an occasional pop. Also, the spectrum from spindown radiation extends to lower frequencies than had previously been expected from supernova events.

VI. DISCUSSION

The discovery of a strong source of gravitational waves that is ubiquitous and is associated with such interesting objects as supernovae and neutron stars inevitably opens up a rich prospect for obtaining astronomical information from gravitational wave observations. We shall discuss here some of the more obvious prospects.

Background radiation from r-modes. Pleasantly, the background requires no detailed modeling of the signal in order to detect it. However, detection of background radiation from r-modes will probably have to wait for the development of "advanced" interferometers (or the construction of two nearby "enhanced" interferometers), even if we assume that a large fraction of neutron stars are born rapidly rotating. For nearby detectors with LIGO III sensitivity, S/N is high enough that one could experimentally measure the spectrum $\mathbf{\Omega}_{gw}(f)$ with reasonable accuracy. This might provide very interesting cosmological information. For instance, imagine that most neutron stars are born rapidly rotating. (This could be verified, at least for neutron stars born today, by direct LIGO detections of nearby supernovae.) The background spectrum between 25 and 50Hz would then give us direct information about the star formation rate in the early universe. And its spectrum between 50 and perhaps 300 Hz would tell us about the distribution of initial rotation speeds of neutron stars.

Individual r-mode events associated with known supernovae. Observations of individual spindown events will be more difficult to achieve but can be very rewarding. The easiest case is if the supernova that leads to the neutron star is seen optically. This gives some hint of when the r-mode radiation should be looked for, but more importantly it gives a position. That reduces the difficulty of extracting the signal from the detector data stream. Detection of the radiation will return the amplitude of the signal, its polarization, the final spin of the star, and the values of the parameters of the waveform. Assuming that the three large detectors (the two LIGO installations

and VIRGO) all detect the signal with $S/N \approx 8$, the effective combined S/N will be $8\sqrt{3} \approx 14$. Values of the various parameters will then typically be determined to 10-20% accuracy. The polarization measures the orientation of the spin axis of the neutron star, which will be difficult to relate to any other observable. So it may not be of much interest. But the power spectrum of the radiation measures, as we have seen, the loss of rotational energy of the star, so it is proportional to I/D^2. If the host galaxy's distance can be determined to better than the accuracy of the gravitational wave measurement, which seems likely, then this will provide a direct measure of the moment of inertia of a neutron star.

There will likely be several detections per year, which will shed light on a number of uncertainties. Even if the parameters are only the Taylor expansion coefficients for the frequency, they will constrain models of the r-mode spindown. We can expect to get some information about cooling rates, viscosity, crust formation, the equation of state of neutron matter, and the onset of superfluidity (or some combination of these). We also expect variability from event to event, due to different initial conditions after gravitational collapse, such as differential rotation or even the mass of the neutron star. Significant differential rotation might affect the final spin rate of neutron stars; hence any variability in the final spin speed might shed light on these initial conditions.

If we find we can detect this radiation with confidence, then the absence of it after a supernova could be a hint that a black hole has formed instead of a neutron star. More rarely it might indicate that the neutron star remained bound in a binary system, and the orbital modulation of the signal made it impossible to find.

Some supernovae will be especially nearby, and some neutron stars will be oriented more favorably, so there might be a handful of events with single-detector $S/N \approx 15 - 20$. These will provide particularly good constraints on the moment of inertia, superfluidity, viscosity, etc. For these events it may also be possible to trace the waveform back to its initial stages, and thereby to measure the initial spin of the

collapsed star. In some cases, a star might be formed with more mass that it can support after spinning down, and so the r-mode spindown would lead to and be interrupted by collapse to a black hole. This would probably happen relatively soon after the star is formed; but for strong events, it might be possible to detect this break.

Using r-mode events as supernova detectors. Perhaps the most exciting use of r-mode observations would be to identify hidden or unnoticed supernovae. If it proves possible to create search strategies that are efficient enough to detect r-mode spindown even without prior positional information from an optical observation, then the gravitational wave detectors will become supernova monitors for the Virgo cluster. Perhaps as many as half of the supernovae in Virgo go unnoticed, hidden in thick dust clouds. LIGO and VIRGO would not give optical observers advance notice of the supernova: they will identify a neutron star only a year or so after it was formed. But they may be able to locate the position of the event with an accuracy of better than one arc-second.

This great precision is achieved from the modulation of the signal produced by the motion of the earth [41]. The angular accuracy is similar to that achieved for pulsar observations in the radio. Fundamentally it is the diffraction limit of a gravitational wave telescope with the diameter of the earth's orbit, because the detector acts like a synthesis array as it builds up signal along its orbit around the Sun. The ratio of the gravitational wavelength of about 1000 km to the diameter of 2 AU is about 3×10^{-6} radians. This angular accuracy improves with S/N as well, but it can be degraded by uncertainties in the spindown parameters. This assumes, as we have in this paper, that neutron-star cooling takes a year or more. If the alternative cooling scenarios are correct and the star cools in a few days, then the angular accuracy of observations will be very poor.

For an event at 20 Mpc, arc-second angular resolution corresponds to distance

resolution of about 60 pc. Observations would therefore not only tell us in which galaxy the event occurred, but even in which molecular cloud. Detailed follow-up searches will then be possible for the expanding nebula, starting perhaps one year after the event.

Other implications for gravitational radiation from supernovae. The r-mode instability also has implications for our expectations of other kinds of gravitational radiation from supernova events. Although detecting supernovae was the goal of initial bar detector development, it has not been possible before now to provide reliable predictions of radiation from gravitational collapse. The r-mode instability is a reliable prediction, but only of radiation long after the collapse event. It is clear that a collapse that produces a rapidly rotating star will be more likely to radiate strongly, especially if it can reach the dynamical bar-mode instability that is seen in the lower-density star-formation simulations. But although rapid rotation is in some sense natural in gravitational collapse, the fact that young pulsars like the Crab are slow rotators seemed to indicate that neutron stars do not form with fast spins. Now the r-mode instability has provided an explanation for the slow spins of young pulsars; there is no longer any observational restriction on the initial spins of neutron stars.

It therefore seems to us much more likely than before that the gravitational collapse event can also be a strong source of gravitational waves. The following scenario seems plausible in at least the extreme cases where rotation completely dominates the last stages of collapse. The collapsed object has so much spin that it forms a bar shape on a dynamical timescale. This radiates away angular momentum in gravitational waves until the star is finally able to adopt a stable axisymmetric shape. The strong gravitational radiation ceases, to be replaced by the developing r-mode radiation. The first burst would be detectable by LIGO II at the distance of the Virgo cluster, and a network of such detectors could give a rough position, which

would allow notification of optical astronomers of the event and multi-wavelength follow-up observations. In the gravitational wave data stream, intensive searching for the r-mode radiation would follow.

The unexpected strength of the r-mode gravitational wave instability in young neutron stars has therefore completely changed the prospects for detection of gravitational waves from supernova events. Not only can we look forward to regular detections of the spindown radiation when enhanced detectors begin operating, but we also now have more reason to expect strong bursts from the collapse events themselves. Particularly exciting is the prospect for using networks of LIGO-type detectors as supernova monitors, able to pinpoint the positions of hidden supernovae with arcsecond precision. In order to achieve these goals, however, much work needs yet to be done to eliminate the uncertainties in our models of young neutron stars and to develop effective ways of searching for signals of this kind.

ACKNOWLEDGMENTS

We thank Patrick Brady, Jolien Creighton, Teviet Creighton, Scott Hughes, Sterl Phinney, Joseph Romano, and Kip Thorne for helpful discussions. This research was supported by NSF grants AST-9417371 and PHY-9796079, by the NSF graduate program, and by NASA grant NAG5-4093.

---

[1] N. Andersson, to appear in Astrophys. J. (gr-qc/9706075).

[2] J. L. Friedman and S. M. Morsink, to appear in Astrophys. J. (gr-qc/9706073).

[3] L. Lindblom, B. J. Owen, and S. M. Morsink, to appear in Phys. Rev. Lett. (gr-qc/9803053).

[4] N. Andersson, K. D. Kokkotas, and B. F. Schutz, in preparation (1998).

[5] A. Abramovici *et al.*, Science **256**, 325 (1992).

[6] A. Giazotto, in *Gravitational Wave Experiments*, edited by E. Coccia, G. Pizzella, and F. Ronga, (World Scientific, Singapore, 1995), p. 86.

[7] K. Danzmann *et al.*, in *Gravitational Wave Experiments*, edited by E. Coccia, G. Pizzella, and F. Ronga (World Scientific, Singapore, 1995), p. 100.

[8] J. Provost, G. Berthomieu, and A. Rocca, Astron. Astrophys. **94**, 126, (1981).

[9] J. Papaloizou and J. E. Pringle, Mon. Not. R. Astron. Soc. **182**, 423 (1978).

[10] J. Ipser and L. Lindblom, in preparation (1998).

[11] K. S. Thorne, Rev. Mod. Phys. **52**, 299 (1980).

[12] J. Ipser and L. Lindblom, Astrophys. J. **373**, 213 (1991).

[13] C. Cutler and L. Lindblom, Astrophys. J. **314**, 234 (1987); R. F. Sawyer, Phys. Rev. D **39**, 3804 (1989).

[14] J. L. Friedman and B. F. Schutz, Astrophys. J. **222**, 281 (1978).

[15] S. L. Detweiler and L. Lindblom, Astrophys. J. **213**, 193 (1977).

[16] D. Lai and S. L. Shapiro, Astrophys. J. **442**, 259 (1995).

[17] S. L. Shapiro and S. Teukolsky, Black Holes, White Dwarfs, and Neutron Stars (Wiley 1983).

[18] L. Lindblom and G. Mendell, Astrophys. J. **444**, 805 (1995).

[19] K. S. Thorne, in *300 Years of Gravitation,*, edited by S. W. Hawking and W. Israel (Cambridge University Press, Cambridge, England, 1987), p. 330.

[20] B. F. Schutz, Class. Quantum Grav. **6**, 1761 (1989).

[21] K. S. Thorne, in *Compact Stars in Binaries*, edited by J. van Paradijs, E. P. J. van den Heuvel, and E. Kuulkers (Kluwer Academic, Dordrecht, 1996), p. 153.

[22] K. S. Thorne, in *Theoretical Principles in Astrophysics and Relativity*, edited by N. R. Lebovitz, W. H. Reid, and P. O. Vandervoort (University of Chicago Press, Chicago, 1978), p. 149.

[23] P. R. Brady, T. Creighton, C. Cutler, and B. F. Schutz, Phys. Rev. D **57**, 2101 (1998).

[24] C. Cutler and É. É. Flanagan, Phys. Rev. D **49**, 2658 (1994).

[25] B. Barish *et al.*, LIGO Advanced Research and Development Proposal, Caltech/MIT, unpublished (1996).

[26] K. S. Thorne, private communication.

[27] S. A. Hughes, private communication.

[28] F. E. Marshall, R. V. Gotthelf, W. Zhang, J. Middleditch, and Q. D. Wang, astro-ph/9803214.

[29] G. Frossati, unpublished.

[30] P. R. Brady and T. Creighton, in preparation (1998).

[31] J. Tohline, J. E. Cazes and H. S. Cohl, "The Formation of Common-Envelope, Pre-Main-Sequence Binary Stars", talk presented by Tohline at *Numerical Astrophysics 1998* Conference in Tokyo, Japan.

[32] A. Vecchio and C. Cutler, in preparation (1998).

[33] É. É. Flanagan, Phys. Rev. D **48**, 2389 (1993).

[34] B. Allen, in *Relativistic Gravitation and Gravitational Radiation* edited by J. P. Lasota and J. A. Marck (Cambridge University Press, Cambridge, 1997), p. 373.

[35] J. Binney and S. Tremaine, *Galactic Dynamics*, (Princeton University Press, Princeton, 1987).

[36] P. J. E. Peebles, *Physical Cosmology*, (Princeton University Press, Princeton, 1971).

[37] B. Allen and J. D. Romano, submitted to Phys. Rev. D (gr-qc/9710117).

[38] H. Spruit and E. S. Phinney, to appear in Nature (astro-ph/9803201).

[39] D. Blair and L. Ju, Mon. Not. R. Astron. Soc. **283**, 648 (1996).

[40] V. Ferrari, in *Proceedings of The 12th Italian Conference on General Relativity and Gravitational Physics*, edited by M.Bassan *et al.* (World Scientific, Singapore, 1997), p. 149.

[41] B. F. Schutz, in *The Detection of Gravitational Waves*, edited by D. Blair (Cambridge University Press, Cambridge, England, 1991), p. 406.